

# The Second Laser Revolution in Chemistry: Emerging Laser Technologies for Precise Fabrication of Multifunctional Nanomaterials and Nanostructures

Alina A. Manshina, Ilya I. Tumkin, Evgeniia M. Khairullina, Mizue Mizoshiri, Andreas Ostendorf, Sergei A. Kulinich, Sergey Makarov, Aleksandr A. Kuchmizhak,\* and Evgeny L. Gurevich\*

The use of photons to directly or indirectly drive chemical reactions has revolutionized the field of nanomaterial synthesis resulting in appearance of new sustainable laser chemistry methods for manufacturing of micro- and nanostructures. The incident laser radiation triggers a complex interplay between the chemical and physical processes at the interface between the solid surface and the liquid or gas environment. In such a multi-parameter system, the precise control over the resulting nanostructures is not possible without deep understanding of both environment-affected chemical and physical processes. The present review intends to provide detailed systematization of these processes surveying both well-established and emerging laser technologies for production of advanced nanostructures and nanomaterials. Both gases and liquids are considered as potential reacting environments affecting the fabrication process, while subtractive and additive manufacturing methods are analyzed. Finally, the prospects and emerging applications of such technologies are discussed.

## 1. Introduction

As a component of chemical reactions, light has been appreciated since long ago. Figure 1 exhibits the chronologically arranged milestones that represent the main developments that gradually led to the subject of this article over decades and centuries. The relationship between chemistry and light was discovered when studying the photosynthesis process in plants by Priestley, Ingenhousz, Mayer, and Pfeffer in the 18<sup>th</sup> and 19<sup>th</sup> centuries. Then Timiriacheff, in his works “Device for studying the decomposition of carbon dioxide” (1868) and “Croonian lecture. - The cosmical function of the green plant” (1904),<sup>[1]</sup> analyzed the photochemical process going on in the green leaf, under the influence

A. A. Manshina, E. M. Khairullina  
St. Petersburg State University 7-9 Universitetskaya Embankment  
St. Petersburg 199034, Russia

I. I. Tumkin, A. Ostendorf  
Ruhr-Universität Bochum  
Applied Laser Technology  
Universitätsstraße 150  
44801 Bochum, Germany

M. Mizoshiri  
Department of Mechanical Engineering  
Nagaoka University of Technology  
1603-1, Kamitomioka, Nagaoka, Niigata 940-2188, Japan

S. A. Kulinich  
Research Institute of Science and Technology  
Tokai University  
Hiratsuka Kanagawa 259-1292, Japan

S. Makarov, A. A. Kuchmizhak  
Qingdao Innovation and Development Center  
Harbin Engineering University  
Qingdao 266000 Shandong, China

S. Makarov  
ITMO University  
Kronverksky pr., 49, St. Petersburg 197101, Russia

A. A. Kuchmizhak  
Institute of Automation and Control Processes  
Far Eastern Branch  
Russian Academy of Science  
5 Radio Str., Vladivostok 690041, Russia  
E-mail: [alex.iacp.dvo@mail.ru](mailto:alex.iacp.dvo@mail.ru)

A. A. Kuchmizhak  
Far Eastern Federal University  
8 Sukhanova str., Vladivostok 690041, Russia

E. L. Gurevich  
Laser Center (LFM)  
University of Applied Sciences Münster  
Stegerwaldstraße 39, 48565 Steinfurt, Germany  
E-mail: [gurevich@fh-muenster.de](mailto:gurevich@fh-muenster.de)

E. L. Gurevich  
Center for Lasers and Optics  
Anhui University  
Hefei 230088, China

 The ORCID identification number(s) for the author(s) of this article can be found under <https://doi.org/10.1002/adfm.202405457>

© 2024 The Author(s). Advanced Functional Materials published by Wiley-VCH GmbH. This is an open access article under the terms of the [Creative Commons Attribution](#) License, which permits use, distribution and reproduction in any medium, provided the original work is properly cited.

DOI: 10.1002/adfm.202405457

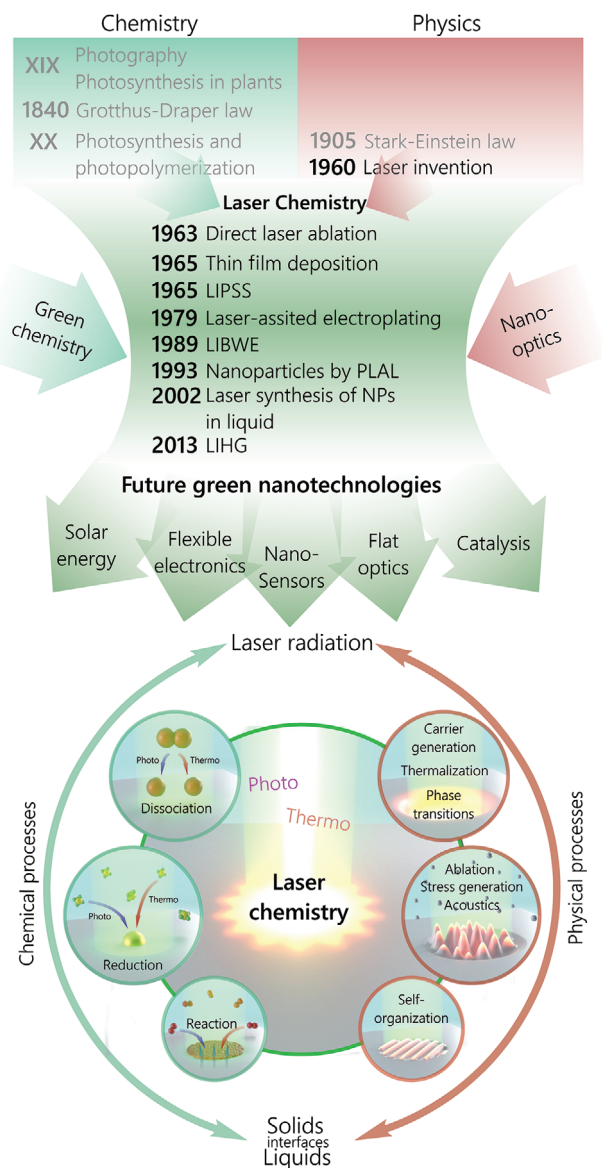


**Figure 1.** (Top panel) Timeline showing key events defining appearance and development of surveyed laser chemistry methods toward several highlighted future technologies. (Bottom panel) Sketch illustrating diversity of physical and chemical processes involved in the formation of nanostructures and nanotextured materials by laser chemistry methods.

of light, which resulted in the concept of “the chemical effect of light”.

It should be noted that in parallel, research in the field of developing photographic images also led to the recognition of the chemical effect of light. Silver salts were found to be easily reduced to metallic silver under the action of light; this observation permitted to develop photosensitive compounds used for image fixing. The first photographs, or “silver pictures”, were taken back in 1802 by Wedgwood who captured images with light sensitive materials. Subsequent research led to the expansion of photosensitive compositions to include photosensitive glasses, and

gradual understanding that the image consisted of submicroscopic particles of gold, silver, or copper.<sup>[2,3]</sup>

Subsequently, the chemical effect of light was discovered for a remarkably wide range of substances and phenomena, and classified according to the types of initiated chemical transformations, such as oxidation and reduction, polymerization, condensation, isomeric, and stereoisomeric changes, ring scission and hydrolysis.<sup>[4]</sup> The importance of light wavelength in initiating chemical reactions has also been established, as well as asymmetric synthesis with circularly polarized light, etc.<sup>[5–13]</sup> In the 1950s, the light absorption and photochemistry were considered and generalized for a wide list of organic molecules, thus providing conceptualization of photo-polymerization processes.<sup>[14]</sup>

Thus, in the beginning of the 20<sup>th</sup> century, the basic principles of photochemistry were established. The first law of photochemistry (also known as the Grothuss–Draper law, 1840) stated that the light must be absorbed by a chemical substance in order for a photochemical reaction to take place, while the second law of photochemistry (the Stark–Einstein law or photochemical equivalence, 1908) stated that each photon of light absorbed by a chemical system can activate no more than one molecule). Thus, photo-excitation was recognized as the first step in a photochemical process, followed by further chemical transformations.

By the middle of the 20<sup>th</sup> century, the main concepts, postulates and laws of photochemistry were already formulated, while this scientific direction was established as a significant branch of chemistry. By then, a wide range of inorganic and organic compounds had been discovered that undergo chemical reactions when exposed to light.

In this regard, Maiman’s demonstration of the ruby laser that took place on May 16, 1960 hit “a fertile ground” and caused an immediate reaction from researchers. As early as in November 1960, Schawlow reported on the prospects of using laser radiation in chemistry.<sup>[15]</sup> Subsequently, a large number of brilliant scientists joined this topic (A. Zewail, V.S. Letokhov, A. M. Ronn, N.V. Karlov and many others) who ensured a rapid progress in this area.<sup>[16–19]</sup> As a result, a new direction in chemistry and, in particular, photochemistry was formed, i.e., laser chemistry.

Thus, it can be argued that the first laser revolution in chemistry occurred in 1960, i.e., when first lasers were built. The use of a new light source, which was able to provide high monochromaticity, coherence, intensity, and directionality of optical radiation, made it possible to launch and study completely new chemical processes and phenomena. The main new research directions focused on stimulation of chemical reactions via selective excitation of vibrational levels in molecules induced by IR lasers, chemical reactions induced by single UV or visible laser photons, selective two-step reactions requiring two photons for their induction, isotope separation by selective laser excitation, and so on refs. [16,20–22].

Almost simultaneously with ruby laser invention, first demonstrations of laser ablation phenomena were published by several groups in 1963<sup>[23–26]</sup> followed by the development of thin-film deposition techniques demonstrated by Smith and Turner in 1965.<sup>[27]</sup> In the same year, self-organised periodically-arranged damages were reported on semiconductor surfaces exposed to high-intensity Q-switched ruby laser radiation.<sup>[28]</sup> Such structures, referred to as ripples or LIPSS (laser-induced periodic surface structures) now, have their period comparable, or up

to ten times finer than the laser wavelength used for their production. The creation of new types of lasers (with wider spectral and energy characteristics, as well as continuous and pulsed generation modes) entailed their immediate introduction into laser chemistry related research. All this helped develop and promote new ideas about homogeneous and heterogeneous chemical processes induced by photo-chemical or/and thermo-chemical effects under laser radiation, thus contributing to the rapid progress of synthetic chemistry.<sup>[29,30]</sup> As a result, by the end of the 20<sup>th</sup> century, laser chemistry became a dynamically developing science, considering not only fundamental issues of the synthesis/transformation of substances, but also analytical problems of their characterization.

The possibility of forming metal tracks in the laser irradiated area at the liquid/substrate interface was first demonstrated in 1979,<sup>[31]</sup> being an idea of localizing the process of metallic coating formation during electroplating by means of laser radiation. Von Gutfeld and colleagues from IBM succeeded in deposition of metallic Au, Ni, and Cu lines on a cathode surface immersed in electroplating bath. The localization of the plating process was achieved by highly localized heating caused by an argon or krypton laser beam focused on the cathode, which resulted in  $\approx 1000$ -fold enhancement of plating rates.<sup>[32–34]</sup> Strictly speaking, this process was laser-enhanced electrodeposition due to temperature increase at the metalsolution interface, which resulted in the shift of the rest potential, an increase in charge transfer rate, and strong microstirring.<sup>[32]</sup>

Further experiments demonstrated that conductive metal lines could be obtained without applying electric field.<sup>[35–38]</sup> Thus, well-localized, a few  $\mu\text{m}$  wide, and highly conductive structures were deposited as a result of laser exposure of the substrate placed in a precursor-containing liquid. Metallic structures appeared on the substrates within laser focal spot via photo-thermally driven redox processes. Later, this approach was called laser-induced chemical liquid phase deposition (LCLD), by analogy with laser chemical vapor deposition (LCVD). Formation of dispersed nanoparticles (NPs) generated by laser ablation of solid targets immersed into a liquid phase was reported by Fojtik and Henglein as early as in 1993.<sup>[39,40]</sup> Later, this discovery transformed into an efficient technology of pulsed laser ablation in liquids (LAL or PLAL, see Section 5.4), a family of convenient approaches that often allow for nanostructures with defined composition, sizes, and morphology. Not only additive manufacturing but also subtractive processes can be improved by laser-induced chemistry. Heating and chemical decomposition of absorbing liquids can be applied for ablation of transparent materials in the laser-induced back-side wet etching (LIBWE) process demonstrated for the first time by Ikeno and coauthors in 1989.<sup>[41]</sup>

Since the beginning of 2000, synergistic joining of several important factors affecting the laser chemistry direction could be observed (Figure 1, top panel). First of all, a rapid development of nanotechnology as an independent and highly demanding field of human activity has stimulated the need for flexible and high-performing synthesis approaches (including environment-friendly or green ones). At the same time, laser systems generating ultrashort (femtosecond) laser pulses have become more and more widespread for applications related with a laser-matter interaction (including laser nanopatterning and nano-optics). In our opinion, this has led to the second laser revolution in chem-

istry, where the laser focal spot can be considered as a precisely localized chemical reactor providing unique experimental conditions for fabrication of functional nanomaterials unattainable via classical chemistry. Brief analysis through the Web of Science database confirms the mentioned timeline and gives an enlightening statistics, where the annual number of publications containing laser, chemical and nanostructures keywords in either abstract or title has been growing rapidly since 2001. Consequently, the citation of such papers also started growing at the same time and exceeds 7000 citations per year now.

At the turn of the 20<sup>th</sup> and 21<sup>st</sup> centuries, there was an explosive growth in publications demonstrating both the transformation of known effects (for example, laser ablation) into potent techniques for the synthesis of a wide range of nano-objects and the development of new approaches of laser synthesis. In parallel, many concise and informative reviews on nanostructures produced under laser illumination have been published to date. However, most of them deal with thorough description of a particular method, followed by discussing generated materials and their applications. Moreover, their attention was mainly focused on long-history laser approaches such as laser ablation, pulsed laser synthesis, laser melting/fragmentation in liquids, etc.<sup>[42–50]</sup>

Meanwhile, the sweeping development of laser chemistry brings forward a rich variety of recently developed approaches such as LCLD, PLAL, laser-induced hydrothermal growth (LIHG), etc., all being associated with laser effect on various media and have their own peculiarities in terms of experimental realization and underlying mechanisms. At the same time, there is still a lack of detailed reviews on each such method, and, what is more important, no integral visio of the laser-accompanying processes resulting in nanostructured materials.

Therefore, this review intends to provide generalization and systematization of laser-assisted chemistry approaches for synthesis of nano-objects and nanomaterials with a specific focus on the interplay of chemical and physical processes driven by laser irradiation, and the resulting formation of nanomaterials and nanostructures. In addition, it also discusses the examples of chemical activity control through various processes, such as photochemical or thermochemical regimes of laser exposure, with the overall goals being consideration of laser-induced processes' variety from unified standpoints, and systematizing the “toolbox of laser approaches” for modern nanotechnology.

## 2. General Description of Laser-Matter Interaction

Initially, the interactions between matter and light are fundamentally non-thermal processes. When using lasers for processing, the relevant stimulations can be categorized into the substrate's solid excitations, the medium's excitations, and the adsorbate-adsorbent system's excitations. In solids, light can interact with optically active elementary excitations such as different types of electronic excitations: phonons, excitons, polaritons, magnons, polarons, and localized or non-localized electronic or vibrational states related to defects, impurities, or the solid surface. On the other hand, the light pulse duration and intensity can significantly affect the regime of interaction governing the types of processes involved in the light-matter interaction on different time-scales from femtoseconds up to milliseconds. As a result, the

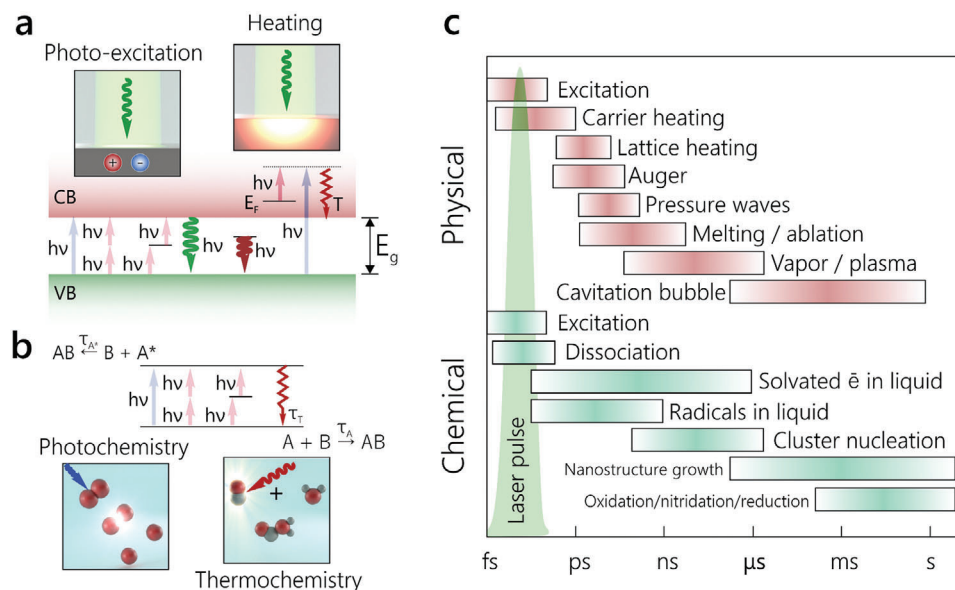


**Figure 2.** a) Light interaction with solids related to photo-excitation via interband transitions between the valence band (VB) and conduction band (CB); and optical heating via intraband transitions in the conduction band (CB) b) Light interaction with a molecular system 'A', where the upper part is a scheme for the competition between thermal and photochemical reactions with different times  $\tau_A$  and  $\tau_{A^*}$  for ground and excited states, respectively.  $\tau_T$  is the characteristic recombination time accompanied by heat generation. c) Schematic illustration of the timescales of main physical (upper part) and chemical (lower part) processes.

selection of wavelength, pulse duration, and intensity of incident light is critical to control laser-induced processes.

## 2.1. Electron-Hole Pair Generation in Solid-State Materials

Generation of free charge carriers is essential for surface chemistry because the electrons and holes at the surface stimulate chemical reactions acting as a reducing/oxidizing agents. First, let's consider light interaction with solid-state dielectric or semiconductor materials, which can play the role of substrate for further chemical reactions on interfaces solid-liquid or solid-gas. When materials with bandgap  $E_g$  are exposed to light with energy  $h\nu > E_g$ , it is primarily absorbed by bound electrons from the valence band (VB) which is called interband transition (Figure 2a). This process increases concentration of electrons  $n_c$  in conduction band (CB), which is around  $<10^{18} \text{ cm}^{-3}$  for low-power excitation (almost no heating),  $10^{18}$ – $10^{21} \text{ cm}^{-3}$  for mid-power excitation (considerable heating), and  $>10^{21} \text{ cm}^{-3}$  for high-power excitation (material melting and ablation). The general equation of the photoexcited carrier density  $n_c$  kinetics can be expressed as:<sup>[30]</sup>

$$\frac{\partial n_c}{\partial t} = D \frac{\partial^2 n_c}{\partial z^2} - An_c - Bn_c^2 - Cn_c^3 + G \quad (1)$$

where  $D$  is the diffusion coefficient,  $G \sim I_i \cdot e^{-\alpha z}$  is a carrier generation rate ( $\alpha = \alpha_L + \alpha_{NL}$  is the sum of linear and nonlinear absorptions of the solid material,  $I_i$  is the incident light intensity), while  $A$  is the coefficient related to non-radiative trap recombination,  $B$  is the bimolecular radiative recombination (in the case without considerable fraction of excitons), and  $C$  is the Auger recombination. The excited or hot carrier will quickly thermalize

the lattice via phonon emission and generate heat at a characteristic time that can be from sub-ps timescale. The radiative recombination processes are relatively slow and typically not faster than 0.1 ns except stimulated emission processes, which occur from  $\approx 10 \text{ ps}$ <sup>[51]</sup> down to sub-ps<sup>[52]</sup> time-scales in various nanostructures, which require quite specific conditions (resonator and narrow fluence range) and usually are not relevant to the processes discussed here. This allows for neglecting the coefficient  $B$  in many practical cases.<sup>[53,54]</sup> For photon energy comparable with the work function of the electrons, the list of the electron loss mechanisms can be extended by the photoionization<sup>[53,55]</sup> and thermionic emission.<sup>[54]</sup> The source term for the electrons  $G$  in the Equation (1) is sometimes described as ref. [54].

$$G = \frac{\alpha_L}{h\nu} I + \frac{\beta_{TPA}}{2h\nu} I^2 + \delta_{II} n_c \quad (2)$$

where  $\beta_{TPA}$  is the two-photon absorption coefficient and  $\delta_{II}$  is the frequency of collisional impact ionisation.

At the same time, at high carrier concentrations  $n_c > 10^{18} \text{ cm}^{-3}$  (i.e., at laser fluence closer to material ablation threshold) contribution of the Auger recombination, a band-to-band three-particle scattering, becomes significant at time-scale starting from  $10^{-12} \text{ s}$ . This process involves either a collision of two electrons in the conduction band and recombination with a hole in the valence band or a collision of two holes in the valence band followed by recombination with an electron in the conduction band. Charge carrier recombination on defects is typically slow and occurs in time-scale  $10^1$ – $10^3 \text{ ns}$ , being important only for the cases of low-fluence excitation, when faster processes are negligible (e.g., in solar cells or optoelectronic devices), which is also out of the scope of our review.

Equation (1) can also be applied not only for bulk materials, but also for nanoparticles and nanostructures. Taking into account their optical resonances<sup>[56]</sup> is critical, because local field enhancement can strongly affect generation rate  $G$  and spatial distribution of free carriers.<sup>[57]</sup>

There are other processes, which change the energy-distribution function but do not reduce the number of free carriers: electron–electron and electron–phonon relaxations occurring in the valence band. The time between electron-to-electron collisions ( $\tau_e$ ) is very short and ranges from 10 fs to 1 ps. In contrast, electron–phonon relaxation times are much longer due to the significant difference in mass between electrons and ions and hence, a small fraction of the kinetic energy exchanged in each collision. Depending on the strength of electron–phonon coupling, relaxation time can range from several to hundreds of picoseconds.<sup>[58]</sup> Similar electron–phonon relaxation times are observed for quasi-free electrons in semiconductors like silicon.<sup>[59]</sup> In many applications like photocatalysis,<sup>[60]</sup> photovoltaics,<sup>[61]</sup> or generally, in photochemistry,<sup>[62,63]</sup> it is important to extract such “hot” electrons before their relaxation to the bottom of CB. However, generally, the electron–phonon interaction results in material heating, which we discuss in the next Section 2.2.

## 2.2. Heat Generation and Dissipation, Slow and (Ultra)Fast Heating

In the case of metals, conduction band electrons have very high density  $\approx 10^{23} \text{ cm}^{-3}$  and absorb incident light via intraband transitions within a thin layer of around 10–30 nm (known as intraband transitions, see Figure 2a). As we discussed in the previous section, the concentration of free carriers in semiconductors and dielectrics can be controlled by laser intensity, and these electrons can also absorb light via intraband transitions. In both cases, the excess of energy in the electronic sub-system is converted to heat via electron–photon relaxation.

Temperature distributions induced by the absorption of laser radiation can be calculated based on the heat equation. In the most general case, the temperature  $T = T(x, t)$  is a function of both the spatial coordinates  $x$  and the time  $t$ . With fixed laser parameters the temperature distribution depends on the optical absorption within the irradiated zone, and on the transport of heat out of this zone. In the absence of heat transport by convection and thermal radiation, the heat equation can be written as:

$$\rho(T)c_p(T) \frac{\partial T(x, t)}{\partial t} - \nabla[\kappa(T)\nabla T(x, t)] = Q(x, t) \quad (3)$$

where  $\rho$  is the mass density,  $c_p(T)$  is the specific heat at constant pressure,  $\kappa$  is thermal conductivity and  $Q(x, t)$  is a heat source (typically Gaussian function in time and space).

Within the electron system, the excitation energy is thermalized within, typically, 10 fs to 1 ps. Thermalization between the electron subsystem and the lattice is much slower, typically of the order of 1100 ps, depending on the strength of electron–phonon coupling  $\Gamma_{e-ph}$  in various materials. If the pulse duration is longer than the characteristic time of electron–phonon relaxation, one can assume that electron and lattice sub-systems are in equilibrium and apply Equation (3). Thus, femtosecond laser excitation generates a hot electron gas with temperature  $T_e$  up to

$10^4$  K in the regime of laser melting or ablation. The transient non-equilibrium state between the hot electrons and the lattice is manifested in temperatures  $T_e$  and  $T$ , which can be calculated from the corresponding heat equations. This description is denoted as the two-temperature model.<sup>[64,65]</sup> In the laboratory system, the coupled nonlinear equations for  $T_e$  and  $T$  can be written, in a general form, as:

$$C_e(T_e) \frac{\partial T_e}{\partial t} = \nabla[\kappa_e(T_e, T)\nabla T_e] - \Gamma_{e-ph}(T_e)[T_e - T] + Q(x, t) \quad (4)$$

and

$$C(T) \frac{\partial T}{\partial t} = \nabla[\kappa(T)\nabla T] + \Gamma_{e-ph}(T_e)[T_e - T] \quad (5)$$

where  $C_e$  and  $C$  are the heat capacities (per unit volume) of the electron and lattice subsystems, respectively. The temperature dependence of the lattice thermal conductivity  $\kappa(T)$  is important for semiconductors<sup>[66]</sup> but is usually neglected for metals.<sup>[54]</sup>

The system of Equations (4) can be also applied for semiconductors along with the equation for photo-excited carriers generation, diffusion, and recombination Equation (1). Based on this fundamental background, one can model the behavior of a solid substrate, which is critical to predict the conditions for various laser-induced processes: heating, melting, and ablation, as well as the spatial and temporal distribution of these phenomena. One of the important predictions that can be made, if one estimates the speed of lattice heating that can be converted to the speed of material thermal expansion, resulting in pressure waves generation at sub-nanosecond time scale.<sup>[67]</sup> These pressure waves can be as high as 1–100 GPa assisting to laser ablation (see more details in Section 5.4) and even to the bubble formation in surrounding liquid.

All this knowledge on thermal dynamics in the irradiated material is crucially important for laser-assisted thermally-induced growth at the solid–liquid interface (Section 5.2), direct laser metallization (Section 5.2), laser surface texturing (Section 5.3), doping (Section 5.4), pulsed laser ablation (Section 5.4), and laser-induced wet etching (Section 5.5). In principle, Equations (1), (4), and (5) along with modified absorption coefficient using Mie theory<sup>[68]</sup> can be applied for laser interaction with nanoparticles<sup>[69,70]</sup> during or after their growth, which is especially important to take into account for the description of fragmentation, autocatalytic growth, or doping (Section 5).

## 2.3. Photochemical Processes

### 2.3.1. Photochemical Versus Thermal

Photochemical processes are often quite complex and they usually overlap with parallel thermal processes affecting them. One of the general scenarios is shown in Figure 2b. A and A\* characterize the system in the ground state and in the photoexcited state, respectively. If we neglect radiative recombination, non-radiative transitions  $A^* \rightarrow A$  can be described by the thermal relaxation time  $\tau_T$ . The characteristic times for the reaction of A and A\* with species B are  $\tau_A$  and  $\tau_{A^*}$ , which are also functions of temperature. In the case of  $\tau_T < \tau_{A^*}$  and  $\tau_A < \tau_{A^*}$ , the excitation energy is rapidly dissipated into heat and the molecules

in the ground state react more actively than in the photoexcited state. In this case, the reaction is thermally activated. In the case of  $\tau_T > \tau_{A^*}$  and  $\tau_A > \tau_{A^*}$ , the process is mainly photochemically activated. The reaction takes place via excited species  $A^*$ . In the case of  $\tau_T < \tau_A$ ,  $\tau_T < \tau_{A^*}$ , but  $\tau_A > \tau_{A^*}$ , or if all these times are comparable, both the 'thermal channel and the photochemical channel are important.

Photochemical synthesis is known to be a useful approach for creating molecules that are hard to make using heat-assisted reactions. However, controlling photochemical reactions is more complicated because the excited states involved are very short-lived and highly reactive, even at low temperatures. Usually, changing the shape or electronic properties of the reactant molecule alters the reaction pathways in photochemical reactions.<sup>[71]</sup> Purely photochemical processes typically occur in organic molecules, where multiple transitions are possible, leading to charge transfer with potential dissociation or isomerization processes, such as the transition between cis and trans isomers. For example, upon photon absorption, the covalently bound 11-cis retinal isomerizes to the all-trans form, enabling rhodopsin to activate transducin, its G protein. All-trans retinal is then released from the protein and reduced to all-trans retinol.<sup>[72]</sup>

There are a few types of photochemical charge transfer processes in organic and organometallic molecules including Ligand-to-Metal Charge Transfer (LMCT), Metal-to-Ligand Charge Transfer (MLCT), Photoredox Catalysis in Organic Synthesis<sup>[73]</sup> and in Organic Photovoltaics.<sup>[74]</sup> For example, the population of the LMCT excited states upon light irradiation of abundant and inexpensive 3d-metal complexes represents an effective platform to access open-shell intermediates of high synthetic value.<sup>[75]</sup> Examples of such metals in the 3d-block include Ti(IV), Fe(III), and Cu(II). Irradiating Cu(II)-X complexes is one of the oldest methods for generating radicals ( $X\cdot$ ) via LMCT excited states. When Cu(II) salts are dissolved in specific organic solvents and exposed to the full spectrum of a mercury lamp (UV+visible light), they undergo photoreduction from Cu(II) to Cu(I).

Additionally, photochemical processes may be considered in photochromic complexes<sup>[76]</sup> where photo switchable organic compounds are attached to metal complexes.<sup>[77]</sup> The photoinduced mechanism in photochromic complexes involves photon absorption, electronic excitation, structural reorganization, formation of a new isomer or state, relaxation to the ground state, and reversibility. For the photocontrollable parts, thermally and photochemically stable chromophores (azobenzene, diarylethene, spiropyran, etc.) are usually used. And for the metal complexes, a wide variety of compounds that have various functions (redox response, luminescence, magnetism, etc.) are applied.<sup>[78]</sup>

Photochemical laser processing dominates when the excitation energy's overall thermalization is slower than the characteristic time of the reaction (see Scheme in Figure 2b). This condition is often true for chemical reactions of excited molecules with themselves or with the substrate surface, photoelectron transfer, chemisorption of species on solid surfaces, and photochemical desorption of species from surfaces. For instance, if we consider the case where the molecules are already adsorbed on the semiconductor surface, photoexcited charge carriers (see Section 2.1) can interact directly with the adsorbate to initiate a reaction. In

purely photochemical processes, the system's temperature remains almost unchanged under laser-light irradiation. Laser photochemistry can differ significantly from standard photochemistry that uses lamps due to the high excitation densities, which can result in multiphoton absorption (see Equation (2)) or induce other nonlinear optical effects.

### 2.3.2. Molecular Systems Photo-Excitation

As discussed in the previous Section 2.3.1, in liquid media and gases, light can induce electronic, vibrational, and rotational transitions within single molecules  $A \rightarrow A^*$  (Figure 2b). When molecules or atoms adhere to a solid surface, their electronic and vibrational characteristics are altered, leading to variations in absorption cross-sections and selection rules for optical absorption, as well as additional vibrational transitions. Light can either increase or decrease the density of adsorbed species by exciting the solid, gas, or liquid-phase molecules, or the adsorbate-adsorbent complex.

There are some typical scenarios of single-photon (linear) excitation. If a molecule in the excited electronic state is unstable, the excitation results in a rapid dissociation within a time range of around  $10^{-14}$  to  $10^{-13}$  s, as shown in Figure 2c. In the gas phase, it is unlikely that relaxation and energy transfer between molecules will occur in such a short period and the dissociation dominates. If the excited electronic state is stable, dissociation only occurs for photon energies ( $h\nu$ ) larger than the energy of dissociation ( $E_d$ ). However, dissociation of isolated molecules is sometimes observed even for smaller photon energies. This phenomenon is known as spontaneous predissociation and is related to transitions from the initially excited electronic state to an unstable state or to a stable electronic state whose dissociation energy is below the originally excited state. The final state can also be the electronic ground state itself; then, the molecule dissociates if  $h\nu > E_d$ . The typical times for predissociation are between  $10^{-12}$  and  $10^{-6}$  s.<sup>[30]</sup>

One of the most important examples of photo-excitation playing key role in many laser-induced nanofabrication processes is photo-ionization of water, where electrons become hydrated on a timescale of  $\approx 300$  fs with lifetimes up to 100 ns in pure water and up to 40 ps in strongly acidic solution.<sup>[79]</sup> In organic liquids, solvated electrons can have lifetimes up to several microseconds.<sup>[80]</sup> Water radical cations rapidly decompose into water molecules within 50 fs.<sup>[81]</sup> Finally, a hydrated electron can also recombine with two molecules of water within  $\approx 1$  ns producing hydroxyl anion  $\text{OH}^-$  and stable  $\text{H}_2$  in the reaction  $2\text{H}_2\text{O} + 2e^- = 2\text{OH}^- + \text{H}_2$ .<sup>[82]</sup> These processes are schematically illustrated in Figure 2c. One can compare these time scales with those from previous Sections 2.1 and 2.2 to better understand the overall dynamics of various laser-induced thermal and photo-chemical processes that occur during laser-matter interaction.

The primary drawback of single-photon excitation/dissociation processes concerning laser-chemical processing is the inflexibility of available lasers to match the maxima of dissociative transitions in the medium to far ultraviolet range.

Multi-photon processes (MP) provide another efficient way to excite and dissociate molecules using laser light at a specific wavelength or a wider range of precursor molecules. The number

of excited molecules in MP processes is dependent on the photon flux in a nonlinear manner. Coherent two-photon absorption occurs when the single photon energy is smaller than the energy difference between the first excited state and the ground state, while sequential two-photon absorption occurs when a molecule is transferred to the first excited state by absorbing a single photon and dissociates upon absorbing an additional photon. The first step in this sequential excitation is usually referred to as ground state absorption, the following absorptions as excited state absorption. For multiphoton absorption of order  $n$ , the absorption rate is proportional to the  $n$ -th power of the incident intensity, meaning that such absorption rates can be very small for relatively low or moderate optical intensities, but can become dominant for high light intensities. Therefore, pulsed lasers with high peak intensity are required for efficient MP processing, but they may cause substrate damage, so irradiation geometry where the laser beam propagates parallel to the substrate surface is often used. By using ultrashort laser pulses these harmful effects can be additionally minimized and localized in space because of the nonlinear character of absorption.

In single, isolated molecules, electronic excitations decay within  $10^{-14}$  to  $10^{-6}$  s, while low excited vibrational levels have a lifetime of approximately  $10^{-3}$  s. With high molecular densities used in laser-chemical processing, energy randomization between molecules with vibrational mismatches  $< kT$  occurs via collisions within  $10^{-10}$  to  $10^{-4}$  s leading to partial quenching of the excited state. It is important to note that at high laser intensities, excitation and energy relaxation mechanisms can be significantly altered compared to those observed at low to medium intensities. For instance, in polyatomic molecules, highly excited vibrational states may have lifetimes of only in the range between hundreds of femtoseconds up to the picosecond scale.

### 2.3.3. Homogeneous Versus Heterogeneous Photo-Induced Processes

Laser-induced chemical synthesis and processing of materials is the activation of chemical reactions resulting in the new nanophase formation, coating, patterning, or physicochemical modification of surfaces. Namely, this includes such reactions in volume or on the surface as oxidation, nitridation, etching, synthesis, alloying, doping, exchange of surface atoms/molecules, metallization, decomposition, reduction, and polymerization. For such processes as gas-flow mediated oxidation, nitridation, and reduction, the time scale of reaction initiation can be as short as sub-nanosecond similarly to the time needed for nucleation, while considerable growth of layers or nanostructures based on these reactions is usually longer than microseconds.<sup>[83,84]</sup>

Remarkably, modern laser technologies together with basic fundamental principles can make all these processes both macro-scale and micro-scale. Indeed, the main reason is that laser-induced activation or enhancement of a chemical reaction can take place homogeneously, heterogeneously, or via a combination of both. A homogeneous reaction is activated simultaneously within the volume of the homogeneous gas, liquid, or solid medium. A heterogeneous reaction is induced at nucleation centers, which can be e.g., solid–gas or solid–liquid interfaces, various defects, within the solid surface itself or in adsorbate/adsorbent systems.

Both heterogeneous and homogeneous laser-induced reactions may be activated photothermally, or photochemically, or photophysically (i.e., by a combination of both). It should be noted that homogeneous nucleation requires relatively high supersaturation compared to heterogeneous processes.<sup>[85]</sup> On the other hand, heterogeneous processes developing at the interface are much more complex compared to homogeneous reactions because of a large number of interphase effects (various types of sorption, diffusion, catalytic reactions, mutual solubility of components, evaporation, etc.), mutual influence contacting media, various processes, and conditions at the interface. It is believed that the activation of reactions developing under heterogeneous conditions requires less energy compared to the activation energy of homogeneous chemical reactions. This leads to significantly high sensitivity of heterophase reactions to external, in particular optical, influence. It should be noted that heterogeneous reactions themselves have a huge impact on chemical processes, while the effect of laser radiation on the interface provides additional ways to control these processes: changing the chemical activity of each of the contacting media, influencing the process of sorption of chemical reagents or chemical reaction products in the field of laser exposure.

The possibility of controlling heterogeneous chemical reactions by laser irradiation is discussed in a number of theoretical works.<sup>[86,87]</sup> For example, issues of resonant excitation of adsorbed atoms and molecules and their subsequent transition to the desorbed state, surface selective diffusion and changes in the catalytic properties of adsorbents, control of the interaction potential of the adsorbate with the surface are considered due to laser exposure in the UV or IR ranges.<sup>[88,89]</sup> In addition, laser radiation can have a significant impact on the processes of heterogeneous catalysis by changing the concentration of reactants through selective desorption or changing the number of active sites on the surface of the adsorbent. At the same time, the chemical reaction at the interface can be stimulated either by thermo- or photo-effect of laser radiation.

Such a variety of possible homogeneous and heterogeneous chemical reactions determines the general structure of this review - consideration of laser-induced processes in homogeneous (liquid) and heterogeneous (liquid/solid, gas/solid) systems. More details and regimes for these processes are given in Sections 3, 4, and 5.

## 2.4. Optical Effects

Large-area photo-chemical or thermal processing can be performed with the weakly focused laser beam propagating either perpendicular (normal incidence) or parallel to the surface. Such irradiation geometries permit the fabrication of nanoparticles or nanostructures at high throughput. In addition to this, laser-induced processes make it possible to ensure spatial and temporal localization of initiated chemical reactions, which predetermines the conditions for the formation of substances and materials structured at the nanoscale over large areas. Remarkably, the products of these reactions can strongly interact with the incident light, where the optical resonances (i.e., plasmons<sup>[90]</sup> or Mie resonances)<sup>[68,91]</sup> play a key role. More specifically, metallic NPs are known to exhibit resonant light absorption and

related thermalization when the incident laser wavelength matches the excitation of localized plasmonic resonances (LPR) associated with oscillations of free electron plasma in the resonant cavity formed by the NP.<sup>[92]</sup> LPR spectral position is largely defined by the nanoparticle geometry and material optical constants, which opens up pathways to achieve resonant light-matter interaction at practically any spectral range spanning from UV to IR wavelengths. LPR-mediated resonant absorption allows to enhance efficiency of light-to-heat conversion within the nanoscale volume defined by the NP dimensions rather than diffraction-limited focusing capabilities of the optical lenses.<sup>[69,93]</sup> This provides deep-subwavelength heat localization having important practical applications including high-resolution plasmonic nanolithography and information recording,<sup>[94–97]</sup> nanoscale localization of plasmon-assisted chemical reactions<sup>[98–102]</sup> and anti-cancer therapy,<sup>[103,104]</sup> just to name a few. Ultrafast heating of LPR-supporting nanoparticles and surrounding reacting media with pulsed laser exposure is of high interest for promoting specific chemical reactions that can not be realized under slow bulk heating conditions.<sup>[101,105]</sup>

In addition to plasmonic heating effects, the resonant thermalization in semiconductor and dielectric nanoparticles supporting so-called magnetic- and electric-type Mie resonances have recently gained substantial research interest.<sup>[70]</sup> Excitation of such resonances in low-loss materials leads to strong localization of the electromagnetic energy inside the Mie-resonant nanoparticles as opposed to the LPR-based absorption in plasmonic ones.<sup>[91]</sup> Despite the absorption coefficient of common materials used to create Mie-resonant NPs for visible spectral range (such as TiO<sub>2</sub>, Si, GaSe, or Ge) is not that large, such resonant light localization was found to give rise to strong photothermal effects in some cases overcoming those for plasmonic-based nanomaterials.<sup>[106–111]</sup> Light localization in Mie-resonant nanostructures boosts inherent Raman scattering and nonlinear optical effects<sup>[112–114]</sup> being also promising for improving efficiency of localized chemical reactions.<sup>[115–119]</sup>

Additionally, excitation of material surfaces/interfaces by relatively large laser spot have gained increasing interest in recent years, particularly in nano-optics, where surface waves or localized modes excited at nanostructured interfaces, as well as waveguided modes in thin films lead to strongly enhanced and inhomogeneous light intensity distribution (see examples in Sections 4.1, 5.2, 5.3, and 5.4.5) resulting in LIPSS formation.

Spatially localized laser-induced chemical processing allows for single-step direct substrate patterning with lateral dimensions down into the nanometer range. This can be performed by scanning a focused laser beam across the substrate surface<sup>[120,121]</sup> (direct writing), by projecting the laser light via a mask,<sup>[122]</sup> by interference of laser beams,<sup>[123]</sup> by means of microlens arrays<sup>[124]</sup> or spatial light modulators,<sup>[125]</sup> by techniques based on scanning probe microscopy,<sup>[126,127]</sup> by using adaptive optics,<sup>[128]</sup> or by formation of strong near-field around various nano-objects.<sup>[129–131]</sup>

## 3. Laser Synthesis in Liquids

### 3.1. Homogeneous Growth

In liquids, the laser energy absorbed by a molecule can exceed the binding energy of valence electrons, which can cause generation

of various types of highly excited radicals and solvated electrons (see Section 2.3.2) potentially launching chemical reactions. Such homogeneous laser-induced chemical reactions take place under specific conditions and kinetics, thus resulting in unique products. In 2002, Abid et al. demonstrated pioneering results on laser synthesis of metallic NPs in solution of metal salt.<sup>[132]</sup> In sharp difference to classical chemical synthesis, the demonstrated process, referred to as laser synthesis in liquid (LSL), required no reducing agents in the working liquid that only contained aqueous solution of silver nitrate.

**Figure 3a** demonstrates schematically a typical LSL experiment where laser radiation is directed through a cell wall and focused inside the liquid. There, highly intense laser radiation promotes development of nonlinear processes (multiphoton absorption, tunnel and avalanche ionization) and plasma formation. As a result, dissociation of the solution components and generation of solvated electrons, hydrogen, hydroxyl radicals, etc. take place, all such species then participating in the reduction of metal ions. Thus, an important feature of the method is the possibility of using solutions with no reducing agents, with the reduction of metal ions taking place due to high-energy electrons and radicals generated in situ under laser exposure.<sup>[133,134]</sup>

To date, direct laser synthesis has been widely applied to produce monometallic NPs of Au,<sup>[141–144]</sup> Ag,<sup>[132,145]</sup> Pt,<sup>[146]</sup> and Pd,<sup>[147,148]</sup> for which solutions of corresponding metal salts and typically either ns-pulsed visible-range or fs-pulsed near-IR lasers were used. Through the multiphoton ionization of the solvent, the high power density laser radiation was found to generate solvated electrons and active radicals, the latter species then reducing metal ions in the solution.<sup>[149]</sup> A distinctive feature of NPs obtained in this way was their small size (less than 10 nm in almost all presented cases) and narrow size distribution.

The reduction efficiency of metal ions per incident photon is known to be 10<sup>−3</sup>.<sup>[150]</sup> Kinetics of multiphoton photolysis and radical-mediated reduction of Au NPs was discussed in ref. [151] revealing the importance of initial solution's pH on such nucleation mechanisms.

The LSL approach was further evolved toward fabrication of bimetallic NPs (such as Au-Ag) via exposure of mixtures of corresponding metal precursors to fs-laser pulses.<sup>[152,153]</sup> Formation of Au-Ag nanoalloy was found to result from the reduction of metal ions by laser-generated radicals followed by alloy formation due to collision and coalescence of formed metal atoms. Optical spectroscopy confirmed formation of heterometallic NPs with an absorption band around 440–510 nm, *i.e.*, between the plasmon-mediated absorption bands of pure silver and gold NPs. Laser exposure duration was also found to affect the reaction kinetics: A deviation of the Au/Ag ratio in the produced NPs from that in the pristine solution was observed under short irradiation times (shorter than 60 min). Other important bimetallic structures (such as Pt-Au and Pt-Fe) in the form of NPs were also produced under fs-laser irradiation of aqueous solutions containing H<sub>2</sub>PtCl<sub>6</sub> and HAuCl<sub>4</sub> and iron (III) chloride FeCl<sub>3</sub>, respectively.<sup>[154,155]</sup> Diverse carbon nanomaterials were also produced by means of LSL upon direct laser exposure of organic liquids (such as acetone, toluene and benzene as well as water/benzene and ferrocene/benzene solutions).<sup>[156–162]</sup> The effect of pulse duration on the resulting products formed upon laser ablation of neat organic liquids (acetone, ethanol, n-hexane, and

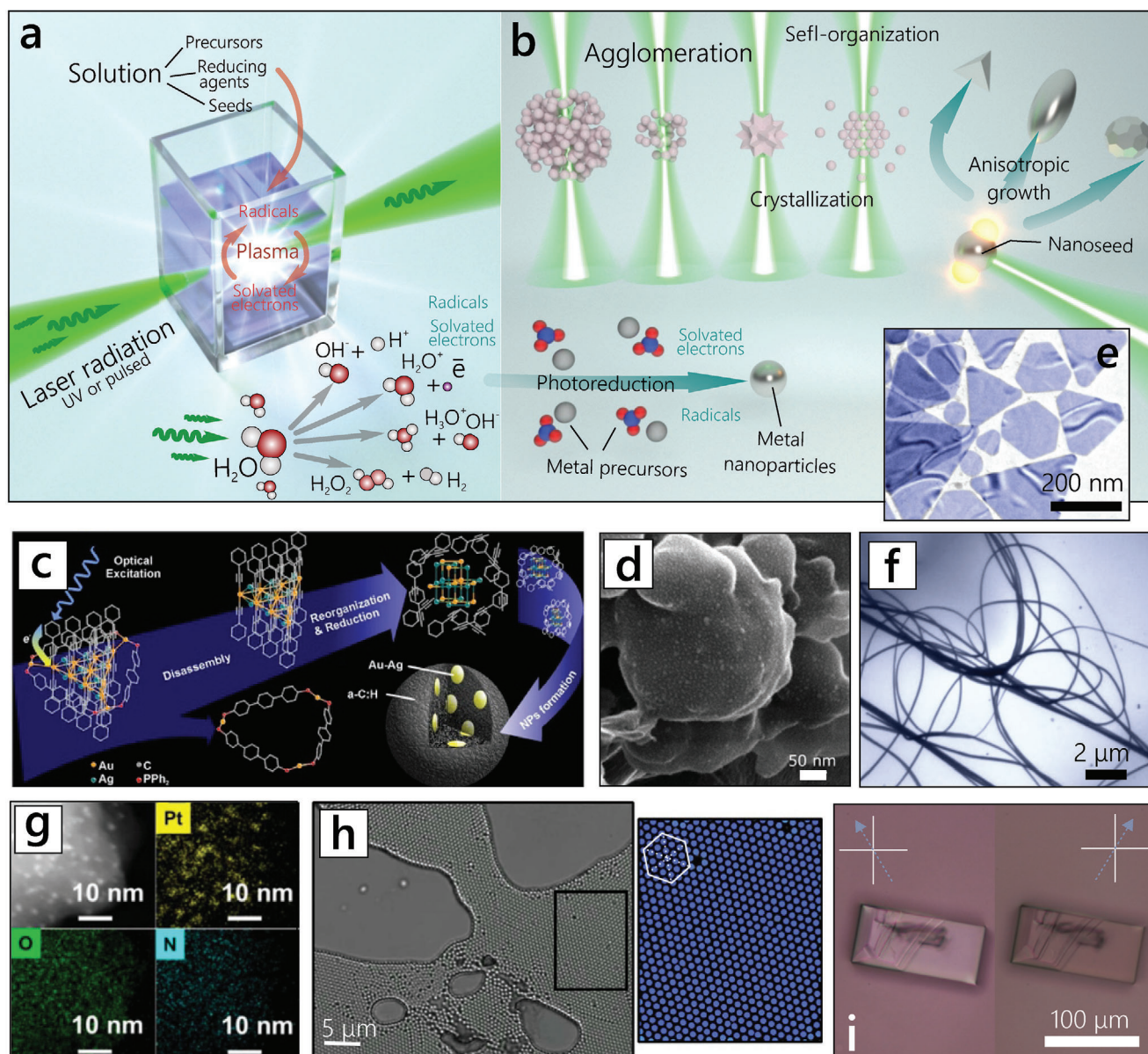


**Figure 3.** a) Schematically illustrated setup of typical LSL experiment. Bottom of panel (a) illustrates diversity of light-induced decomposition channels of water molecules serving as a source of solvated electrons and radicals that take part in reductive LSL reactions. b) Graphically illustrated reduction assisted by generated radicals and solvated electrons, agglomeration driven by optical forces, self-organization and light-driven anisotropic growth taking part in LSL of functional nanomaterials. c) Schematic representation of Au-Ag@carbon nanoparticle formation, with SEM of product shown in panel (d). e) TEM image of Ag nano-triangles produced by plasmon-mediated laser-induced reshaping of Ag seeds in precursor-containing liquid. f) SEM image of LSL-grown Ag nanowires. g) EDX mapping images of Pt-loaded (1 wt.%) covalent organic framework. h) Optical photograph of colloidal crystal solution self-organized into square lattice via laser-driven hydrodynamic flows. Magnified color image provides Lindemann analyses of the highlighted photograph area. i) Crossed-Nicols polarized optical images of the laser-grown d-form  $\text{NaClO}_3$  chiral micro-crystal. Reproduced with permission from [135] Copyright 2010, Springer Nature (c and d), [136] Copyright 2010, American Chemical Society (e), [137] Copyright 2010, Elsevier (f), [138] Copyright 2022, Springer Nature (g), [139] Copyright 2017, Springer Nature (h) and [140] Copyright 2023, Optical Society of America (i).

toluene) was recently studied by Frias Batista et al.<sup>[163]</sup> Both the reaction kinetics and product distribution were found to change upon laser pulse extension from femtoseconds to picosecond pulses: The formation of solvent molecule dimers and oxidized molecules was suppressed, while enhancing the yield of gaseous molecules, sp-hybridized carbons and fluorescent carbon dots was enhanced.

In the processes described above, the redox reactions are triggered by electrons and radicals generated by intense laser radiation. Alternatively, the chemical reactions can be photostimulated at significantly lower intensities of the laser radiation. In this case the solution should contain not only the metal precursor, but also some reducing or photosensitizing agents. The photocatalyzed effect results in reduction of metal ions to

metal, the following nucleation and metal NPs grow. The detailed review of photochemical synthesis is presented by Jara et al.<sup>[134]</sup>

The LSL approach was also adopted to produce metal@carbon nano-composites through UV-laser exposure of precursor solutions containing diverse supramolecular complexes having a central bimetallic core stabilized by the alkynyl and phosphine ligands.<sup>[135]</sup> The authors showed that depending on chosen complex composition and irradiation time, multi-yolk-shell nanostructures with bimetallic Au-Ag NPs (15 nm) encapsulated into carbon nanospheres (20–200 nm) could be produced (see Figure 3d). The mechanism of metal@carbon nanostructure formation was found to include: i) photo-induced decomposition of precursor molecules, ii) transformation of the heterometallic cluster core to bimetal NPs via red-ox intramolecular reaction and aggregation of metal species, and iii) simultaneous aggregation of carbon-rich organic building blocks formed from carbonaceous matrix and multi-yolk-shell architecture as schematically shown in Figure 3c,d.

### 3.2. Seed-Mediated Growth

Photochemical growth of NPs can also be realized using the LSL technique under rather mild laser intensities well below plasma formation threshold. However, additional reducing agents (such as, e.g., citrates) are typically required in this case.<sup>[164,165]</sup> Laser illumination was shown to initiate photochemical nanoparticle growth from metal ions adsorbed on colloidal metal NPs used as seeds in the presence of citrate. An important modality of such a method is its ability to control the shape of the resulting NPs through laser radiation. For example, Maillard et al. demonstrated spherical, triangular and disk-like Ag NPs by irradiating colloids of metallic Ag seeds, silver nitrate and citrate with a CW Ar-laser.<sup>[166]</sup> The initially spherical Ag NPs were shown to evolve into triangular ones as a result of photochemical reactions that stimulated asymmetric NP growth (reshaping; Figure 3b) coming from the specific polarization- and shape-dependent distribution of plasmon-mediated electromagnetic hot spots.

Light-driven reshaping of Ag NPs with even more diverse geometries was reported by Stamplecoskie and Scaiano<sup>[136]</sup> who applied multiple LEDs with wavelengths from 405 to 720 nm to control the morphology of resulting NPs. They demonstrated that radiation wavelength affected the hot spot distribution associated with various localized plasmon mode excitation in the Ag seeds, which provided diverse opportunities to control the growth of NPs and their optical properties. Figure 3e shows a representative TEM image of such triangular Ag NPs produced through the above-mentioned route. High-aspect-ratio NPs (such as nanorods, nanowires, or nanofibers) are also of high importance, since their plasmonic properties can be shifted toward the near-IR spectral range, i.e., the range of optical transparency of biological tissues and telecom-band laser sources. The LSL technique was adopted to produce such nanostructures using UV irradiation of solutions with metal precursor in the presence of a catalyst and stabilizing agent or through the template synthesis via UV-photocrosslinking of PVA/DNA scaffolds in the presence of negatively charged seed particles.<sup>[137,167–169]</sup> Figure 3f demon-

strates an example of Ag nanowires grown under UV-laser exposure of a precursor containing silver nitrate and phosphomolybdic acid that acted as a catalyst and stabilizing agent.<sup>[167]</sup>

Similar to metallic nano-seeds stimulating the above-mentioned anisotropic plasmon-mediated growth of NPs, other types of nano-inclusions in the form of colloids or powders can be added into the liquid containing precursors (and sometimes reducing agents) to produce nanomaterials with even more sophisticated morphology and composition. Hence, here, we only mention several nano-composites produced through photo-induced growth, to distinguish them from those fabricated by means of thermal-assisted PLAL discussed in Section 5.6. Hu et al. reported LSL of the binary alloy PtX (X = Ag, Cu, Co, and Ni) NPs generated by ns-laser irradiation of Pt nanopowders aqueous salt solutions.<sup>[170]</sup> The formation of such bimetallic NPs was described to occur through laser fragmentation of the pristine Pt powder followed by its alloying by precursor metal ions reduced by solvated electrons and free radicals.

Semiconductor seeds can also be applied to produce hybrid NPs by means of LSL. In this approach, also referred to as photodeposition,<sup>[171]</sup> laser irradiation can cause excitation of valence-band electrons which then migrate to seed's surface and take part in the photoreduction of metal-ion precursors from the surrounding liquid. In this respect, nanoscale semiconductor seeds act as optical radiation absorbers, reducing agents and provide active surface sites for preferential growth of metallic NPs. This route was widely applied for fabrication of diverse metal-semiconductor nano-composites, including Pt/TiO<sub>2</sub>,<sup>[172–174]</sup> Pd/TiO<sub>2</sub>,<sup>[175]</sup> Au/TiO<sub>2</sub> NPs,<sup>[176]</sup> Au/ZnO nanopencils,<sup>[177]</sup> and Pt-decorated covalent organic frameworks.<sup>[138]</sup> Finally, similar LSL routes were widely adopted to produce nano-hybrids made of common 2D nanomaterials decorated with noble metal NPs, such as, e.g., Pt/TiS<sub>2</sub>, Pt/TaS<sub>2</sub>, Ag/MoS<sub>2</sub> and Pt/MoS<sub>2</sub> nanocomposites,<sup>[178–180]</sup> as well as NP-decorated graphene<sup>[181]</sup> or reduced graphene oxides,<sup>[182,183]</sup> to name just some. For more details, those who are interested can address recent review on photodeposition of metal NPs over semiconductor seeds by Wenderich et al.<sup>[171]</sup>

### 3.3. Laser-Trapping-Assisted Growth

Laser-induced agglomeration, which can further lead to nucleation and crystallization, is known to happen in homogeneous molecular solutions or in suspensions when laser power is high enough either to induce a hydrodynamic flow<sup>[139]</sup> or optical trapping forces<sup>[184]</sup> overcoming the Brownian motion. This type of growth has a purely physical nature and does not involve chemical reactions, but we shortly address it here for its similarity to the LSL process discussed earlier in this section. Such laser-induced agglomeration processes permit to grow microcrystals in the focal laser spot directly in a precursor-containing liquid as schematically illustrated in Figure 3b. The first use of this approach was reported by Sugiyama et al.<sup>[185]</sup> who focused a near-IR CW laser inside evaporating DO<sub>2</sub> containing glycine molecules, which resulted in formation of glycine crystals after 15 min of exposure. The authors attributed this effect to optical attraction and trapping due to a large dipole moment of glycine molecules. In this method, the laser beam power was found to

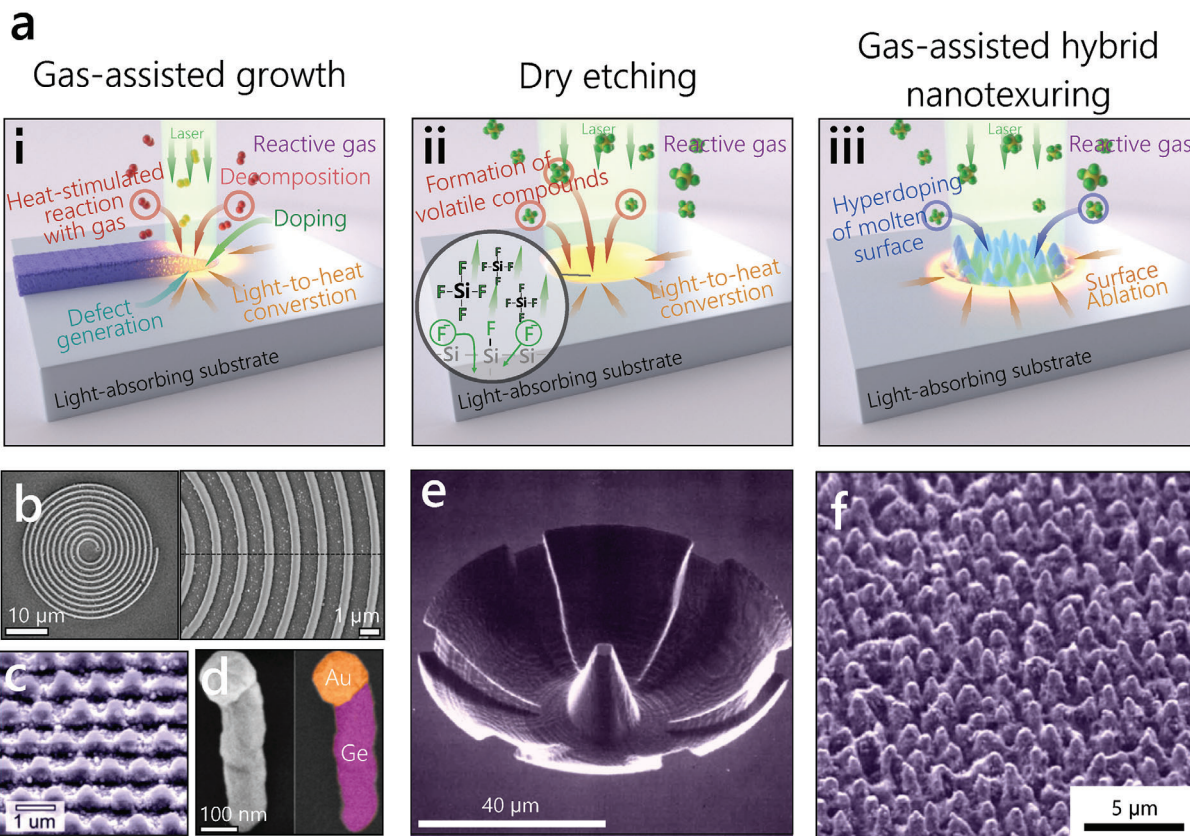


**Figure 4.** a) Scheme illustrating methods of gas-assisted laser nanostructuring of materials: i) gas-assisted growth of nanostructures, ii) gas-assisted etching of semiconductors and iii) hybrid surface nanotexturing. b–d) SEM images providing examples of gas-assisted nanotextured morphologies: b) spiral-shape  $\text{SiO}_2$  ridge recorded on the Si substrate, c) Grating-like structures composed of  $\text{SiO}_2$  ridges produced on the Si wafer surface by its laser-induced periodic surface structuring, d) Ge nanowire grown from the Au nanoparticle in Ar atmosphere containing  $\text{Ge}_2\text{H}_6$  precursor, e) etched Si in chlorine gas at 100 Torr and f) hyperdoped spiky Si surface laser-patterned in  $\text{SF}_6$ . Reproduced with permissions from<sup>[189]</sup> Copyright 2024, Elsevier (b),<sup>[190]</sup> Copyright 2020, John Wiley & Sons (c),<sup>[191]</sup> Copyright 2015, American Chemical Society (d),<sup>[192]</sup> Copyright 1993, Elsevier (e) and<sup>[193]</sup> Copyright 2006, AIP Publishing (f).

be less important for optical trapping than the gradient of optical field.<sup>[186]</sup>

An interesting development of the LSL technique was recently suggested by Toyoda et al.<sup>[140]</sup> who demonstrated formation of chiral  $\text{NaClO}_3$  microcrystals with high crystal enantiomeric excess (a merit of structural chirality) using an optical vortex beam with a helical wavefront. It was shown that the crystal chirality could be flexibly controlled by manipulating the direction of helical wavefront rotation of the vortex beam and its topological charge, thus providing pathways to locally grow enantioselective microcrystals. An example of such microcrystals is provided in Figure 3(i).

The self-organization and agglomeration in the laser-trapping-assisted growth is usually assigned either to the laser-induced hydrodynamic flow or to the optical trapping forces.<sup>[139,184]</sup> In ref. [187] silver nanoparticles were generated in colloidal polymers under action of a  $\lambda = 532$  nm CW laser with  $P = 0.1$  W. The growth of the nanoparticles increases the light absorption, the polymer temperature grows and the Marangoni convection moves the particles to the edge of the beam forming a dark ring surrounding the laser beam. The opposite flow was observed by Yusupov et al.:<sup>[188]</sup> a filament of up to 14 cm length and 10–80  $\mu\text{m}$

in diameter was formed in the direction of the laser light propagation as a 400- $\mu\text{m}$  optical fiber was immersed into a suspension of Ag nanoparticles in the form of Ag/albumin complex. The laser power was in the range 0.3–8.0 W and the filament was stable during the illumination. As the laser was switched off, the filament disappeared due to the Brownian motion.

#### 4. Laser-Assisted Chemistry at the Solid–Gas Surfaces

Next, we will further consider the case when pulsed laser radiation is focused on the interface between a fully transparent gas environment and a solid light-absorbing material (Figure 4a). Once the electrons in the exposed material absorb the incident photons, an electron–phonon relaxation subsequently thermalizes the lattice establishing at picosecond timescale a certain temperature distribution that follows, to some extent, the lateral profile of the laser beam with the largest temperature induced near the interface. Laser-generated heat in the irradiated material is a well-known phenomenon allowing to boost the kinetics of the interface chemical reactions. Potential reactions involve structural transformations of the near-surface material atoms

stimulated by interaction with surrounding gas molecules such as doping, oxidation, nitridation, or carbonization. Noteworthy, the temperature increase also enhances the diffusion of near-surface atoms facilitating penetration of the gas molecules deeper inside the material. The laser patterning experiments can be carried out in the vacuum chamber under control of the gas precursor pressure and content that allows to regulate the onset of laser-driven physical and chemical processes. Depending on the stability of the compounds formed within the laser-irradiated surface area either additive (such as gas-assisted growth; Section 4.1) or subtractive/hybrid (such as gas-assisted etching or texturing/doping; Sections 4.2 and 4.3) nanofabrication techniques can be realized, yet the underlying mechanisms are rather similar in most of the cases.

#### 4.1. Gas-Assisted Localized Growth

Achieving a certain temperature ( $T_{act}$ ) can activate the chemical reactions before the material will proceed to the molten state, while ultrashort pulse duration ensures heat confinement within the focal spot area and highest lateral resolution, in its turn. For example, efficient oxidation of titanium can be initiated above  $T_{act} = 600$  °C under ambient atmosphere,<sup>[194]</sup> allowing to locally grow nanocrystalline TiO<sub>2</sub> nanoridges within the laser focal spot<sup>[195]</sup> (Figure 4a(i)). The transparent oxide ridges focus the incident laser radiation at their bottom increasing the temperature at the metal-oxide interface and stimulating the diffusion of the metal and oxygen ions.<sup>[196]</sup> This provides one of the possible positive feedback mechanisms stimulating the ripple growth. Scanning the sample surface by a laser beam allows free-form writing of the oxide ridges at high spacial resolution.<sup>[189,195]</sup> Example of the produced spiral-shape ridge on the crystalline silicon surface is shown in Figure 4b. Alternatively, highly regular nanogratings made of oxide ridges can be created through the more convenient way using interference of the incident and scattered laser radiation. Such oxidized nanogratings typically referred to as LIPSS were demonstrated on diverse materials including Ti,<sup>[197–199]</sup> Si,<sup>[190]</sup> W,<sup>[198]</sup> Cr,<sup>[196]</sup> Ni<sup>[200]</sup> and Hf.<sup>[201]</sup> Growth of the TiN-containing LIPSS upon patterning of the titanium films in nitrogen-rich atmosphere was demonstrated in ref. [202] Figure 4c demonstrates hierarchical LIPSS formed by periodically arranged oxide protrusions on the crystalline Si surface upon its scanning with linearly polarized laser beam.<sup>[190]</sup>

Laser-driven growth of the surface protrusions can be considered as non-ablative self-terminating processes that stops once the oxide thickness reaches a certain level preventing further interaction of the material atoms beneath oxide layer with gas molecules. The process can be also characterized by minimal amount of the surface debris and molten-state ejecta, while control over the gas pressure provide additional opportunity for regulation of the nanofabrication process. Typically, the larger the difference between the oxidation ( $T_{act}$ ) and melting ( $T_{melt}$ ) temperatures of the certain laser-processed material, the more regular and stable nanotextures can be recorded with broad range of laser processing parameters. Considering high regularity of the formed morphology, their facile production and rather unique ability to imprint high-quality LIPSS even on the curvy surfaces, the potential application areas of this technology include diffrac-

tive color marking,<sup>[198,203,204]</sup> sensing and production of grating-type templates for subsequent coating with other materials (for example, noble-metal-coated gratings for plasmonic biosensors). Structural surface coloring via growth of the uniform oxide layer over the highly reflective pristine material was considered as promising technology for optical filtering, information encryption and anti-counterfeiting.<sup>[204–206]</sup> Additionally, Pomenidis et al. recently reported laser-patterned Ni and Fe electrodes for both enhanced hydrogen production and increased charge storage.<sup>[207]</sup> Surface oxidation simultaneously with nanomorphology growth can also create anti-reflective layer reducing refractive index jump at the air-material interface.<sup>[190]</sup> Such an approach typically works well for IR-transparent crystalline materials (such as silicon, germanium, ZnS, etc.) having rather large refractive index and high Fresnel reflection at the interface, in its turn.

Localized heat-activated growth of the isolated upright-standing Ge nanowires in the presence of 3% germane (GeH<sub>4</sub>) in hydrogen was reported in ref. [208]. By controlling the growth temperature and exposure time, the authors demonstrated the ability to vary the height and geometry (cross-section) of the nanowires. Another interesting example of laser gas-assisted growth technique was suggested by Martino et al., realizing local formation of the Ge nanowires upon thermal decomposition of the Ge<sub>2</sub>H<sub>6</sub> precursor in Ar atmosphere.<sup>[191]</sup> High localization of the growth process was achieved by placing the Au nanoparticles of the substrate acting as local nano-heaters under CW-laser exposure for precursor molecule decomposition as shown on Figure 4d. The technology holds promise for diverse optoelectronic and nanophotonic applications, where metal-semiconductor nanostructures are highly demanding.<sup>[209]</sup>

#### 4.2. Gas-Assisted Dry Etching

Laser-assisted dry etching is technically very similar to the above mentioned laser gas-assisted growth (Section 4.1), yet a change in the environment leads to the opposite effect: the etching is usually done in the atmosphere of halogen-containing molecules providing free halogen atoms. Three main etching mechanisms can be identified:<sup>[210]</sup> 1) The increase in the surface temperature above the activation temperature leads to a chemical reaction between the surface and the environment. 2) The incident laser light excites the free charge carriers at the surface, which activate the chemical reaction between the surface and the gas. 3) The gas photolysis takes place and the active atoms or radicals destroy the solid surface. The products of these laser-activated reaction are gases, the gas molecules leave the surface and create no passivation layer, so that the laser-illuminated solid surface can further react with the molecules coming from the gaseous state. The etch rate depends on the laser intensity, wavelength and on the concentration of the etching molecules in the environment.<sup>[211]</sup> The experiments show that the etched depth per pulse is proportional to the square root of the gas pressure in the lower pressure range but this dependence saturates at higher pressures.<sup>[210,212]</sup>

Dry laser etching of semiconductors is usually performed in halogen-containing gaseous environments like e.g., SF<sub>6</sub>, CCl<sub>4</sub>, CH<sub>3</sub>Br or Cl<sub>2</sub>.<sup>[30,192,210,213–216]</sup> Comparison of the etching rates of Si in CCl<sub>4</sub>, CHCl<sub>3</sub>, CH<sub>2</sub>Cl<sub>2</sub>, CH<sub>3</sub>Cl shows that the etching rate

grows with the number of Cl atoms per molecule.<sup>[210]</sup> The most probable chain of reactions in this case is as follows: first free Cl atoms are generated either by photolysis or by electrons excited to the conduction band of the Si. In the second step gaseous silicon tetrachloride is formed in the reaction  $\text{Si} + 4\text{Cl} = \text{SiCl}_4 \uparrow$  if the surface temperature is above 57.7 °C (see Figure 4a(ii)). Example of the Si surface laser patterned in the  $\text{SF}_6$  atmosphere is shown in Figure 4e. Similar reactions happen in  $\text{SF}_6$  with silicon tetrafluoride formation at the final stage. Usually UV excimer lasers are used due to high photon energy able to break the gas molecule more easily than visible or infrared lasers. However the energy of the stretching mode between the S and F atoms in the  $\text{SF}_6$  molecule is exactly at  $\lambda = 10.6 \mu\text{m}$  ( $943 \text{ cm}^{-1}$ ) corresponding to one of the wavelengths of the  $\text{CO}_2$  laser<sup>[217]</sup> enabling its application for etching in  $\text{SF}_6$  environment. Although the later should absorb at least 30 photons at the  $\lambda = 10.6 \mu\text{m}$  wavelength, in pure  $\text{SF}_6$  gas in the pressure range between 0.1 and 5 mBar, the collisions between the molecules lead to redistribution of the excitation between them, but not to decrease in the average vibrational energy.<sup>[30]</sup> Such multiphoton dissociation excited by  $\text{CO}_2$  laser radiation is also observed in  $\text{CF}_3\text{I}$ .<sup>[218]</sup> The etching of metals and oxides involves more complex processes, since salts appearing at the surface during the etching are solid and form a passivating layer. However, the correlation between the experimentally-observed etching rates and the vapor pressures of these salts shows that they can be removed by the incident laser radiation.<sup>[219]</sup>

Gas-assisted dry etching can take place as a side effect in the process of laser ablation under atmospheric conditions due to approximately 20% of oxygen content in the atmospheric air. Kononenko et al. studied ablation of diamond in different atmospheres and observed that the ablation threshold in experiments done in oxygen-free environments are higher, than that performed in the air.<sup>[220]</sup> This observation highlights the role of the laser-assisted etching in air at low laser fluences.

Additionally, hybrid processes combining material oxidation followed by its etching was recently reported by Bronnikov et al. upon fs-laser texturing of amorphous germanium (*a*-Ge) in ambient air and vacuum environments.<sup>[221]</sup> The authors showed that laser-induced heating of *a*-Ge initially drives its oxidation  $\text{Ge} + \text{O}_2 \Rightarrow \text{GeO}_2$  at temperature above 470 °C and partial reduction of the formed dioxide to less stable configuration  $\text{GeO}_x$  ( $\text{GeO}_2 \Rightarrow \text{GeO}_x + \text{Ge}$ ) that can sublime at temperatures comparable to those required for oxidation.<sup>[222]</sup> This allows ultra-clean ablation-free laser etching of Ge without generating any debris typically ejected at the molten state in the form of nanoparticles. Reduction of the amount of oxygen in the processing chamber by vacuuming was found to regulate the oxidation/sublimation speed allowing to control the grating morphology.<sup>[221]</sup>

### 4.3. Gas-Assisted Hybrid Nanotexturing

Laser-induced heating below phase transition can stimulate formation of vacancies and defective sites in the irradiated material. These sites can be occupied by the thermally decomposed surrounding gas molecules causing local doping of the material within the focal spot. Doping is well known method for tailoring key optoelectronic properties of the common semiconduc-

tors such as silicon and germanium.<sup>[223–225]</sup> Appearance of novel 2D semiconducting materials (*e.g.*, graphene or transition metal dichalcogenides) commonly synthesized in the form of micro-scale flakes has pushed forward the development of the methods allowing localized or site-selective doping. Kim et al. reported laser exposure of 2D  $\text{MoS}_2$  nanoflakes in phosphene  $\text{PH}_3$  gas environment resulting in controllable p-type doping of the material by phosphorus within the irradiation area.<sup>[226]</sup> Noteworthy, photo-decomposition of the precursor gas molecules can be realized with UV light also inducing doping of the target material nearby, as it was recently reported for graphene doping in  $\text{Cl}_2$  gas environment.<sup>[227]</sup>

Laser-induced transition from the solid to the molten state allows the surrounding gas precursor molecules adsorbed on the surface of the irradiated material to easily penetrate inside the material producing a highly hyper-doped near-surface layer (Figure 4a(iii)). Extensive studies of the laser-induced hyperdoping of monocrystalline Si in the  $\text{SF}_6$  gas atmosphere was carried by Mazurs group last two decades stimulated by high importance of this material for optoelectronic devices and its transparency at IR wavelengths.<sup>[193,228,229]</sup> These studies showed the possibility to create sulfur-rich near-surface layer rendering initially IR-transparent Si with the ability to absorb the photons with below-bandgap energies through the formation of impurity-mediated absorption levels. Laser texturing of the Si surface that proceeds simultaneously with its hyperdoping can create a well-developed surface morphology resulting from the material melting, redistribution driven by electromagnetic/hydrodynamic mechanisms and ablative removal.<sup>[230]</sup> An example of such spiky morphology with nearly 100% absorbance at wavelength up to mid-IR range formed on the monocrystalline Si laser-textured in  $\text{SF}_6$  atmosphere is provided in Figure 4f.<sup>[231]</sup> Noteworthy, ultrafast thermalization/quenching rates driven by multi-pulse laser exposure upon texturing create defects in the monocrystalline Si that also contributes to enhanced absorbance of the sub-band photons along with impurity-mediated levels.

## 5. Laser-Assisted Chemistry at the Solid–Liquid Interface

In a sharp contrast to the case of laser structuring in reactive gas surrounding discussed in Section 4, transparent liquid environment offers potentially much higher concentrations of the reacting chemical species within a focal laser spot opening diverse pathways for photo- and thermo-assisted nanostructure formation. In this respect, precursor-containing liquid can act as a source of newly formed nanostructures that will be precisely deposited over the solid target (substrate) within laser focal spot. The substrate in this case can provide charge carriers and active surface sites for nucleation and growth of the nanostructures via diverse photo- or thermal-induced redox reactions. Transparent liquid layer enhances a heat dissipation from the light absorbing material facilitating its faster cooling/quenching, while uneven temperature distribution established in the liquid layer creates convection flows naturally mixing chemical precursors. Such an interplay between physical and chemical light-driven processes at the solid–liquid interface provides a set of additive methods, which allow hydro-thermal growth of the semiconducting crystals (Section 5.1), photo-induced decoration

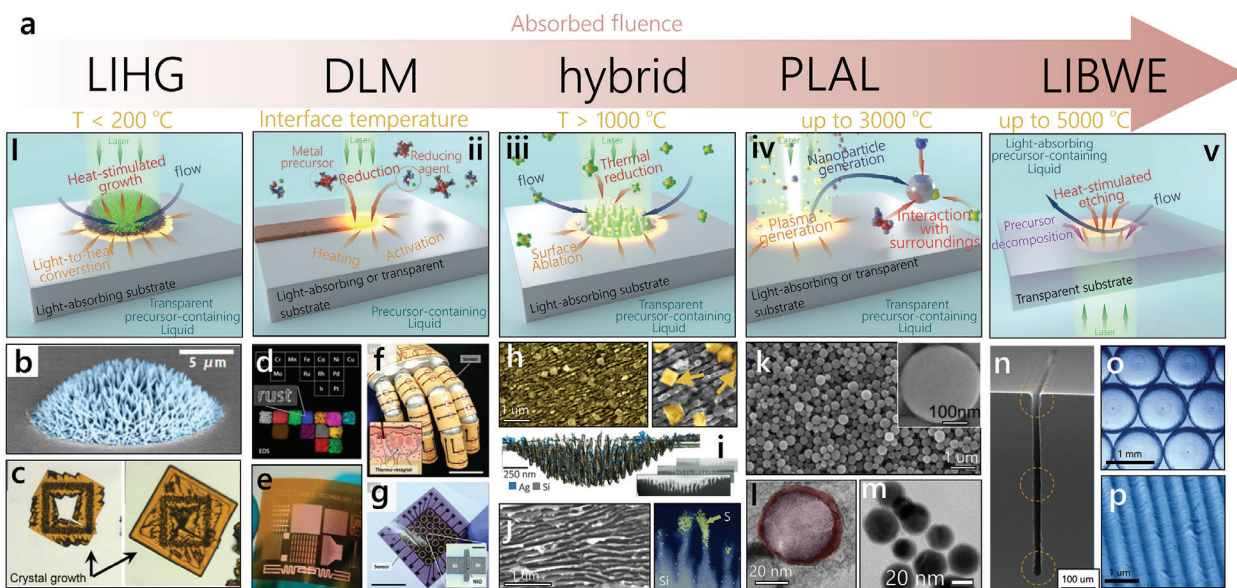


**Figure 5.** a) Diversity of laser nanostructuring methods in reacting liquids (from left to right): laser-induced hydrothermal growth (LIHG) in precursor solution, Direct laser metallization (DLM), hybrid nanotexturing that combines ablative patterning of the surface with its decoration/doping by atoms from precursor solution, PLAL and laser-induced back-side wet etching (LIBWE). b) SEM image of ZnO nanowire array locally grown on a flexible PI substrate. c) Optical image of  $\text{CH}_3\text{NH}_3\text{PbBr}_3$  perovskite microcrystals produced by laser-induced growth in precursor solution followed by lamp exposure. d) EDX map of deposited metals and their positions in the periodic table. e) Photograph of copper electrodes on a polyimide film. f) The NiO temperature sensor on the model hand with temperature-sensitive artificial skin and enlarged illustration of skin thermosensors. g) Thermoreceptor array based on NiO subsensors with an enlarged image of the subsensor (scale bars: 4 cm and 100  $\mu\text{m}$  (inset)). h) Monocrystalline Si patterned in aqueous  $\text{Cu}(\text{NO}_3)_2$  solution resulting in formation of LIPSS decorated by cubic Cu nanoparticles. i) 3D model of a Ag-decorated Si nanograting reconstructed from a series of SEM images of cross-sectional FIB cuts. j) Monocrystalline Si surface laser-patterned in liquid  $\text{CS}_2$ . TEM images of PLAL-generated Co/CoO (k), Pb/PbS (l) and MoC/C core/shell NPs (m). n) High-aspect-ratio channels produced in glass substrate using absorbing liquid with absorbent with phosphoric acid (40 wt.%). o) Microlens array produced on a quartz substrate. p) SEM image of sapphire surface with a grating structure produced by LIBWE. Reproduced with permission from [235] Copyright 2015, American Chemical Society (b), [236] Copyright 2016, American Chemical Society (c), [232] Copyright 2016, American Chemical Society (d), [233] Copyright 2011, American Chemical Society (e), [234] Copyright 2019, John Wiley & Sons (f,g), [237] Copyright 2021, American Chemical Society (h), [238] Copyright 2022, John Wiley & Sons (i), [239] Copyright 2018, American Chemical Society (j), [240] Copyright 2010, John Wiley & Sons (k), [241] Copyright 2010, American Chemical Society (l), [242] Copyright 2010, American Chemical Society (m), [243] Copyright 2020, Elsevier (n), [244] Copyright 2007, IOP Publishing (o), [245] Copyright 2007, Optical Society of America (p).

of free from interface by metallic nanoparticles, as well as localized surface metallization with conductive microstructures. The set of diverse methods for direct laser metallization (DLM) (Figure 5a(ii),d–g) [232–234] - Laser-Induced Chemical Liquid Phase Deposition (LCLD), Laser-Induced Deposition (LID) via photoreduction, 2PP-assisted laser-induced deposition, DLM with viscous precursors, as well as localized laser-induced surface activation followed by chemical deposition - are carefully surveyed in Section 5.2.

In contrast to the additive methods, ablative (or subtractive) laser texturing of solid targets affected by the presence of the precursor-containing liquid layer can also be realized. Upon such patterning, morphological perturbations caused by laser exposure of the solid target can proceed simultaneously with thermal decomposition of the precursors molecules in the vicinity of ablation area, resulting in hybrid (subtractive + additive) patterning discussed in Section 5.3. The liquid layer also helps to collect and remove the ejected debris formed upon laser-textured surface sites resulting in formation of more clean morphology. Atoms, clusters and nanoparticles ejected under laser ablation of target material can react with the surrounding liquid that is commonly used in the so-called Pulsed Laser Ablation (Modification or Fragmentation) in Liquid (PLAL) for generation of suspen-

sions of functional nanomaterials [39,40] discussed in Section 5.4. Moreover, additional effects such as formation of vapor bubbles and plasma at the material-liquid interface also come into action affecting the patterning process. The former typically results in deterioration of the laser beam profile for subsequently incident laser pulses, once the generated vapor bubbles usually exist in the system much longer as compared to micro- or millisecond timescale of the interval between the laser pulses. [246] Finally, the liquid layer itself can be used to absorb laser energy transferring the laser-generated heat to the substrate and causing its modification (Section 5.5). Similarly to the laser-texturing of the materials in the reactive gas environment, patterning below a reacting liquid layer can be formally divided into additive, subtractive, and hybrid approaches that are schematically illustrated in Figure 5a and arranged according to typical fluence/temperature maintained at the interface.

### 5.1. Laser-Assisted Hydrothermal Growth at the Solid-Liquid Interface

Laser-assisted thermally-induced growth also referred to as Laser-Induced Hydrothermal Growth (LIHG) represents a sort of

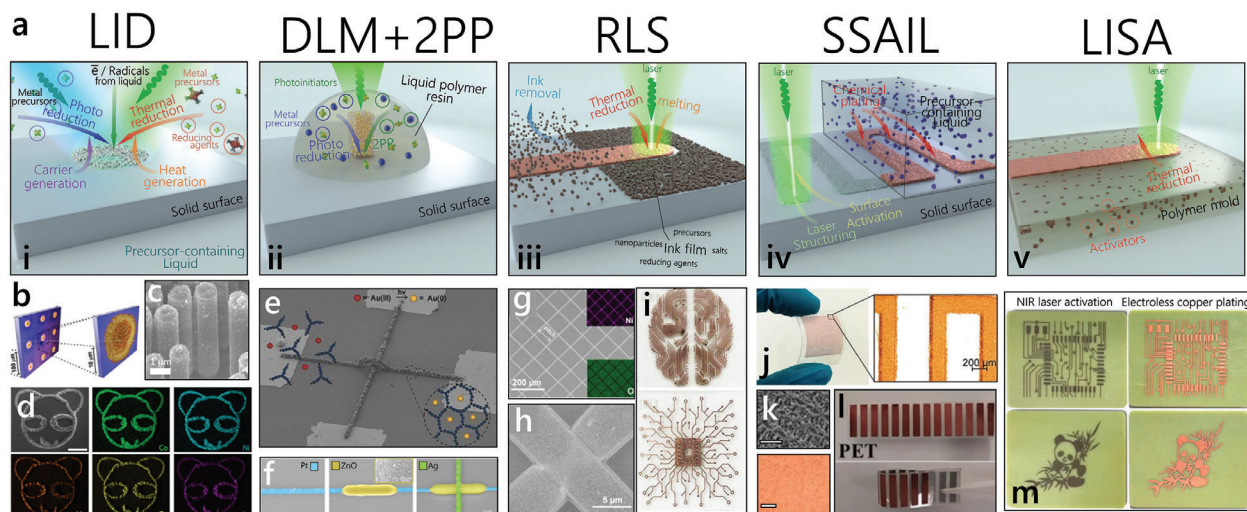


**Figure 6.** a) Schematically illustrated diversity of DLM-related methods: i) Laser-induced deposition (LID) involving either photo- or thermal-induced processes, ii) LID assisted by two-photon polymerization (2PP) for spatial localization of the LID process, iii) Laser reductive sintering of oxide NPs ink film, iv) Selective surface activation induced by a laser followed by electroless copper plating, v) Laser-induced selective structuring of polymer loaded with activator. b) Si nanowires decorated with Au-Ag-C NPs. c)  $\mu$ -chip of 20  $\mu$ m diameter spots of plasmonic nanoparticles. d) EDX maps and SEM image of complex oxides deposited by LITV (scale bar: 1 mm). e) 3D conductive Au microstructures fabricated by simultaneous photopolymerization and LID. f) SEM images of laser-printed multi-layered (Pt-ZnO-Ag) functional electronic element. g,h) SEM images of transparent mesh-type Ni electrodes. i) Copper patterns deposited from DES by picosecond laser. j) A flexible PET with a circuit pattern made by SSAIL. k) Optical micrographs and SEM images of copper deposited on PEN. l) Photographs of copper structures on PET produced by SSAIL. m) Laser activated ABS (left) and circuit patterns after electroless copper plating (right). Figures reproduced with permission from: [253] Copyright 2016, Royal Society of Chemistry (b), [254] Copyright 2023, IOP Publishing (d), [255] Copyright 2016, John Wiley & Sons (e), [256] Copyright 2023, Springer Nature (f), [257] Copyright 2014, American Chemical Society (g,h), [258] Copyright 2023, Elsevier (i), [259] Copyright 2020, Elsevier (j), [260] Copyright 2022, Springer Nature (k,l), [261] Copyright 2016, American Chemical Society (m).

bottom-up fabrication approach allowing to create microscale structures within a laser focal spot via thermally-induced self-organization processes in the liquid precursor solution. Substrate in this case acts as a light-absorbing medium hosting localized heat source within a focal laser spot, as well as providing defective surface sites for preferential growth. Laser-generated heat can activate decomposition of the precursor molecules to neutral atoms in the vicinity of the interface or initiate nucleation and subsequent growth of the self-organized nanocrystals from liquid-phase precursors. The mechanism of the growth is similar to the diffusion-limited aggregation (DLA), which is able to generate localized dendrite structures.<sup>[247]</sup> The convection stimulated by the laser-induced localized temperature gradient induces the directional up-streaming flow around the structure and turns the dendritic pattern to a bunch of flow-oriented nanowires. For example, Yeo et al. reported laser-induced hydrothermal localized growth of ZnO and TiO<sub>2</sub> nanowires by CW-laser exposure of the substrates in zinc nitrate hexahydrate/hexamethylenetetramine/polyethylenimine and hydrochloric acid/distilled water/titanium butoxide precursor solutions, respectively.<sup>[235,248]</sup> Example of the grown micro-scale structure composed of densely arranged ZnO nanocrystals is provided in Figure 5b. Once the typical activation temperatures of the growth process is rather low (typically below 200°C that does not cause intense boiling of the precursor solution), any type of the substrate can be used including flexible polymer substrates with rather low melting temperature. Considering simplicity of realization, flexibility of the process and diverse choice of alternative metal oxide materials,<sup>[249,250]</sup> the method is attractive for realization of catalytically active sur-

faces, super-capacitors, UV photodetectors and other optoelectronic micro-devices. Another example is laser-induced localized growth of the light-emitting perovskite microcrystals on the substrate from the precursor solution containing CH<sub>3</sub>NH<sub>3</sub>Br and PbBr<sub>2</sub> dissolved in dimethylformamide.<sup>[236,251]</sup> Considering outstanding optoelectronic and light-emitting properties of halide perovskite, on-demand laser-controlled growth of microcrystals holds promise for diverse applications including optical circuits, micro-optics and gas sensors.<sup>[252]</sup>

## 5.2. Direct Laser Metallization at the Solid–Liquid Interface

### 5.2.1. Photo-Induced Deposition of Metal Nanoparticles Over Solid Interfaces

Photoreduction of metal precursors can be driven at the solid–liquid interface by photons with energies adjusted to the absorption band of the related liquid. The corresponding single-step method referred to as laser-induced deposition (LID) allows to precisely cover highly irregular free-form interfaces with metal nanoparticles using rather low-intense radiation. Photo-induced reduction ensures high spatial localization of the deposition process at the interface with minimized thermal impact, while variation of both laser parameters and chemical composition of the working solution provide diverse opportunities for controlling the morphology and properties of the resulting deposits (Figure 6a(i)).

Bjernelund et al. first reported photo-reduction-assisted deposition of silver NPs over the transparent glass substrates covered by an aqueous solution of Ag salt and citrate,<sup>[262]</sup> which is known as a classical solution for the Turkevich method.<sup>[263]</sup> The authors also highlighted the role of the surface in the LID process by comparing the deposition efficiencies of aminopropyltriethoxysilane-coated and bare glasses. LID of the Au NPs over glass substrates was further demonstrated via CW-laser radiation of a water solution of HAuCl<sub>4</sub> and citrate (1:1).<sup>[264]</sup> Interesting development of the approach was presented by Setoura et al.<sup>[265]</sup> showing Ag NP deposition over the glass surface using aqueous solution of silver salt without reducing reagents and diverse CW laser wavelengths spanning from 325 to 1064 nm. It was found that formation of Ag<sub>2</sub>O sites associated with glass surface defects is responsible for the NP deposition followed by aggregation of small Ag clusters under CW laser irradiation. Authors declared only photo-reduction mechanism of the NP formation, yet related thermal effects cannot be totally excluded taking into account moderate intensities used, as well as plasmon-mediated enhancement of the absorbed light intensity near the formed Ag nano-clusters.

LID of Au, Ag, Pt, and Ru NPs was demonstrated in a series of publications<sup>[266–269]</sup> using metal precursors in water or organic solvents without any reducing or stabilizing agents and UV (266 nm) laser radiation. The related solutions were typically prepared from common commercially available precursors CH<sub>3</sub>COOAg, C<sub>7</sub>H<sub>5</sub>AgO<sub>2</sub>, (CF<sub>3</sub>SO<sub>2</sub>)<sub>2</sub>NAg, C<sub>6</sub>H<sub>5</sub>COOAg, C<sub>6</sub>H<sub>9</sub>AuO<sub>6</sub>, HAuCl<sub>4</sub>, Pt(NH<sub>3</sub>)<sub>4</sub>(OH)<sub>2</sub>, (C<sub>8</sub>H<sub>12</sub>)Cl<sub>2</sub>Pt, C<sub>8</sub>H<sub>18</sub>OPtSi, Ru<sub>3</sub>(CO)<sub>12</sub> - dissolved in water, methanol, acetonitrile, ethanol, or isopropanol. NP formation was explained through the decomposition of the metal precursor resulting in formation of the substrate-supported metal seeds and their subsequent growth. Potential contribution of the anion radicals of photo-decomposed metal precursors that can act as reducing agents were also discussed. Similar LID process was also reported for bi- or tri-metal Ag-Pt, Au-Pt, Au-Ag, Au-Ag-Pt core-shell nanoparticles using solutions containing mixture of corresponding metal precursors.<sup>[266]</sup>

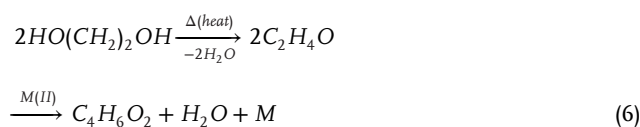
LID procedure is typically carried out with low-intense laser radiation causing weak destructive effects on the deposited NPs/substrate, as well as ensuring high spatial localization of the process that does not degrade through thermal diffusion. Figure 6b provides an example of the an array of LID-produced NP arrangements localized within 20-μm diameter surface area.<sup>[253,270]</sup> Applicability of the LID for decoration of free-form (including high-aspect ratio) interfaces is another important advantage of the method.<sup>[266,271]</sup> Examples of such interfaces (e.g., anodic aluminum oxide nanomembranes<sup>[269,272–274]</sup> or semiconductor nanowire arrays)<sup>[253]</sup> can be readily found in different applications areas spanning from optical/electrochemical sensing to optoelectronics and solar energy. Figure 6c gives an illustrative example of high-aspect-ratio Si nanowires uniformly decorated by noble-metal nanoparticles using LID method.

### 5.2.2. Laser Thermo-Induced Deposition

Advancing along the temperature continuum (Figure 5a) can lead to conditions where the incident laser radiation results in a minor substrate modification, triggering only localized forma-

tion of defects.<sup>[275]</sup> Such defects can serve as active sites for promotion of chemical reactions, as well as crystallization of new phases. Therefore, under such conditions, simultaneous activation of the substrate and its patterning takes place,<sup>[276,277]</sup> making it very useful in the field of metallization of dielectric surfaces, also known as direct laser metallization (DLM). Diverse thermal-induced DLM approaches are characterized by common precursor composition, containing a metal source (salts or complexes), reducing agents, and optional additives aimed to improve the characteristics of the fabrication process (e.g., processing speed) or properties of final materials<sup>[232,278]</sup> (Figure 6a(i)). In this case, reduction of metal complexes results from temperature increase within the laser-irradiated area at the solid-liquid interface. Noteworthy, thermo-induced processes are highly specific for each precursor system. In general, reactions can be initiated due to overcoming the activation barrier, for example, via changing oxidation/reduction potential or due to localized laser-induced formation of an active intermediate. CW or high repetition rate pulsed lasers are mostly used to provide a stable and uniform heating of the system ensuring efficient thermal reduction of the metal precursors. Thermo-induced approaches comprise a wide family of techniques spanning from common LCLD<sup>[279]</sup> to recently emerging ones, such as Laser-Induced Thermal Voxels (LITV).<sup>[280]</sup> LCLD appeared as a modification of the traditional chemical plating, where a laser heating was used to speed up and localize the process. After pioneering works by Kordas and Shafeev<sup>[276,277]</sup> establishing a concept of simultaneous surface activation and Cu structure formation, subsequent studies have explored aspects of deposition of diverse noble and transition metals, deepening an understanding regarding influence of the solution composition onto the resulting structure characteristics.<sup>[281–286]</sup>

Conventional LCLD allows to produce a wide range of advanced materials, yet the method suffers from rather low writing speed, as well as low patterning resolution above tens of microns. At the same time, tight focusing of the laser radiation can be easily achieved in a liquid environment, for example, using oil-immersion optics adopted in so-called LITV technique.<sup>[254,280,287]</sup> LITV can be considered as a miniature solvothermal reactor, where commonly used inorganic precursors undergo localized chemical transformations resulting in formation of diverse metal and metal oxide structures.<sup>[232]</sup> These structures can be produced even within a single substrate by altering the precursor solution in the process of LITV as illustrated in Figure 5d. Metal (e.g., Ag, Au, Cu, Ni, etc.) structures produced by LITV typically preserve nanocrystalline structure with an estimated crystallite sizes ranging from 15 to 200 nm. The mechanism of metal formation under laser irradiation was thoroughly investigated in case of nickel, wherein ethylene glycol served as a reducing agent. Ethylene glycol (C<sub>2</sub>H<sub>6</sub>O<sub>2</sub>) was thermally dehydrated via laser-induced photothermal heating to produce acetaldehyde (C<sub>2</sub>H<sub>4</sub>O). This acetaldehyde can subsequently reduce Ni<sup>2+</sup> to Ni, with diacetyl (C<sub>4</sub>H<sub>6</sub>O<sub>2</sub>) as the main oxidation product (see reaction Scheme (6)).



Importantly, the method allows to produce metastable mixed transition metal oxides promising for n-type and p-type gas sensors ( $\text{H}_2\text{S}$ ,  $\text{NO}_2$ ,  $\text{NH}_3$ , ethanol, and acetone)<sup>[287]</sup> and catalysts for the oxygen evolution reaction.<sup>[254,288]</sup> For example, Figure 6d presents the results of a teddy bear patterns microfabrication of high entropy oxides. An aqueous solution of nitrate salts ( $\text{M}(\text{NO}_3)_2$ , where  $\text{M} = \text{Mg}$ ,  $\text{Co}$ ,  $\text{Ni}$ ,  $\text{Cu}$ ,  $\text{Zn}$ ) with a concentration of 0.2 M for each metal was used as a precursor. The synthesis of the composite material, which contains a mixture of all five metals in oxide form, was achieved through laser thermo-induced decomposition by localized heating at the focus of a 532 nm laser.

Finally, not only metals but also 2D materials can be printed with the laser thermo-induced deposition. Pioneering work by James M. Tour and colleagues demonstrated a one-step  $\text{CO}_2$  laser scribing on commercial polymer films in air to form 3D-graphene layers.<sup>[289]</sup> Subsequently, the laser-induced graphene was extended to other synthetic materials such as polyetheretherketone, polyimide, polycarbonate, and polyethylenimine, as well as natural materials including silk, lignin, wood, xylan, paper, coconut shell, and potato skin. Graphene formation in this case is believed to involve the material carbonization, where  $\text{sp}^3$  carbons are converted to  $\text{sp}^2$  ones upon reaching characteristic temperatures around 2500 °C. At such conditions, functional groups are removed, and bonds between atoms such as CC and CH or those in aromatic compounds are broken.<sup>[289,290]</sup> Another example to mention is a femtosecond laser-induced graphene oxide reduction that represents a thermal-induced conversion of non-conductive graphene oxide to the so-called reduced graphene oxide (r-GO) suitable for high-resolution flexible electronics, transistors, etc.<sup>[291]</sup> LIPSS can also accompany the r-GO formation.<sup>[292]</sup> Recently, formation of periodic stripes and self-organised hexagonal patterns was observed simultaneously with  $\text{MoS}_2$  laser reduction from the  $(\text{NH}_4)_2\text{MoS}_4$  precursor.<sup>[293,294]</sup> Noteworthy, the described reduction processes require no reaction of the laser-heated material with the surrounding atmosphere, so the described techniques appears to be slightly outside the scope of present review. Interested readers are further referred to recent excellent reviews surveying this field.<sup>[295,296]</sup>

### 5.2.3. Laser-Induced Deposition Assisted by Two-Photon Polymerization

Another promising approach for achieving strong light localization consists in using nonlinear absorption phenomenon that can be realized with ultrashort pulses providing high peak intensities.<sup>[297,298]</sup> In sharp contrast to “classic” photo-chemistry, where laser wavelength is usually adjusted to the absorption band of precursor molecules/liquids, the wavelength  $\lambda_0$  can be chosen in such a way that the liquid medium is transparent for  $\lambda_0$  but absorbs  $\lambda_0/2$ . Thus, chemical reactions will only be triggered when two photons are absorbed simultaneously,<sup>[299]</sup> which is solely possible at high peak intensities readily achieved with tightly focused ultrashort laser pulses. If such a chemical reaction occurring in the liquid environment triggers its transition to the solid state, e.g., polymerization, the method permits to write 3D nanostructures of organic and inorganic polymers or nanocomposites.<sup>[300]</sup> The pure two photon polymerisation (2PP) processes are out of the scope of this article, once there are a lot of timely reports

on this topic.<sup>[298,301,302]</sup> At the same time, a sort of DLM method can be realized combining 2PP with a specially designed photoresists containing metal precursors as schematically illustrated in Figure 6(ii).

Wegener’s group demonstrated an approach with a novel water-based photoresist for preparation of 3D conductive microstructures by simultaneous photopolymerization and photoreduction of a metallic salt via a two-photon process.<sup>[255]</sup> Acrylate-functionalized poly(ethylene glycol) derivative (PEG-triacryl) was used as a water-based photoresist containing  $\text{HAuCl}_4$  as a gold precursor and *Irgacure 2959* as a photoinitiator. One of the main challenges was the local heating of the irradiation region during writing due to the light absorption of the gold species, which was solved by decreasing the repetition rate and reducing the heat accumulation between consecutive pulses. Using the proposed approach, 3D Au nano-architectures with a feature size below 3  $\mu\text{m}$  and electric conductivity comparable to those for gold films were demonstrated (see Figure 6e). The synthesis of 3D silver nanostructures with minimum line width below the optical diffraction limit has also been demonstrated.<sup>[303]</sup> The introduction of surfactants such as amino acids, carboxylate, and n-decanoylsarcosine sodium to the silver ion solution facilitated uniform growth of surfactant-capped primary-precipitated nanoparticles and led to the formation of finer silver patterns.<sup>[304,305]</sup> In the paper,<sup>[256]</sup> the authors developed the complex technique that combines the multi-photon absorption of near-infrared femtosecond laser pulses for synthesizing metal structures with LIHG for the fabrication of ZnO structures. The proposed approach allows printing a multi-layer Pt-ZnO-Ag composite with precise layer positioning for creating security circuits. SEM images of the consecutively deposited layers are presented in Figure 6f. For efficient reduction of Pt ions, an iron oxalate photosensitizer was added to the precursor ink. Meanwhile, for Ag, the process involved direct multiphoton absorption of the  $\text{Ag}(\text{I})$  complex, followed by the reduction of the excited state in the presence of a citrate reducing agent ( $\text{Na}_3\text{C}_6\text{H}_5\text{O}_7$ ). In the meantime, a fundamentally different method was proposed for fabricating ZnO structures. Under laser-induced local temperature field, the “ink” composed of  $\text{Zn}(\text{NO}_3)_2$  dissolved in ammonia solution forms an insoluble  $\text{Zn}(\text{OH})_2$  precipitate, which is subsequently transformed into ZnO. Thus, the photothermally induced reaction locally converts the ink into polycrystalline ZnO deposited on a platinum wire to form a direct electrical contact.

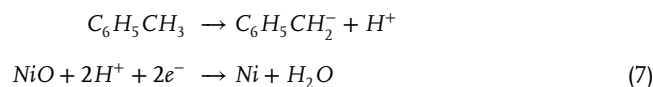
### 5.2.4. Direct Laser Metallization with Viscous Precursors

An alternative strategy to enhance printing speeds and increase the industrial potential of the DLM technology involves the utilization of more viscous systems with high concentrations of metal precursors compared to conventional solvents (water, acetonitrile, dimethylformamide, etc.) (Figure 6a(iii)). In the scientific literature, such compositions are commonly referred to as inks. Apart from laser irradiation conditions and chemical properties of the chosen system, the precursor coating method and roughness of the substrate have crucial influence on the fabrication process. Due to the lower melting temperatures of polymers as compared to bulk inorganic materials, the optimal parameters for the chemical reaction and decomposition of the

precursor need to be adjusted carefully to avoid excessive damaging the substrate. For example, several studies used Copper Nitrate ( $\text{Cu}(\text{NO}_3)_2$ ) with  $0.2 \text{ g ml}^{-1}$  aqueous polyethylene glycol (PEG) and  $0.1 \text{ g ml}^{-1}$  aqueous polyvinyl pyrrolidone (PVP) to create micropatterns on polycarbonate surface.<sup>[306–309]</sup> Mixed metal salts ( $\text{Cu}(\text{NO}_3)_2 \cdot 3\text{H}_2\text{O}$  and  $\text{AgNO}_3$ ) and low-cost liquid ionic precursor were recently applied to fabricate a flexible Cu-Ag structures.<sup>[310]</sup> Deep eutectic solvents (DES) represents a special class of viscous precursors previously used as effective extractants in analytical chemistry<sup>[311]</sup> and media for electrochemical metallization and sensing.<sup>[312]</sup> Shishov et al. first demonstrated that utilization of DES-based coating instead of common liquid precursors increases the efficiency of metallic pattern formation, at least, two orders of magnitude.<sup>[313]</sup> Figure 6(i) presents Cu micropatterns fabricated on glass by a one-step, picosecond laser-assisted approach. The precursor was a DES composed of choline chloride, copper(II) acetate, and citric acid.<sup>[258]</sup> The main benefits of using a DES for DLM includes its low cost, straightforward synthesis, eco-friendliness, and the ability to dissolve a broad range of metal salts in high concentrations. Further studies confirmed advances of using DES for DLM-related applications.<sup>[258,314–317]</sup>

Reductive Laser Sintering (RLS) represents another DLM technique (Figure 6a(iii)) in which viscous suspensions of metal oxide NPs with high linear and nonlinear absorption are typically used as precursors. For linear absorption regime, visible to near-IR laser wavelengths are mainly used. For instance, NPs made of copper (II) oxide with its bandgap of 1.2 eV were thermochemically reduced and sintered into conductive patterns using near-IR (1070 and 808 nm) and visible (532 nm) CW lasers, ethylene glycol as a reducing agent, and light-absorbing PVP as a dispersant.<sup>[233,318,319]</sup> Pulse duration was found to affect the reduction/sintering process allowing to tailor the resulting composition of the produced structures. In particular, fs-laser pulses were found to cause complete reduction of copper (II) oxide NPs to metallic copper, while sub-picosecond one yield in either Cu-rich or  $\text{Cu}_2\text{O}$ -rich composites depending of the processing parameters.<sup>[320–322]</sup> Insufficient photon energy and reoxidation contribute to  $\text{Cu}_2\text{O}$ -rich composite formation, with resulting patterns showing negative semiconductor-like temperature coefficients of resistance in contrast with Cu-rich patterns displaying a slight positive metal-like behavior.<sup>[320]</sup> An effective strategy to improve the conductivity of RLS-prepared Cu patterns involves the careful design of the ink compositions, which includes the usage of copper (II) oxide NPs of various sizes. The incorporation of smaller CuO NPs (<100 nm) into the inks containing larger ( $\approx 3.68 \mu\text{m}$ ) NPs has been demonstrated to significantly enhance the conductivity of the fabricated patterns.<sup>[323]</sup> The potential application of metal oxide NPs for laser reductive sintering can be guided by the Ellingham diagram, which illustrates the relationship between the Gibbs free energy of oxidation and temperature. Apart from copper, RLS has extensively been investigated for the fabrication of nickel,<sup>[257]</sup> cobalt,<sup>[324]</sup> and metal alloys such as copper-nickel.<sup>[325]</sup> For example, D. Paeng and D. Lee et al.<sup>[257,326]</sup> demonstrated fabrication of high-resolution Ni patterns from NiO NPs thin film without the need for vacuum, lithography, or solution processing (Figure 6g,h). The ink was made from synthesised NiO NPs dispersed in toluene ( $\text{C}_7\text{H}_8$ ). The solvent played a crucial role in the reduction of the NiO NPs,

as the toluene molecules adsorbed on the surfaces of the NiO NPs provided protons essential for the reduction of  $\text{Ni}^{2+}$  by a CW laser with a wavelength of 514.5 nm, as described in the following reactions (7):



Laser reductive sintering via single-photon absorption has been applied for fabrication of conductive patterns,<sup>[233]</sup> transparent electrodes<sup>[257]</sup> (Figure 6g,h), temperature sensors,<sup>[234,321]</sup> planar Bragg gratings,<sup>[327]</sup> micro-opto-electrical systems,<sup>[328]</sup> flow sensors,<sup>[329]</sup> thermo-electric couples,<sup>[330]</sup> nickel-based microgears,<sup>[331]</sup> and copper and nickel porous electrodes for non-enzymatic D-glucose detection.<sup>[332]</sup>

RLS involving multi-photon absorption processes and laser-transparent inks typically allows to produce conductive patterns with lower feature size.<sup>[333]</sup> For example, NPs made of copper (I) oxide NPs with its bandgap of 2.1 eV, are commonly used as a raw material for such fabrication, while related inks containing 2-propanol and PVP exhibited high transparency at common near-IR/visible wavelengths.<sup>[334,335]</sup> Upon absorption of laser pulses, 2-propanol and PVP generate formic acid, that reduces the copper (I) oxide nanoparticles to metallic copper, in its turn. The nonlinear absorption properties of the copper (I) oxide NPs were characterized using an open-aperture z-scan technique.<sup>[335,336]</sup> Two-photon processes have been demonstrated to be effective for the reduction of glyoxylic acid complexes of copper and nickel.<sup>[337,338]</sup> The glyoxylic ligands effectively prevent the reoxidation of the precipitated metal nanoparticles, resulting in metal patterns (Cu, Ni, Cu-Ni alloys) with high conductivity.

### 5.2.5. Laser Direct Structuring Followed by Chemical Metallization

Several two-step fabrication methods, such as Selective Surface Activation Induced by a Laser (SSAIL) and Laser Induced Selective Activation (LISA), should be also mentioned within DLM family (Figure 6(iv–v)). Both methods entail the activation step of the solid surface under its laser exposure followed by either chemical or electrochemical metallization.<sup>[339]</sup> SSAIL activation largely depends on the substrate material and is typically carried out in air resulting in laser-induced formation of active sites that facilitate electron transfer in the redox reactions. In the case of polymer substrates, laser exposure causes decrease of the oxygen content in the surface layer, which can be associated with the breaking of carbonyl and ether bonds, as well as the formation of aldehyde groups.<sup>[340]</sup> These aldehyde groups can reduce silver ions from the sensitization solution, followed by final localized electroless plating of the activated area. The flexibility in pattern fabrication suggests that the SSAIL technique holds significant potential for a wide range of industrial applications, as highlighted by several research groups.<sup>[341,342]</sup> For instance, flexible patterns were fabricated on the commonly used polyethylene terephthalate (PET) polymer substrate, serving as support layer<sup>[259]</sup> (Figure 6j) and as electrochemical sensors for glucose detection. Figure 6k,l shows optical and electron microscopy images of Cu micropatterns used as electrodes for non-enzymatic

sensors.<sup>[260]</sup> Additionally, it has been found that for the metallization of polyurethane, the activation step can be improved by irradiating copper(II) L-tyrosine with an excimer ArF laser to form a tunable layer of copper seeds used for further metallization.<sup>[343]</sup>

LISA typically uses a specially designed polymer composite doped with a sensitizer, which can be activated upon laser irradiation<sup>[344]</sup> (Figure 6a(v)). The sensitizer absorbs the laser irradiation, resulting in the polymer ablation, carbonization, and outgassing that creates a surface microroughness, metal particles and amorphous carbon.<sup>[345]</sup> After the activation step, conventional electroless plating can be implemented. In a series of studies by Zhou et al., different designs of this process have been developed for the metallization of a variety of polymer surfaces. For example, copper-free antimony-doped tin oxide was proven to be an effective additive in a polymer mold for fabricating high-resolution copper patterns on the polystyrene (PS) surface under pulsed near-IR laser activation.<sup>[346]</sup> In turn, copper oxalate  $\text{Cu}_2\text{O}_4$  and copper acetylacetonate  $\text{Cu}(\text{O}_2\text{C}_5\text{H}_7)_2$  can be used for high-performance copper plating of acrylonitrile-butadiene-styrene as illustrated in Figure 6m.<sup>[261,347]</sup> For polydimethylsiloxane metallization, the effective sensitizer is  $[\text{Cu}_2(\text{OH})\text{PO}_4]$  and ATO.<sup>[348]</sup> Recently, a new type of  $\text{MoO}_3$ -based sensitizer, suitable for both 355 nm UV and 1064 nm near-infrared lasers, has been reported to form Cu layers, followed by Ni-Cu, Ag-Cu, and Au-Ni-Cu layers based on it.<sup>[349]</sup>

### 5.3. Hybrid Processing in Reacting Liquid: Simultaneous Laser Texturing and Functionalization

At a certain absorbed fluence, laser radiation can cause direct material patterning at the interface with surrounding liquid. Such patterning can be driven by redistribution in a molten phase, ablation, ejection facilitated by thermomechanical processes or direct solid-to-vapor transitions in a similar way as it was described in Section 2. The main effect of the liquid is in fact that melting temperatures of the solid material is typically much larger as compared to evaporation temperature of the surrounding liquid. Strong heating of the liquid at the interface causes vapor formation and generation of bubbles that can remain in the systems for milliseconds (Figure 2c). Excessive bubbling usually causes unpredictable deterioration of the intensity profile of the subsequently incident laser pulses for laser setups with vertically arranged optical path limiting both maximal pulse repetition rate and applied fluence.<sup>[44,246]</sup> At the same time, several studies utilized the bubble-assisted modulation of the laser beam profile to modify the surface nanopatterning process.<sup>[350–353]</sup> Presence of the liquid with a certain refractive index ( $n_L > 1$ ) also modifies the effects associated with propagation of laser-excited surface plasma waves that play a key role when fs laser pulses are used. Typically, processing in liquid reduces the surface plasmon wavelength by a factor of  $n_L$  resulting in imprinting of LIPSS with a shorter grating periodicity (as compared to the case of similar laser patterning in air).<sup>[354,355]</sup> For strongly oxidizing materials (such as transition metals and semiconductors), oxygen-free liquids can be used to efficiently suppress the laser-induced oxidation in the process of nanopatterning. At the same time, precursor molecules contained in a liquid can be decomposed via thermal or photo-reduction near the laser-textured interface. Gener-

ated atoms can react with an irradiated molten material allowing its doping or decoration (encapsulation) and eventually resulting in formation of composite (core-shell or alloyed) nanotextured surfaces (Figure 5(iii)).

This topic was widely explored in the context of creating metal-semiconductor nanotextured interfaces promising for diverse applications spanning from optoelectronics and nanophotonics to heterogeneous catalysis and biosensing. For example, monocrystalline Si wafers were laser-textured in liquids containing different salt/acid metal precursors (such as  $\text{HAuCl}_4$ ,  $\text{AgNO}_3$ ,  $\text{H}_2\text{PdCl}_4$ ,  $\text{K}_2[\text{PtCl}_6]$ , or  $\text{Cu}(\text{NO}_3)_2$ ) to produce within a single and direct fabrication route a nanotextured semiconductor surface decorated with metal nanoparticles.<sup>[237,238,356–359]</sup> Similarly to gas-phase hyperdoping of Si, its laser texturing in liquid  $\text{CS}_2$  was also carried out to produce nanotextured interface with high concentration of sulfur atoms.<sup>[239,360]</sup> Processing of Si was also carried out using liquid  $\text{CCl}_4$  contain traces of chlorine, whereas processing in liquid  $\text{C}_2\text{Cl}_3\text{F}_3$  strongly enriches the surface with fluorine due to a higher chemical activity of the latter.<sup>[361]</sup> Apart from high IR absorption of nanotextured hyperdoped silicon, Kudryashov et al. also reported strong anti-bactericidal performance of the patterned composite interfaces preventing appearance of a *Staphylococcus aureus* bacterial biofilm.<sup>[239]</sup> Material texturing in common organic solvents (such as acetone, isopropanol, hexane, etc.) allows surface encapsulation with carbon atoms (carbonization) via thermal decomposition of the solvent molecules, as well as promotes carbide formation. Zhang et al. reported comprehensive study of fs-laser texturing of different transition metal species in acetone, showing the ability to produce highly nanotextured surfaces capped with amorphous carbon and carbides rendering the surface with strong and spectrally broadband optical absorption.<sup>[362]</sup> Direct laser patterning of titanium was carried out in liquid hydrocarbon to produced nanotextured TiC,<sup>[363]</sup> iron carbides were observed on the surface of iron ablated in acetone and toluene<sup>[364]</sup> and titanium nitride by ablation of NiTi in liquid nitrogen.<sup>[365]</sup> Nitrides and carbides can be characterized by extremely high melting temperatures (above 2000 °C), making the technology promising for production of devices for diverse high-temperature applications.

### 5.4. Pulsed Laser Ablation in Liquid (PLAL): Controlling Nanoparticle Properties via Surrounding Liquid

Historically, PLAL was apparently the first method to be formally considered as a new direction for the production of various nanomaterials since the 1990s.<sup>[39,40,366,367]</sup> Then, during several decades of its application, this approach has gradually led to the emergence and development of several offshoots, such as laser irradiation in liquid, laser melting in liquid or laser fragmentation in liquid.<sup>[42,47,367–371]</sup> Classically, in PLAL, as shown in Figure 5(iv), a solid target was placed in a liquid, with laser beam focused at the liquid-target interface, generating NPs.<sup>[42,44,47,366,368,370,371]</sup> These nanoparticles are usually well dispersed in the liquid, although the vapor bubbles formed upon the laser ablation<sup>[372]</sup> and the electrostatic forces<sup>[373]</sup> can facilitate the particle redeposition onto the surface. As a result, the morphology and chemical composition of produced nanostructures were found to depend primarily on the target (metal, pressed ceramic,

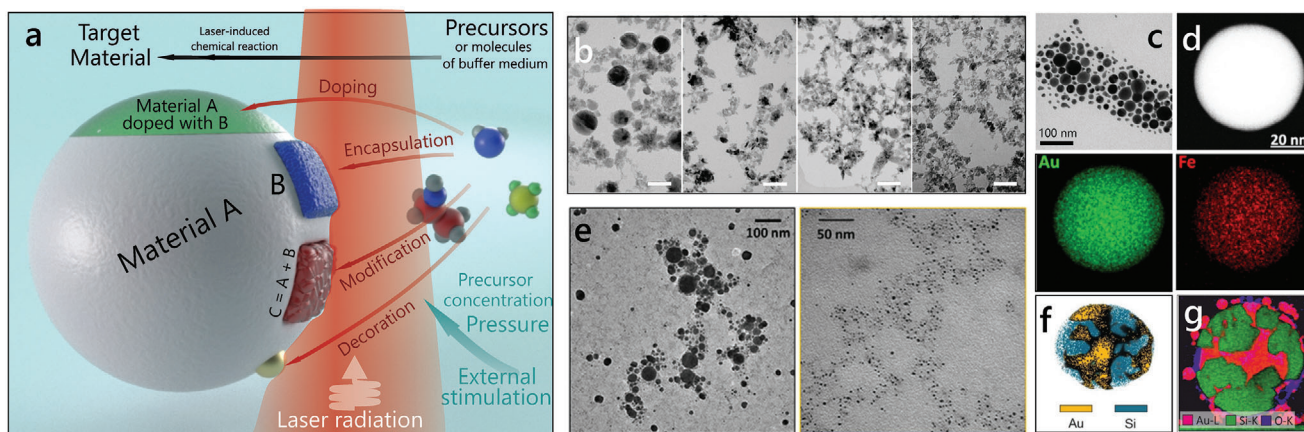


**Figure 7.** Controlling nanoparticle morphology in PLAL. a) Schematic illustration of pathways for NP structure/composition via laser-driven reactions with precursor molecules or those of buffer liquid. b) Reduction of the average size of ZnO NPs prepared via ablation of Zn in water at 1 atmosphere, 15, 22, and 31 MPa (from left to right). Scale bar of TEM images indicates 100 nm. c) Representative TEM image of Au-Fe NPs, and d) elemental analysis showing homogeneous distribution of Au and Fe atoms in an isolated Au-Fe NP. f, g) Elemental analysis of hybrid Au-Si NPs showing their composite structure with Si nanocrystals wrapped by Au. e) TEM images illustrating reduction in size of hybrid AuFe NPs after 4 h incubation at 37 °C with EDTA in 20% v/v FCS/water. Reproduced with permission from<sup>[391]</sup> Copyright 2013, AIP Publishing (b),<sup>[393]</sup> Copyright 2019, American Chemical Society (c, d),<sup>[394]</sup> Copyright 2020, American Chemical Society (e),<sup>[395]</sup> Copyright 2018, American Chemical Society (f),<sup>[396]</sup> Copyright 2023, American Chemical Society (g).

silicon wafer, etc.) and laser parameters applied (wavelength, frequency, pulse duration, fluence, etc.).<sup>[42,367,368,370,371,374,375]</sup> PLAL method can be easily adopted to produce practically any kind of product including pure metallic,<sup>[376–378]</sup> semiconductor<sup>[379–381]</sup> and dielectric nanoparticles,<sup>[382,383]</sup> as well as advanced composite nanomaterials with complex multi-element structure.<sup>[384–389]</sup>

At the same time, since nanostructure formation during PLAL processes often involves chemical reactions, it is obvious that liquid itself, its temperature, pressure, and chemical composition (reactivity and/or dissolved additives or components), should also play some role and hence influence the morphology and composition of the product.<sup>[241,242,367–369,390–392]</sup> Potentially, processes involving laser-induced chemical reactions can be classified as doping, decoration, or encapsulation of the initial NP material (A) by material (B) formed upon thermal decomposition of precursor molecules or those of buffer liquid, as well as compositional/structural modification that results in formation of material (C) through a reaction of (A) with (B), as schematically illustrated in **Figure 7a**.

Because chemical reactions often take place during PLAL processing, the temperature of liquid medium predictably plays some role. However, because the local temperatures generated inside the ablated zone are very high and can reach thousands of degrees K,<sup>[397]</sup> in most experiments, PLAL is nominally carried out at room temperature (without temperature control of the liquid). Nevertheless, the effect of medium temperature was observed in case of nanostructures that could recrystallize at elevated temperatures, such as, for example, ZnO NPs, as was reported in works.<sup>[398,399]</sup> At the same time, water cooled with ice was used to produce smaller NPs, which was explained by higher cooling rates and faster quenching.<sup>[400,401]</sup> Temperature-dependent water compressibility influences the dynamics of the laser-induced cavitation bubble. This could explain the non-monotonic variation (of approx. 20%) in the diameter of gold colloids observed by Menendez-Manjon and coauthors when water temperature was changed in the range of 283–353 K at one atmosphere.<sup>[402]</sup>

#### 5.4.1. PLAL in Non-Reactive and Reactive Liquids

Along with the target material, the solvent medium is another important factor in PLAL that can control not only the shape and size of NPs but also their structure and composition.<sup>[401]</sup> When the ablated target is a noble metal (e.g., gold), normally metallic NPs are obtained irrespective of the liquid used. However, if the target is a more reactive metal, products with different degree of oxidation should be expected in liquid media with different oxidizing potential.<sup>[241,242,369]</sup> In a wider sense, using liquids with more oxidizing/reducing properties is a convenient way to produce nanostructures with a wider spectrum of properties.<sup>[401]</sup> Probably, the most illustrative example of how using liquid media with different reactivity can affect the product was demonstrated by Niu and coworkers who used millisecond-long pulses.<sup>[241,242]</sup> Because metal species were ablated in the form of nanodroplets, such droplets were then, depending on the reactivity of medium, either quenched as metallic NPs, or oxidized partially or completely. As a result, the products ablated in oxygen-containing (or sulfur-containing) liquids with different reactivity were metal NPs, core@shell metal@metal oxide (sulfide) NPs, or purely oxidized metal oxide (sulfide) nanocubes<sup>[241,242]</sup> (see **Figure 5k–m**). In most laboratories, however, nanosecond or pico-/femtosecond pulsed lasers are used which evaporate ablated material to its plasma state. No nanodroplet formation is expected in such experiments, which is why less contrasting morphologies are typically observed as products produced by shorter pulses in different media.<sup>[369,401]</sup> Apart from tuning the composition of the generated NPs, the liquid was also found to affect the size distribution of the product.<sup>[403,404]</sup> For example, Amans et al. reported that the size of PLAL-synthesized Gd<sub>2</sub>O<sub>3</sub> NPs can be reduced and narrowed by adding reacting organic molecules to the deionized water.<sup>[385]</sup> More details on the nanomaterials produced by different lasers ablating various targets in a wide range of organic and inorganic media, including the effect of pH, can be found in the concise review recently published by Zhang et al.<sup>[401]</sup>

#### 5.4.2. PLAL in Pressurized Liquid

Typically, PLAL is run as a simple and convenient preparation technique with very easy-to-use and inexpensive setups, with lasers being the most complex part of the setup. That is why, in most cases, nominally room temperature is used, and targets are ablated in liquids at atmospheric pressure. However, along with the influence of temperature and reactivity of liquid, the pressure of liquid medium can also affect the product. Because of technical complexity of setups designed for high-pressure PLAL experiments, the number of studies in this direction is rather limited, with only several groups reporting on experiments carried out in either pressurized CO<sub>2</sub>,<sup>[405,406]</sup> or water,<sup>[390,391,407]</sup> or water-ethanol mixtures.<sup>[408]</sup> The choice of CO<sub>2</sub> is explained by its mild critical point parameters, which is why it can be pressurized and used as a fluid at rather low pressures and temperatures. For this reason, in their recent work, using the same setup, Singh *et al.* reported ablation of Ti plate in CO<sub>2</sub> in the form of gas, liquid and supercritical fluid.<sup>[406]</sup> Sasaki and coworkers were first to report on the effect of pressure on the size of the cavitation bubble when ablating Ti plate in deionized water by means of a nanosecond pulsed laser.<sup>[390,409]</sup> The dynamics (maximum size and lifetime duration) were shown to be pressure-dependent, so that the cavitation bubble grew smaller and collapsed faster at higher medium pressures.<sup>[390]</sup> This was later related to the sizes of ZnO NPs produced by PLAL in pressurized deionized water.<sup>[391]</sup> It was experimentally shown that smaller ZnO NPs with narrower size distribution were produced at higher pressures (see Figure 7b), which was explained by the shorter lifetimes of the cavitation bubble (and thus faster quenching rates) at higher medium pressures.<sup>[391]</sup> In addition, the NPs generated at elevated pressures demonstrated stronger green emission, with their UV emission blue-shifted.<sup>[391]</sup> Later on, Goto and coauthors ablated Zn in pressurized water-ethanol mixtures, showing that the produced ZnO NPs had different defects and therefore differed in their light emission.<sup>[408]</sup>

Partially because of technical and engineering limitations related to the cost and complexity of equipment needed for ablation at high pressures, related research has not been very active in this direction. However, the reported results suggest that the use of pressurized liquids during ablation is another way to control the sizes and defects in produced nanomaterials. Further research, however, is needed to expand the number of materials involved as so far, the related research was mainly limited to Ti and Zn ablation (and thus TiO<sub>2</sub> and ZnO NPs as product). It can be postulated that the above conclusions drawn for PLAL in pressurized liquids (or supercritical fluids) could probably be extended onto ablation in pressurized gas/air where somewhat similar effects could be expected.

#### 5.4.3. Doping and Functionalization of Produced Nanostructures

Because PLAL is carried out in a liquid medium, it can be predicted that this method should be attractive for preparing doped NPs, with the dopant element being added as part of the liquid. To prepare  $\alpha$ -Ni(OH)<sub>2</sub> nanosheets doped with Mn, Zhang *et al.* ablated metallic Mn in aqueous NiCl<sub>2</sub>,<sup>[368]</sup> while Cu-doped ZnS NPs were reported after ablation of Zn plate in mercaptoethanol

in the presence of copper nitrate.<sup>[410]</sup> The method, however, is not very straightforward. As an example, when ablating Ti in aqueous Ce(NO<sub>3</sub>)<sub>3</sub>, a CeO<sub>2</sub>-TiO<sub>2</sub> hybrid was produced rather than Ce-doped TiO<sub>2</sub> NPs.<sup>[411]</sup> Thus, despite the apparent simplicity and ease of this approach, the number of publications in this direction is not very large. This can probably be explained by the necessity of individually studying each dopant-NPs system, also taking into account that many salts containing dopant ions are able to change the pH of the medium after dissolution. In addition, the effect of salt presence in the liquid medium on the size of obtained NPs,<sup>[412]</sup> as well as the additional stage of purification of the obtained product, should be taken into account.

#### 5.4.4. Hybrid Nanomaterials Produced by PLAL

Hybrid nanomaterials are defined as unique chemical conjugates of two or more phases which could be both inorganic and/or organic materials. Such mixtures of two or more phases are different from a simple mixture of its components but a synergistic material with properties and performance, thus resulting in applications with unique properties, which are determined by the interface of the components at the atomic/molecular level. Such hybrid nanomaterials are highly anticipated for advanced catalytic and photocatalytic, electrochemical and biochemical, optoelectronic, and photonic, magnetic and thermal, and sensing applications, to name just several. Because of extreme conditions, both during ablation and quenching stages, laser treatment can provide very close and tight conjugating between immiscible phases, thus providing conditions for preparation of a wide variety of hybrid nanomaterials based on organic-inorganic, and especially inorganic-inorganic materials. The most common laser related strategies to produce diverse nanohybrids A-B are as follows: i) ablating or irradiating a solid target A in a liquid with a dissolved precursor B (or nanoparticles made of B);<sup>[396,413-417]</sup> ii) ablating subsequently two different targets, A and B<sup>[418,419]</sup> or one composite target containing both materials,<sup>[420]</sup> iii) mixing ablated nanomaterials A and B followed by their further annealing as dry powders or laser-processing in liquid state,<sup>[421-426]</sup> iv) laser irradiation of mixed dispersion of both components A and B (where one of them can be obtained by synthesis method other than PLAL).<sup>[415,427]</sup>

The above mentioned PLAL routes open up pathways for bridging contrasting materials within unified nano-hybrids some of which are hard to prepare through other approaches. For instance, substantial efforts were made to combine optically resonant noble metal materials (such as Au and Ag) with common magnetic materials (such as Co or Fe; Figure 7c,d).<sup>[420,428-430]</sup> The resulting nano-hybrids were demonstrated to be promising for diverse applications, e.g., in nano-medicine, where photo-thermal treatment of cancer cells can be combined with photoacoustic or magnetic resonance imaging techniques.<sup>[394,431,432]</sup> Torressan *et al.* reported Au-Fe nano-hybrids acting as contrasting agents for magnetic resonance imaging and demonstrating remarkable self-degradation properties, which facilitates their removal from the body<sup>[394]</sup> (Figure 7e).

Guiding and agglomeration of PLAL-generated hybrid NPs by means of magnetic field was also found promising for realization of advanced Surface-Enhanced Raman Scattering

(SERS)-based plasmonic biosensors for molecular fingerprinting.<sup>[433]</sup> Common semiconductors (such as Si, Ge, or TiO<sub>2</sub>) and noble metals present another intriguing combination showing promise for sensing, nanophotonics and nano-medicine. Formation of Au-Si nano-hybrids through PLAL was extensively studied by several groups. This resulted in a diversity of produced nanomaterials with different composition and structure (such as nano-alloys, hybrids, core-satellites, etc.) controlled through processing parameters.<sup>[396,413,416,434–438]</sup> Insolubility of silicon in gold was found to give rise to NPs with a unique structure where isolated Si nanocrystals were wrapped by a Au matrix, as shown in Figure 7f,g. Such Au-Si hybrids demonstrated strong light-to-heat conversion,<sup>[416]</sup> nonlinear light emission<sup>[395,439]</sup> and advanced SERS sensing performance mediated by a strong plasmonic response combined with temperature-feedback modality of Raman-active Si nanocrystals embedded in Au matrix.<sup>[396]</sup>

### 5.5. Laser-Induced wet Etching

Laser-induced back-side wet etching (LIBWE) is a promising method for micro-patterning of common transparent materials (such as glasses, quartz, and sapphire).<sup>[440]</sup> In a sharp contrast to laser-induced growth, where the heat from laser-irradiated material is used to stimulate chemical reactions, a heat-generating opaque liquid is used in LIBWE to ablate or pattern the material at the liquid–solid interface (see Figure 5(v)). This method is similar to the DLM and LIHG methods discussed above, but changing the absorption of the liquid and increasing the fluence in LIBWE can permit to switch between the additive and subtractive effects. Several mechanisms of surface patterning can be identified: a) laser-induced chemical degradation of the absorbing liquid with consequent generation of active molecules that etch the surface;<sup>[441–443]</sup> b) direct heat transfer from an overheated liquid to a transparent surface;<sup>[444,445]</sup> c) the shock wave from the cavitation bubbles in a boiling absorbing liquid is transferred to break a solid transparent surface;<sup>[446,447]</sup> d) a combination of the above mechanisms. In other words, the LIBWE process can be considered as ablation of an opaque liquid, which then patterns a transparent solid sample. The transition between the photochemical to photothermal mechanism of etching can be demonstrated by changing the concentration of dissolved active molecules.<sup>[441]</sup> For low concentrations, the ablation threshold does not correlate with the chemical activity of the solute molecules whereas at higher concentrations such a correlation was observed. Moreover, in the latter case, etching was detected at a lower threshold even if the interface temperature of the liquid was much lower than the boiling point.

The common liquids utilized for such process include solution of pyrene in different organic solvents,<sup>[444,448]</sup> toluene,<sup>[446,449]</sup> chlorobenzene<sup>[245]</sup> or strong oxidants like KMnO<sub>4</sub>, CrO<sub>3</sub>, FeCl<sub>3</sub>, NiSO<sub>4</sub>, and CuSO<sub>4</sub>.<sup>[41,447,450,451]</sup> Usually ns UV lasers are used,<sup>[444,448]</sup> whose radiation is well absorbed by pyrene and benzene.<sup>[441]</sup> Shorter wavelengths of the UV laser radiation were shown to provide higher etching rates at comparable fluences.<sup>[452]</sup> Nanosecond green lasers are used with red, orange and violet colored solutions like CrO<sub>3</sub>, FeCl<sub>3</sub> and KMnO<sub>4</sub>.<sup>[450,451]</sup> Lasers with wavelength corresponding to the absorption bands

of water can be effectively used in a combination with aqueous solution of sodium and potassium salts. In this case, water serves as the absorbing layer providing high temperatures and pressure and facilitating sapphire etching by alkali ions.<sup>[453]</sup>

Application of picosecond and femtosecond laser pulses is seldom<sup>[245,443,449,454]</sup> since short pulse duration provides no advantages but increases the risk of unwelcome non-linear optical effects like e.g., light filamentation, frequency conversion,<sup>[455]</sup> multiphoton absorption, and defect generation in the transparent media and LIPSS formation.<sup>[454]</sup> The lateral resolution of the LIBWE is defined by the width and shape of laser intensity distribution at the processed interface. The average etching rate per pulse depends on laser fluence and applied materials, being usually in the sub-micrometer range. The minimal values range from several nanometers per pulse (as it is e.g., for etching with pyrene and nanosecond UV laser pulses)<sup>[448,456]</sup> to hundreds of picometers per pulse (as it was reported for etching with toluene and picosecond UV laser pulses).<sup>[449]</sup> Application of liquid metals as absorbing liquids was shown to enable elevated etching rates up to one micrometer per pulse.<sup>[457]</sup>

The chemistry of the LIBWE can be illustrated on the example of SiO<sub>2</sub> etched in aqueous solution of KMnO<sub>4</sub> exposed to  $\lambda = 515$  nm laser pulses.<sup>[443]</sup> In the first step, potassium oxide is synthesized through the reaction:  $4\text{KMnO}_4 + h\nu = 2\text{K}_2\text{O} + 4\text{MnO}_2 + 3\text{O}_2 \uparrow$ . In the second step, it reacts with water forming potassium hydroxide:  $\text{K}_2\text{O} + \text{H}_2\text{O} = 2\text{KOH}$ . The latter hydroxide then etches fused silica forming potassium silicate:  $\text{SiO}_2 + 2\text{KOH} = \text{K}_2\text{SiO}_3 + \text{H}_2\text{O}$ . However, the MnO<sub>2</sub> produced in the first reaction covers the silica surface playing a dual role in the LIBWE process. On one hand, it forms a passivating layer that reduces etching rate. On the other hand, it serves as an absorption layer that facilitates ablation at the surface. Hence, the LIBWE process can also be used for epitaxial growth of thin oxide films from inorganic etching solutions.<sup>[451]</sup> The role of the absorbing layer during LIBWE in organic solutions is played by carbon deposited on the surface, whose traces were revealed with Raman spectroscopy.<sup>[458,459]</sup> Formation of such absorbing layers (along with commonly used models of defect generation in transparent media)<sup>[460]</sup> can provide an LIBWE-specific explanation of the incubation effect.<sup>[452,459]</sup> Moreover, such deposited oxide or carbon layers, if remained on the surface upon laser processing, turn the LIBWE to a surface-coating method.<sup>[451]</sup>

Laser-assisted wet etching of semiconductors with visible and UV lasers differs from LIBWE in the following aspects: 1) semiconductors are usually not transparent to these laser wavelengths; 2) electron-hole pairs generated by laser light at the surface (see Section 2.1) provide a photocatalytic effect, which influences the etching process.<sup>[30,213,214]</sup> The opacity of the semiconductor material makes the backside etching impossible and hence the configuration is inverted: the laser radiation propagates through a transparent etching agent and makes the groove on the laser-facing side (i.e., frontside) of the wafer. If NIR lasers are used in a combination with materials transparent to the laser wavelength, the backside etching<sup>[461,462]</sup> or absorbing layers<sup>[463]</sup> can be used. The concentration of active molecules in the solution<sup>[30]</sup> and the temperature of etching liquid<sup>[464]</sup> are usually chosen in the range so that they are not enough to start a chemical etching spontaneously, but the etching process can be activated by the laser radiation locally. In comparison with gas

etching, see Section 4.2, liquids provide additional mechanisms to remove debris of laser-ablation and products of chemical reactions, which results in higher etching rates.<sup>[464,465]</sup> Analytical analysis of GaN etched in HCl showed several possible reaction channels, which can be reduced to a simple reaction:  $\text{GaN} + 3\text{HCl} = \text{GaCl}_3 + \text{NH}_3 \uparrow$ .<sup>[466]</sup> This model agrees with experimental observations that reported on a Ga-rich layer at the surface.<sup>[465]</sup>

LIBWE can also be used to selectively etch metals.<sup>[467]</sup> The laser-induced elevation of surface temperature activates reactions that would not take place at room temperature. The forming salts are either soluble in water or are removed due to either thermal expansion caused by laser-induced surface heating or by shock waves in the liquid. Increase in ablation rate was also observed when water was replaced with hydrogen peroxide, thus indicating that in the second case ablation was assisted by LIBWE.<sup>[468]</sup>

Sometimes the chemical etching process was found to be activated by laser radiation, as was reported for industrial stainless steels in  $\text{H}_3\text{PO}_4$ .<sup>[469]</sup> Such steels are not etched by  $\text{H}_3\text{PO}_4$  spontaneously due to a surface chromium oxide layer. However, at elevated temperatures locally generated by laser beam, the following reaction converted such a passivating  $\text{Cr}_2\text{O}_3$  layer into water-soluble  $\text{CrPO}_4$ :  $\text{Cr}_2\text{O}_3 + 2\text{H}_3\text{PO}_4 = 2\text{CrPO}_4 + 3\text{H}_2\text{O}$ . After that,  $\text{H}_3\text{PO}_4$  could etch the steel surface as long as its temperature remained high. When the laser radiation was off, the passivating layer started forming again thus inhibiting further etching.

## 6. Outlook: Laser Chemistry Technologies of Future

In this section, we overview recent trends and potential directions of further commercialization of the laser-induced photo-chemical and hybrid nanotechnologies. As shown in Figure 1, we are now in a unique historical point where the fusion of previously established and emerging approaches can give rise to an explosive growth of applications for the above mentioned laser-assisted technologies.

### 6.1. Technological Aspects and Challenges

#### 6.1.1. Green Chemistry

As the global population and its corresponding technological demands continue to grow, the request for more efficient and clean methods to synthesize nanomaterials will gradually intensify. For example, nanoparticles are extensively utilized across various industries including agriculture, environmental remediation, coatings, optics, electronics, cosmetics, food, medicine, textiles, plastics, paints, fuel additives, and wastewater treatment. The use of NPs is widespread, with over 600 products and almost 3000 products containing NPs according to nanotechnology-based consumer products and online databases, respectively.<sup>[470]</sup> During the last decade, in the field of medicine and biology, the use of NPs has grown significantly, with a reported value of \$17.5 billion in 2011, increasing to \$53.5 billion in 2017, and reaching \$79.8 billion in 2019. The consumption of silver NPs is estimated at 450 tons per year, while the production of zinc NPs is around 5500 tons per year. Therefore, methods of such nanomaterials fabrication should be as clean as possible to avoid hazardous impacts on human health and the environment.

Since the late 1990s and till now, the concept of so-called 'green chemistry' (or sustainable chemistry) has become one of the most important trends in chemical engineering aiming to minimize or eliminate the use and generation of hazardous substances.<sup>[471]</sup> The Green Chemicals Market exceeded \$100 billion in 2022 and is expected to exceed \$200 billion in 2030. The principles of green chemistry are based on such key ideas as the use of safe, environmentally benign substances and materials, as well as avoiding or minimizing the production of any waste as the ideal form of waste management.

In this regard, laser-assisted photo-chemical processes for the fabrication of nanostructures and nanomaterials are very promising for waste-free manufacturing. PLAL is a typical example of a green-chemistry approach that allows for the production of ligand-free NPs with diverse compositions, shapes, and phases<sup>[472]</sup> (for more details, see Section 5.4). Such methods as direct laser writing and laser synthesis in liquids (Section 3) without producing hazardous waste can also be considered as green-chemistry approaches in many cases. However, the aspect of energy efficiency as well as production cost are becoming quite important issues for this direction.

#### 6.1.2. Development of Laser Technologies

**Energy Efficiency:** Addressing energy efficiency and reducing carbon emissions in the industry is increasingly critical, given the volatility of energy markets and the tightening of environmental regulations. In this regard, the laser manufacturing industry is a high energy-consuming one. In gas lasers, such as those using carbon dioxide (which have long been used as powerful continuous-wave sources), efficiencies are typically low, reaching no more than wall-plug efficiency (WPE) 20%. In turn, semiconductor laser diodes and fiber lasers are much more efficient exhibiting WPE of more than 40%,<sup>[473]</sup> while for high-power femtosecond lasers WPE is usually less than 5%. As discussed in Section 2.4, there are various techniques for local near-field enhancement that can also be employed to improve the overall efficiency of laser-assisted photo-chemical processes.

**Cost Efficiency:** The average price per watt of continuous wave (CW) devices designed for high-volume applications decreased exponentially during the past few decades from  $10^3$  \$/W to a value of  $10^0$  \$/W. These values are already reliable for many industrially reasonable photo-chemical manufacturing processes, and they are believed to continue improving. Also, lasers with ultrashort (fs and ps) pulse durations are becoming more and more cheaper going down to  $<10^4$  \$ level. As a result, such technologies as PLAL of gold NPs have become even more economically efficient when compared to chemical technologies based on standard reduction reactions.<sup>[474]</sup>

More detailed comparison of the productivity of three laser systems (40, 10, and 3-ps) for ablation of gold, platinum, silver, and nickel in water was done in the work.<sup>[475]</sup> The picosecond laser system showed the highest absolute productivity in terms of mass per unit time compared to the nanosecond laser system. For gold and silver, the power-specific productivity was lower for the picosecond laser compared to the 10-ns laser, while it was similar for platinum and nickel. The study also revealed that the 10-ns laser outperformed the 3-ps laser in investment-specific

productivity for gold and silver nanoparticle production by 11% and 15% per 1000 \$ investment, respectively. Longer pulses, such as those from a 40-ns laser source, were found to result in lower productivity due to thermal interactions and plasma shielding. Both power and investment costs are essential from an economic standpoint, as even slight differences can translate into significant profits over time. Considering the expenses to the whole technological equipment, the lower initial investment cost of the 10-ns laser system is around 100 000 \$ compared to approximately 3–5 times more expensive the 3-ps high-productive laser systems, which makes it more accessible for small-scale industries looking to invest in environmentally friendly nanoparticle production methods.

Generally, for industrial-scale applications, synthesis costs can be further significantly reduced by employing higher laser power including increase of repetition rate. For example, novel advanced laser systems supporting GHz and even THz level of repetition rate<sup>[476,477]</sup> are already available for extremely high throughput of materials processing or nanomaterials generation.<sup>[478]</sup> Remarkably, modern laser technologies allow for integration with various robot systems to achieve full automatization and remote control. Laser beam multiplexing and shaping by spatial light modulators, diffractive optical elements and interference-based approaches is another promising strategy for fabrication upscaling and increasing the resulting cost efficiency.

*Photo-Excitation Efficiency.* Further progress in the laser-induced photochemistry requires high efficiency of the laser photo-excitation of electrons in different precursor molecules. This opens new challenges for development of suitable lasers, especially that with wavelengths exactly fitting required electron transitions. First of all these are new tunable lasers with precisely adjustable wavelengths with photon energies in the range of several eV (corresponding to the visible-UV range). Now the absorption of the materials is usually adjusted to the available wavelengths of existing lasers, which sometimes needs a difficult chemical process to fabricate the precursor.<sup>[135,273]</sup> Fitting the wavelength of the laser would help solving the efficiency problem “from the other side”. Application of different techniques for shifting the laser wavelength such as optical parametric amplification is also possible but is less advantageous due to its relatively low efficiency.

Highly efficient UV lasers are needed to excite an electron to high levels (over 3 eV). The active medium of such lasers is usually a fluoride crystal (having a good transparency in the UV range) doped with  $Ce^{3+}$  ions<sup>[479]</sup> or with other 4f elements or laser diodes. Energy up-conversion and cross-relaxation<sup>[480–483]</sup> enable the pumping of such materials in the visible or NIR range. Application of higher harmonic generation or UV gas lasers such as excimer lasers can be attractive due to their high power, but is problematic due to low efficiency. If no laser with fitting wavelength can be found, excitation via the excited-state absorption (ESA) can be exploited. For the ESA a sequence of two timely-synchronized pulses with different precisely adjusted wavelengths are needed.

## 6.2. Flexible Electronics

Flexible electronics, which include wearable devices, IoT devices, healthcare monitoring systems, and many other devices, have

been gaining a significant attraction in the market due to their versatility and potential applications in various industries. The current market size for flexible electronics is estimated to be around \$40 billion and is expected to grow at a compound annual growth rate of 11% over the next five years. One of the key drivers for the growth of flexible electronics is the increasing demand for lightweight, portable, and energy-efficient devices.

Innovations in manufacturing technologies are driving the development of fully printed flexible optoelectronic devices. Laser technologies are emerging as a promising tool for creating all functional layers in these devices.<sup>[484]</sup> By using lasers to precisely pattern and deposit materials on flexible substrates, manufacturers can achieve high-resolution, high-performance optoelectronic components. Namely, the discussed in this review lasers-based photo-chemical approaches can be used for the synthesis and deposition of all necessary layers: semiconductors (as photoactive and transport layers, see Section 4), and metals (as contacts, see Section 5.2). As a result, we envision further huge progress in the direction of all-laser-printed flexible electronic devices.<sup>[121]</sup>

## 6.3. Nanophotonics and Flat Optics

Over the past few years, the fields of nanophotonics and metasurfaces have become a rapidly expanding area of research in optics, which is mature enough for some applications.<sup>[485,486]</sup> For example, thin arrays made up of subwavelength meta-atoms allow for precise manipulation of electromagnetic waves and have been suggested for a range of uses including lenses,<sup>[487]</sup> polarization control,<sup>[488]</sup> holography,<sup>[489]</sup> coloration,<sup>[490]</sup> information encryption,<sup>[491]</sup> anti-counterfeiting labeling,<sup>[492]</sup> and many other applications. Thanks to advancements in nanofabrication techniques and significant enhancements in metasurface performance (efficiency, bandwidth, etc.), this technology has now reached a level of maturity that makes it suitable for integration into commercial applications. High-throughput fabrication techniques capable of mass-producing metasurfaces, such as nanoimprinting lithography, injection molding, and roll-to-roll printing, are also available. However, modern laser technologies are also very prospective for this purpose,<sup>[493,494]</sup> and additional photo-chemical approaches for quality improvement or functionalization would make the fabricated devices multifunctional.<sup>[495]</sup>

## 6.4. Sensing

Nanostructures have revolutionized the sensor technologies enabling the development of highly sensitive and selective devices for a wide range of applications. SERS,<sup>[496]</sup> refractive index sensors,<sup>[497]</sup> surface-enhanced IR absorption (SEIRA) biosensors,<sup>[498]</sup> surface-enhanced photoluminescence (SEPL),<sup>[499]</sup> optical gas sensors,<sup>[500]</sup> and other types of sensors based on plasmonics and nanostructures have shown great promise in detecting trace amounts of analytes with high sensitivity and specificity.

The current market size for sensors based on plasmonics and nanostructures is growing rapidly, driven by increasing demand for advanced sensing technologies in various industries such as healthcare, environmental monitoring, food safety, and security.

The global market for plasmonic sensors is projected to reach billions of dollars in the coming years as these sensors continue to gain traction in the market. One of the key advantages of sensors based on plasmonics and nanostructures is their potential for miniaturization and cost-effectiveness. The latter is closely related to the need for single-use handling of sensors with reliable detection, especially in the case of medical diagnostics. Diverse scalable laser technologies surveyed in this review were already applied or can be potentially adopted to fabricate SERS/SEIRA sensors at high precision and efficiency, making them suitable for low-cost mass production.

Some potential applications of laser photo-chemical technologies in creating cheap and efficient sensors include environmental monitoring of pollutants, detection of hazardous gases in industrial settings, food quality control, medical diagnostics, and security screening. By leveraging the unique properties of plasmonics and nanostructures, these sensors can offer improved performance compared to traditional sensing technologies, enabling faster and more accurate detection of diverse analytes. For example, SERS/SEPL sensing elements produced by LID and LIPSS techniques were applied as substrates for detection.<sup>[238,270,501,502]</sup> Additionally, emerging laser technologies also hold promise for another sensor types (i.e., electrochemical or chemiresistive gas sensors), where advanced electrodes and active sensor parts loaded with functional nanomaterials are highly demanded.

### 6.5. Catalysis

Catalysis is a crucial field in the realm of chemical engineering and industrial processes, playing a significant role in accelerating chemical reactions and reducing energy consumption. The global catalysis market size is estimated to be around \$29 billion in 2021 and is projected to grow at a compound annual growth rate of 4.8% till 2026.

One of the emerging trends in catalysis is the utilization of laser photo-chemical technologies to create efficient nanoparticles and nanostructures for catalytic applications. By leveraging laser-induced processes, researchers can precisely control the size, shape, and composition of NPs, aiming at their enhanced catalytic performance. This approach holds great promise for improving the efficiency and selectivity of catalytic processes in various industries, such as pharmaceuticals, petrochemicals, and environmental remediation. Laser photo-chemical technologies for the formation of metallic NPs with controlled morphology, the development of novel catalytic materials for renewable energy production, and the design of catalysts for carbon capture and conversion.<sup>[503,504]</sup>

### 6.6. Supercapacitors

Supercapacitors, also known as ultracapacitors or electrochemical capacitors, are energy storage devices that offer high power density, fast charging and discharging capabilities, and long cycle life compared to traditional batteries. The global super-capacitor market size was valued at approximately \$2.5 billion in 2020 and is expected to witness a significant growth in the coming years,

driven by increasing demand for energy storage solutions in various industries such as automotive, electronics, and renewable energy.

One of the key challenges in supercapacitor technology is the development of high-performance electrode materials that can enhance energy density and power efficiency. Laser photo-chemical technologies have emerged as a promising approach to address this challenge by enabling the precise synthesis of nanostructured materials with tailored properties for supercapacitor applications. By leveraging laser-induced processes such as laser ablation, laser pyrolysis, and laser-assisted chemical vapor deposition, researchers can fabricate electrode materials with controlled morphology, composition, and surface area at the nanoscale. For example, laser photo-chemical technologies in super-capacitors are very promising for the synthesis of graphene-based materials,<sup>[505]</sup> metal oxides,<sup>[506,507]</sup> and conducting polymers with enhanced electrochemical properties.

### 6.7. Solar energy

The future of solar energy looks very promising. The market size of solar energy, particularly photovoltaics and solar water heaters utilizing thin-film technologies, has been steadily growing in recent years.

One area of research that holds great potential for the solar industry is the use of laser photo-chemical technologies to create NPs for the use in solar water heaters. By utilizing lasers to fabricate NPs with specific properties, it is possible to create nano-fluids (volumetric heating) or advanced light-absorbing materials (localized heating) that can significantly improve the efficiency and cost-effectiveness of solar-to-heat converters and water dissalination systems. Such nano-fluids can enhance light absorption and heat transfer properties, leading to more efficient heating of water using solar energy.<sup>[415,508,509]</sup> Additionally, laser-fabricated NPs can also be applied to improve the performance of solar cells. By incorporating such nanoparticles into the design of solar cells, it is possible to enhance light absorption and energy conversion efficiency. Since the price of nanoparticles generated by PLAL is relatively low and is expected to be further reduced during the nearest years, we envision that their applications for solar energy would not affect the final price of devices while improving their efficiency. Thus, laser-produced nanomaterials can be especially promising for solution-processible organic<sup>[510]</sup> and perovskite<sup>[511]</sup> photovoltaic technologies that will be eventually widely commercialized during the next decade.

### 6.8. Theranostics

Transition to a personalized medicine as well as the use of novel low-invasive therapeutic and diagnostic approaches represent global trends in treatment of socially significant diseases such as cancer causing around 12% of all deaths, according to the World Health Organization. Nanomaterials (or nano-agents) hold promise for antitumor therapy expanding existing diagnostic capabilities and providing highly selective and local therapeutic effect on the targeted biological tissues. At the same time, biomedical nanomaterials should simultaneously address multiple requirements including low toxicity, high colloidal stability,

as well as strong absorption and scattering at near-IR laser wavelengths within the so-called therapeutic transparency window of biological tissues. In this regard, the PLAL method permits to produce unique nanomaterials (such as nano-hybrids, magneto-plasmonic nano-alloys, van der Waals NPs, etc.) that have already proved their efficiency for diverse theranostic applications including photothermal therapy and bioimaging.<sup>[387,394,512–514]</sup> Once both the productivity of laser synthesis approaches and cost efficiency of the product are expected to continuously increase, we envision the growing popularity of diverse laser methods (such as PLAL or LSL) for fabrication of advanced nanomaterials for biomedical applications.

## 7. Conclusion

The provided overview of the history and recent achievements in the field of laser chemistry brings us to the conclusion that the development of laser technologies, green-chemistry approaches, and nanophotonics makes a paradigm shift in modern nanofabrication. With nearly the same processing arrangement, one can switch between additive and subtractive manufacturing or between chemical and morphological surface modifications by changing the parameters (such as, e.g., laser beam intensity, composition and absorption spectrum of the environment). The laser radiation triggers these processes in two different ways: 1) photochemical action: the photons excite molecular oscillations or electrons in the environment or generate electron-hole pairs at the surface. In this case the laser wavelength corresponds to some absorption band of the material. As a result, the material is driven out of its thermal equilibrium on the time scales larger than that needed for chemical reactions. The chemical reaction is activated either by the free charge carriers or because its threshold is lowered by this excitation. 2) thermo-induced action: the absorbed laser radiation increases the temperature at the interface and acts as a localized heat source. The thermal equilibrium can be assumed in this case and the chemical reaction is activated by the increased temperature at the interface.

Both physical routes enable considerable energy saving in the production. In the photochemical way one can avoid the Maxwell-Boltzmann energy distribution of the reacting species, in which only the high-energy “tail” is able to overcome the reaction barrier and the rest just dissipates the energy. The efficiency of the laser-induced thermal chemical patterning is higher than that of traditional chemical reactors due to localization of the light only in the area to be processed. The final goal of this direction would be the achievement of high control of reaction product parameters, high spatial precision, low toxicity, and cost efficiency, which can make laser chemistry approaches suitable for industrial scale applications in flexible electronics, flat optics, sensing, catalysis, supercapacitors, and solar energy.

## Acknowledgements

This work was supported by the Russian Science Foundation (Grant no. 21-79-20075) and National Natural Science Foundation of China (project 62350610272).

Open access funding enabled and organized by Projekt DEAL.

## Conflict of Interest

The authors declare no conflict of interest.

## Keywords

laser chemistry, laser ablation in liquids, laser deposition, laser patterning, nanostructures

Received: March 29, 2024

Revised: June 24, 2024

Published online:

- [1] C. Timiriacheff, *Nature* **1909**, 82, 67.
- [2] R. H. Dalton, Glass article and making it., U.S. Patent No. 2,326,012. **1943**.
- [3] S. D. Stookey, *Ind. Eng. Chem.* **1949**, 41, 856.
- [4] W. A. Davis, *Sci. Prog. Twentieth Century (1906-1916)* **1912**, 7, 251.
- [5] M. Bodenstein, *J. Chem. Educ.* **1930**, 7, 518.
- [6] H. D. Roth, *Pure Appl. Chem.* **2001**, 73, 395.
- [7] G. Ciamician, P. Silber, *Ber. Dtsch. Chem. Ges.* **1901**, 34, 1530.
- [8] G. Ciamician, P. Silber, *Ber. Dtsch. Chem. Ges.* **1901**, 34, 2040.
- [9] G. Ciamician, P. Silber, *Ber. Dtsch. Chem. Ges.* **1907**, 40, 2415.
- [10] G. Ciamician, P. Silber, *Ber. Dtsch. Chem. Ges.* **1908**, 41, 1928.
- [11] G. Ciamician, *Science* **1912**, 36, 385.
- [12] N. D. Heindel, M. A. Pfau, *J. Chem. Educ.* **1965**, 42, 383.
- [13] E. Paterno, G. Chieffi, *Gazz. chim. ital* **1909**, 39, 341.
- [14] E. J. Bowen, *Q. Rev. Chem. Soc.* **1950**, 4, 236.
- [15] A. L. Schawlow, *Bell Lab. Rec.* **1960**, 38, 403.
- [16] N. V. Karlov, *Appl. Opt.* **1974**, 13, 301.
- [17] S. Lin, A. Ronn, *Chem. Phys. Lett.* **1977**, 49, 255.
- [18] V. S. Letokhov, *Nature* **1983**, 305, 103.
- [19] A. H. Zewail, *Phys. Today* **1980**, 33, 27.
- [20] J. T. Knudtson, E. M. Eyring, *Annu. Rev. Phys. Chem.* **1974**, 25, 255.
- [21] N. Bloembergen, E. Yablonovitch, *Phys. Today* **1978**, 31, 23.
- [22] A. M. Ronn, *Sci. Am.* **1979**, 240, 114.
- [23] J. F. Ready, *Appl. Phys. Lett.* **2004**, 3, 11.
- [24] J. A. Howe, *J. Chem. Phys.* **2004**, 39, 1362.
- [25] T. J. Harris, *IBM J. Res. Dev.* **1963**, 7, 342.
- [26] D. Lichtman, J. F. Ready, *Phys. Rev. Lett.* **1963**, 10, 342.
- [27] H. M. Smith, A. F. Turner, *Appl. Opt.* **1965**, 4, 147.
- [28] M. Birnbaum, *J. Appl. Phys.* **1965**, 36, 3688.
- [29] R. M. Osgood, T. F. Deutsch, *Science* **1985**, 227, 709.
- [30] D. Bäuerle, *Laser Processing and Chemistry*, Springer, Berlin, Germany, **2000**.
- [31] R. J. von Gutfeld, E. E. Tynan, R. L. Melcher, S. E. Blum, *Appl. Phys. Lett.* **1979**, 35, 651.
- [32] J. C. Puipe, R. E. Acosta, R. J. von Gutfeld, *J. Electrochem. Soc.* **1981**, 128, 2539.
- [33] R. J. von Gutfeld, L. T. Romankiw, R. E. Acosta, *IBM J. Res. Dev.* **1982**, 26, 136.
- [34] R. J. von Gutfeld, L. T. Romankiw, *Gold Bull.* **1982**, 15, 120.
- [35] L. Nánai, I. Hevesi, F. V. Bunkin, B. S. Luk'yanchuk, M. R. Brook, G. A. Shafeev, D. A. Jelski, Z. C. Wu, T. F. George, *Appl. Phys. Lett.* **1989**, 54, 736.
- [36] S. Pflüger, M. Wehner, F. Jansen, T. Kruck, F. Lupp, *Appl. Surf. Sci.* **1995**, 86, 504.
- [37] M. Wehner, F. Legewie, B. Theisen, E. Beyer, *Appl. Surf. Sci.* **1996**, 106, 406.
- [38] H. W. Lee, S. D. Allen, *Appl. Phys. Lett.* **1991**, 58, 2087.
- [39] A. Fojtik, A. Henglein, *Ber. Bunsen-Ges. Phys. Chem.* **1993**, 97, 252.
- [40] A. Henglein, *J. Phys. Chem.* **1993**, 97, 5457.

- [41] J. Ikeno, A. Kobayashi, T. Kasai, *J. Japan Soc. Prec. Eng.* **1989**, *55*, 335.
- [42] D. Zhang, B. Gökce, S. Barcikowski, *Chem. Rev.* **2017**, *117*, 3990.
- [43] M. Kim, S. Osone, T. Kim, H. Higashi, T. Seto, *KONA Powder Part. J.* **2017**, *34*, 80.
- [44] A. Kanitz, M.-R. Kalus, E. L. Gurevich, A. Ostendorf, S. Barcikowski, D. Amans, *Plasma Sources Sci. Technol.* **2019**, *28*, 103001.
- [45] K. A. Teter, L. S. Kabnick, M. Sadek, *Phlebology* **2020**, *35*, 656.
- [46] D. Zhang, Z. Li, K. Sugioka, *J. Phys.: Photonics* **2021**, *3*, 042002.
- [47] R. C. Forsythe, C. P. Cox, M. K. Wilsey, A. M. Müller, *Chem. Rev.* **2021**, *121*, 7568.
- [48] J. Theerthagiri, K. Karuppasamy, S. J. Lee, R. Shwetharani, H.-S. Kim, S. K. K. Pasha, M. Ashokkumar, M. Y. Choi, *Light Sci. Appl.* **2022**, *11*, 1.
- [49] A. Balachandran, S. P. Sreenilayam, K. Madanan, S. Thomas, D. Brabazon, *Results Eng.* **2022**, *16*, 100646.
- [50] H. Park, J. J. Park, P.-D. Bui, H. Yoon, C. P. Grigoropoulos, D. Lee, S. H. Ko, *Adv. Mater.* **2023**, 2307586, <https://doi.org/10.1002/adma.202307586>.
- [51] S. W. Eaton, A. Fu, A. B. Wong, C.-Z. Ning, P. Yang, *Nat. Rev. Mater.* **2016**, *1*, 16028.
- [52] M. A. Masharin, T. Oskolkova, F. Isik, H. Volkan Demir, A. K. Samusev, S. V. Makarov, *ACS Nano* **2024**, *18*, 3447.
- [53] W. Marine, N. M. Bulgakova, L. Patrone, I. Ozerov, *J. Appl. Phys.* **2008**, *103*, 094902.
- [54] P. Balling, in *Handbook of Laser Micro- and Nano-Engineering*, Springer, Cham, Switzerland, **2021**, pp. 3–59.
- [55] N. M. Bulgakova, R. Stoian, A. Rosenfeld, E. E. B. Campbell, I. V. Hertel, *Appl. Phys. A* **2004**, *79*, 1153.
- [56] D. G. Baranov, S. V. Makarov, V. A. Milichko, S. I. Kudryashov, A. E. Krasnok, P. A. Belov, *Acs Photonics* **2016**, *3*, 1546.
- [57] A. Rudenko, K. Ladutenko, S. Makarov, T. E. Itina, *Adv. Opt. Mater.* **2018**, *6*, 1701153.
- [58] Z. Lin, L. V. Zhigilei, V. Celli, *Phys. Rev. B* **2008**, *77*, 075133.
- [59] L. L. Taylor, R. E. Scott, J. Qiao, *Opt. Mater. Express* **2018**, *8*, 648.
- [60] R. J. Maurer, P. K. Jain, *J. Phys. Chem. C* **2024**, *128*, 1863.
- [61] M. L. Brongersma, *Proc. IEEE* **2016**, *104*, 2349.
- [62] Y. Zhang, S. He, W. Guo, Y. Hu, J. Huang, J. R. Mulcahy, W. D. Wei, *Chem. Rev.* **2017**, *118*, 2927.
- [63] H. Tang, C.-J. Chen, Z. Huang, J. Bright, G. Meng, R.-S. Liu, N. Wu, *J. Chem. Phys.* **2020**, *152*, 220901.
- [64] S. Anisimov, B. Kapeliovich, T. Perelman, *Zh. Eksp. Teor. Fiz* **1974**, *66*, 375.
- [65] T. Q. Qiu, C. L. Tien, *J. Heat Transfer* **1993**, *115*, 835.
- [66] C. J. Glassbrenner, G. A. Slack, *Phys. Rev.* **1964**, *134*, A1058.
- [67] B. J. Demaske, V. V. Zhakhovskiy, N. A. Inogamov, I. I. Oleynik, *Phys. Rev. B* **2013**, *87*, 054109.
- [68] G. Mie, *Ann. Phys.* **1908**, *330*, 377.
- [69] G. Baffou, F. Cichos, R. Quidant, *Nat. Mater.* **2020**, *19*, 946.
- [70] G. P. Zograf, M. I. Petrov, S. V. Makarov, Y. S. Kivshar, *Adv. Opt. Photonics* **2021**, *13*, 643.
- [71] H. Yamamoto, K. Ohkubo, S. Akimoto, S. Fukuzumi, A. Tsuda, *Org. Biomol. Chem.* **2014**, *12*, 7004.
- [72] A. Hamedian, M. Vakili, S. A. Brandán, M. Akbari, A. Kanaani, V. Darugar, *Sci. Rep.* **2024**, *14*, 12452.
- [73] M. H. Shaw, J. Twilton, D. W. C. MacMillan, *J. Org. Chem.* **2016**, *81*, 6898.
- [74] L. Sun, K. Fukuda, T. Someya, *npj Flexible Electron.* **2022**, *6*, 89.
- [75] F. Juliá, *ChemCatChem* **2022**, *14*, 202200916.
- [76] C.-C. Ko, V. Wing-Wah Yam, *J. Mater. Chem.* **2010**, *20*, 2063.
- [77] G. C. Thaggard, J. Haimerl, K. C. Park, J. Lim, R. A. Fischer, B. K. P. Maldeni Kankanamalage, B. J. Yarbrough, G. R. Wilson, N. B. Shustova, *J. Am. Chem. Soc.* **2022**, *144*, 23249.
- [78] R. Sakamoto, M. Murata, S. Kume, H. Sampei, M. Sugimoto, H. Nishihara, *Chem. Commun.* **2005**, *2005*, 1215.
- [79] S. Pommeret, F. Gobert, M. Mostafavi, I. Lampre, J.-C. Mialocq, *The Journal of Physical Chemistry A* **2001**, *105*, 11400.
- [80] J. Baxendale, P. Wardman, *Nature* **1971**, *230*, 449.
- [81] Z.-H. Loh, G. Doumy, C. Arnold, L. Kjellsson, S. Southworth, A. Al Haddad, Y. Kumagai, M.-F. Tu, P. Ho, A. March, R. D. Schaller, M. S. Bin Mohd Yusof, T. Debnath, M. Simon, R. Welsch, L. Inhester, K. Khalili, K. Nanda, A. I. Krylov, S. Moeller, G. Coslovich, J. Koralek, M. P. Minitti, W. F. Schlotter, J.-E. Rubensson, R. Santra, L. Young, *Science* **2020**, *367*, 179.
- [82] J. A. LaVerne, S. Pimblott, *The Journal of Physical Chemistry A* **2000**, *104*, 9820.
- [83] P. Camarda, L. Vaccaro, F. Messina, M. Cannas, *Appl. Phys. Lett.* **2015**, *107*, 013103.
- [84] S. Reich, J. Göttlicher, A. Ziefuss, R. Streubel, A. Letzel, A. Menzel, O. Mathon, S. Pascarelli, T. Baumbach, M. Zuber, B. Gökce, S. Barcikowski, A. Plech, *Nanoscale* **2020**, *12*, 14011.
- [85] T. V. Bykov, X. C. Zeng, *J. Chem. Phys.* **2006**, *125*, 144515.
- [86] J. T. Lin, W. C. Murphy, T. F. George, *Ind. eng. chem. prod. res. dev.* **1984**, *23*, 334.
- [87] L. Nanai, I. Hevesi, N. Bunkin, B. Zon, S. Lavishev, B. Luk'yanchuk, G. Shafeev, *Appl. Phys. A* **1990**, *50*, 27.
- [88] V. I. Goldanskii, V. Namiot, R. Khokhlov, *Sov. Phys. JETP* **1976**, *43*, 1226.
- [89] G. Askar'yan, V. Namiot, *Sov. Phys. JETP* **1976**, *42*, 1009.
- [90] S. A. Maier, *Nanoplasmonics: Fundamentals and Applications*, Springer, Berlin, Heidelberg **2007**.
- [91] A. I. Kuznetsov, A. E. Miroshnichenko, M. L. Brongersma, Y. S. Kivshar, B. Lukyanchuk, *Science* **2016**, *354*, 6314.
- [92] K. M. Mayer, J. H. Hafner, *Chem. Rev.* **2011**, *111*, 3828.
- [93] G. Baffou, R. Quidant, *Laser Photonics Rev.* **2013**, *7*, 171.
- [94] W. Sritravanich, N. Fang, C. Sun, Q. Luo, X. Zhang, *Nano Lett.* **2004**, *4*, 1085.
- [95] I. Alessandri, M. Ferroni, L. E. Depero, *ChemPhysChem* **2009**, *10*, 1017.
- [96] I. Alessandri, *Small* **2010**, *6*, 1679.
- [97] K. Ueno, S. Takabatake, Y. Nishijima, V. Mizeikis, Y. Yokota, H. Misawa, *J. Phys. Chem. Lett.* **2010**, *1*, 657.
- [98] I. Alessandri, *J. Colloid Interface Sci.* **2010**, *351*, 576.
- [99] C. Fasciani, C. J. B. Alejo, M. Grenier, J. C. Netto-Ferreira, J. Scaiano, *Org. Lett.* **2011**, *13*, 204.
- [100] I. Alessandri, M. Ferroni, L. E. Depero, *J. Phys. Chem. C* **2011**, *115*, 5174.
- [101] J. Qiu, W. D. Wei, *J. Phys. Chem. C* **2014**, *118*, 20735.
- [102] A. Gelle, T. Jin, L. de la Garza, G. D. Price, L. V. Besteiro, A. Moores, *Chem. Rev.* **2019**, *120*, 986.
- [103] D. Jaque, L. M. Maestro, B. del Rosal, P. Haro-Gonzalez, A. Benayas, J. Plaza, E. M. Rodríguez, J. G. Solé, *nanoscale* **2014**, *6*, 9494.
- [104] R. S. Riley, E. S. Day, *Wiley Interdiscip Rev: Nanomed Nanobiotechnol* **2017**, *9*, e1449.
- [105] A. N. Koya, M. Romanelli, J. Kuttruff, N. Henriksson, A. Stefancu, G. Grinblat, A. De Andres, F. Schnur, M. Vanzan, M. Marsili, M. Rahaman, A. V. Rodríguez, T. Tapani, H. Lin, B. D. Dana, J. Lin, G. Barbillon, R. P. Zaccaria, D. Brida, D. Jariwala, L. Veisz, E. Cortés, S. Corni, D. Garoli, N. Maccaferri, *Appl. Phys. Rev.* **2023**, *10*, 021318.
- [106] G. P. Zograf, M. I. Petrov, D. A. Zuev, P. A. Dmitriev, V. A. Milichko, S. V. Makarov, P. A. Belov, *Nano Lett.* **2017**, *17*, 2945.
- [107] N. Bontempi, I. Vassalini, S. Danesi, M. Ferroni, M. Donarelli, P. Colombi, I. Alessandri, *J. Phys. Chem. Lett.* **2018**, *9*, 2127.
- [108] M. Aouassa, E. Mitsai, S. Syubaev, D. Pavlov, A. Zhizhchenko, I. Jادli, L. Hassayoun, G. Zograf, S. Makarov, A. Kuchmizhak, *Appl. Phys. Lett.* **2017**, *111*, 24.
- [109] S. Danesi, M. Gandolfi, L. Carletti, N. Bontempi, C. De Angelis, F. Banfi, I. Alessandri, *Phys. Chem. Chem. Phys.* **2018**, *20*, 15307.

- [110] E. Mitsai, M. Naffouti, T. David, M. Abbarchi, L. Hassayoun, D. Storozhenko, A. Mironenko, S. Bratskaya, S. Juodkazis, S. Makarov, A. Kuchmizhak, *Nanoscale* **2019**, *11*, 11634.
- [111] D. Ryabov, O. Pashina, G. Zograf, S. Makarov, M. Petrov, *Nanophotonics* **2022**, *11*, 3981.
- [112] I. Alessandri, J. R. Lombardi, *Chem. Rev.* **2016**, *116*, 14921.
- [113] S. V. Makarov, M. I. Petrov, U. Zywiets, V. Milichko, D. Zuev, N. Lopanitsyna, A. Kuksin, I. Mukhin, G. Zograf, E. Ubyvovk, D. A. Smirnova, S. Starikov, B. N. Chichkov, Y. S. Kivshar, *Nano Lett.* **2017**, *17*, 3047.
- [114] S. Syubaev, I. Gordeev, E. Modin, V. Terentyev, D. Storozhenko, S. Starikov, A. A. Kuchmizhak, *Nanoscale* **2022**, *14*, 16618.
- [115] S. J. Kim, I. Thomann, J. Park, J.-H. Kang, A. P. Vasudev, M. L. Brongersma, *Nano Lett.* **2014**, *14*, 1446.
- [116] Y. Huang, N. Wang, Y. Huang, L. Deng, C. Shen, Y. Chen, *Ann. Phys.* **2021**, *533*, 2000557.
- [117] R. T. A. Tirumala, S. Gyawali, A. Wheeler, S. B. Ramakrishnan, R. Sooriyagoda, F. Mohammadparast, N. Khatri, S. Tan, A. K. Kalkan, A. D. Bristow, M. Andiappan, *ACS Catal.* **2022**, *12*, 7975.
- [118] L. Hüttenhofer, M. Golibrzuch, O. Bienek, F. J. Wendisch, R. Lin, M. Becherer, I. D. Sharp, S. A. Maier, E. Cortés, *Adv. Energy Mater.* **2021**, *11*, 2102877.
- [119] R. T. Addanki Tirumala, N. Khatri, S. B. Ramakrishnan, F. Mohammadparast, M. T. Khan, S. Tan, P. Wagle, S. Puri, D. N. McLroy, A. K. Kalkan, M. Andiappan, *ACS Sustainable Chem. Eng.* **2023**, *11*, 15931.
- [120] A. Y. Vorobyev, C. Guo, *Laser Photonics Rev.* **2013**, *7*, 385.
- [121] Y. Li, M. Hong, *Laser Photonics Rev.* **2020**, *14*, 1900062.
- [122] M. Rothschild, *Mater. Today* **2005**, *8*, 18.
- [123] C. Lu, R. Lipson, *Laser Photonics Rev.* **2010**, *4*, 568.
- [124] C. Lim, M. Hong, Y. Lin, Q. Xie, B. LukYanchuk, A. Senthil Kumar, M. Rahman, *Appl. Phys. Lett.* **2006**, *89*, 191125.
- [125] K. Obata, J. Koch, U. Hinze, B. N. Chichkov, *Opt. Express* **2010**, *18*, 17193.
- [126] A. Chimmalgi, T. Choi, C. Grigoropoulos, K. Komvopoulos, *Appl. Phys. Lett.* **2003**, *82*, 1146.
- [127] Y. N. Kulchin, O. Vitrik, A. Kuchmizhak, A. Nepomnyashchii, A. Savchuk, A. Ionin, S. Kudryashov, S. Makarov, *Opt. Lett.* **2013**, *38*, 1452.
- [128] P. S. Salter, M. J. Booth, *Light: Sci. Appl.* **2019**, *8*, 110.
- [129] A. Plech, V. Kotaidis, M. Lorenc, J. Boneberg, *Nat. Phys.* **2006**, *2*, 44.
- [130] A. Plech, P. Leiderer, J. Boneberg, *Laser Photonics Rev.* **2009**, *3*, 435.
- [131] Z. Lin, K. Liu, T. Cao, M. Hong, *Opto-Electron. Adv.* **2023**, *6*, 230029.
- [132] J. P. Abid, A. W. Wark, P. F. Brevet, H. H. Girault, *Chem. Commun.* **2002**, 792.
- [133] K. Guo, A. Baidak, Z. Yu, *J. Mater. Chem. A* **2020**, *8*, 23029.
- [134] N. Jara, N. S. Milán, A. Rahman, L. Mouheb, D. C. Boffito, C. Jeffryes, S. A. Dahoumane, *Molecules* **2021**, *26*, 4585.
- [135] A. A. Manshina, E. V. Grachova, A. V. Povolotskiy, A. V. Povolotckaia, Y. V. Petrov, I. O. Koshevoy, A. A. Makarova, D. V. Vyalikh, S. P. Tunik, *Sci. Rep.* **2015**, *5*, 12027.
- [136] K. G. Stampelcoskie, J. C. Scaiano, *J. Am. Chem. Soc.* **2010**, *132*, 1825.
- [137] S. Kundu, D. Huitink, K. Wang, H. Liang, *J. Colloid Interface Sci.* **2010**, *344*, 334.
- [138] Y. Li, L. Yang, H. He, L. Sun, H. Wang, X. Fang, Y. Zhao, D. Zheng, Y. Qi, Z. Li, W. Deng, *Nat. Commun.* **2022**, *13*, 1355.
- [139] S. Ilday, G. Makey, G. B. Akguc, Ö. Yavuz, O. Tokel, I. Pavlov, O. Gülseren, F. Ö. Ilday, *Nat. Commun.* **2017**, *8*, 14942.
- [140] K. Toyoda, H.-T. Su, K. Miyamoto, T. Sugiyama, T. Omatsu, *Optica* **2023**, *10*, 332.
- [141] T. Nakamura, Y. Mochidzuki, S. Sato, *J. Mater. Res.* **2008**, *23*, 968.
- [142] J. A. Bobb, S. P. Fisenko, C. J. Rodrigues, M. S. El-Shall, K. M. Tibbetts, *J. Eng. Phys. Thermophys.* **2019**, *92*, 369.
- [143] K. K. Ashkhalieva, V. V. Kononenko, A. L. Vasil'ev, E. V. Akhlyustina, V. M. Gololobov, N. R. Arutyunyan, A. M. Romshin, V. I. Konov, *Phys. Wave Phen.* **2022**, *30*, 17.
- [144] P. H. D. Ferreira, M. G. Vivas, L. D. Boni, D. S. dos Santos, D. T. Balogh, L. Misoguti, C. R. Mendonca, *Opt. Express* **2012**, *20*, 518.
- [145] A. A. Manshina, I. E. Kolesnikov, M. D. Mikhailov, *Acta Chim. Slov.* **2016**, *63*, 850.
- [146] T. Nakamura, K. Takasaki, A. Ito, S. Sato, *Appl. Surf. Sci.* **2009**, *255*, 9630.
- [147] G. Fan, S. Qu, Q. Wang, C. Zhao, L. Zhang, Z. Li, *J. Appl. Phys.* **2011**, *109*, 023102.
- [148] G. Fan, S. Ren, S. Qu, Z. Guo, Q. Wang, Y. Wang, R. Gao, *Opt. Commun.* **2013**, *295*, 219.
- [149] L. M. Frias Batista, M. Moody, C. Weththasingha, E. Kaplan, I. Faruque, M. S. El-Shall, K. M. Tibbetts, *Phys. Chem. Chem. Phys.* **2023**, *25*, 18844.
- [150] N. Nakashima, K. ichi Yamanaka, M. Saeki, H. Ohba, S. Taniguchi, T. Yatsuhashi, *Journal of Photochemistry and Photobiology A: Chemistry* **2016**, *70*, 319.
- [151] K. Moore Tibbetts, B. Tangeysh, J. H. Odhner, R. J. Levis, *J. Phys. Chem. A* **2016**, *120*, 3562.
- [152] Y. Herhani, T. Nakamura, S. Sato, *J. Nanomater.* **2010**, *2010*, 15421.
- [153] Y. Herhani, T. Nakamura, S. Sato, *J. Phys. Chem. C* **2011**, *115*, 21592.
- [154] J. L. H. Chau, C.-Y. Chen, M.-C. Yang, K.-L. Lin, S. Sato, T. Nakamura, C.-C. Yang, C.-W. Cheng, *Mater. Lett.* **2011**, *65*, 804.
- [155] J. L. H. Chau, C.-Y. Chen, C.-C. Yang, *Arabian J. Chem.* **2017**, *10*, S1395.
- [156] R. Srinivasan, A. Ghosh, *Chem. Phys. Lett.* **1988**, *143*, 546.
- [157] J. Pola, M. Urbanova, Z. Bastl, Z. Plzak, J. Šubr, V. Vorlíček, I. Gregora, C. Crowley, R. Taylor, *Carbon* **1997**, *35*, 605.
- [158] T. Nakamura, Y. Mochidzuki, S. Sato, in *2007 Conference on Lasers and Electro-Optics (CLEO)*, IEEE, Piscataway, NJ, **2007**, pp. 06–11.
- [159] M. Wesolowski, S. Kuzmin, B. Moores, B. Wales, R. Karimi, A. Zaidi, Z. Leonenko, J. Sanderson, W. Duley, *Carbon* **2011**, *49*, 625.
- [160] M. Wesolowski, S. Kuzmin, B. Wales, J. Sanderson, W. Duley, *J. Mater. Sci.* **2013**, *48*, 6212.
- [161] T. Hamaguchi, T. Okamoto, K. Mitamura, K. Matsukawa, T. Yatsuhashi, *Bull. Chem. Soc. Jpn.* **2015**, *88*, 251.
- [162] T. Yatsuhashi, T. Okamoto, in *High-Energy Chemistry and Processing in Liquids*, Springer, Berlin, Heidelberg **2022**, pp. 331–356.
- [163] L. M. Frias Batista, E. Kaplan, C. Weththasingha, B. Cook, S. Harris, A. Nag, K. M. Tibbetts, *J. Phys. Chem. B* **2023**, *127*, 6551.
- [164] A. M. Ahern, R. L. Garrell, *Anal. Chem.* **1987**, *59*, 2813.
- [165] E. J. Bjerneld, K. Murty, J. Prikulis, M. Käll, *ChemPhysChem* **2002**, *3*, 116.
- [166] M. Maillard, P. Huang, L. Brus, *Nano Lett.* **2003**, *3*, 1611.
- [167] L. Liu, C. He, J. Li, J. Guo, D. Yang, J. Wei, *New J. Chem.* **2013**, *37*, 2179.
- [168] S. Kundu, V. Maheshwari, R. F. Saraf, *Langmuir* **2008**, *24*, 551.
- [169] G. Bikbaeva, A. Belhadi, D. Pankin, D. Mamonova, I. Kolesnikov, Y. Petrov, T. Ivanova, D. Ivanov, A. Manshina, *Nano-Structures & Nano-Objects* **2023**, *36*, 101037.
- [170] T. Hu, Y. Fan, Y. Ye, Y. Cai, J. Liu, Y. Ma, P. Li, C. Liang, *Catalysts* **2023**, *13*, 1018.
- [171] K. Wenderich, G. Mul, *Chem. Rev.* **2016**, *116*, 14587.
- [172] J. Yu, L. Qi, M. Jaroniec, *J. Phys. Chem. C* **2010**, *114*, 13118.
- [173] L. Qiu-ye, Z. Lan-lan, L. Chen, C. Yu-hui, W. Xiao-dong, Y. Jian-jun, *Adv. Condens. Matter Phys.* **2014**, *2014*, 316589.
- [174] J. Lv, H. Gao, H. Wang, X. Lu, G. Xu, D. Wang, Z. Chen, X. Zhang, Z. Zheng, Y. Wu, *Appl. Surf. Sci.* **2015**, *351*, 225.
- [175] K. H. Leong, H. Y. Chu, S. Ibrahim, P. Saravanan, *Beilstein J. Nanotechnol.* **2015**, *6*, 428.
- [176] J.-J. Chen, J. C. S. Wu, P. C. Wu, D. P. Tsai, *J. Phys. Chem. C* **2011**, *115*, 210.

- [177] T. Wang, R. Lv, P. Zhang, C. Li, J. Gong, *Nanoscale* **2015**, *7*, 77.
- [178] Z. Zeng, C. Tan, X. Huang, S. Bao, H. Zhang, *Energy Environ. Sci.* **2014**, *7*, 797.
- [179] Y. T. Lei, D. W. Li, T. C. Zhang, X. Huang, L. Liu, Y. F. Lu, *J. Mater. Chem. C* **2017**, *5*, 8883.
- [180] X. Huang, Z. Zeng, S. Bao, M. Wang, X. Qi, Z. Fan, H. Zhang, *Nat. Commun.* **2013**, *4*, 1.
- [181] K. Xia, W.-Y. Chiang, C. J. Lockhart de la Rosa, Y. Fujita, S. Toyouchi, H. Yuan, J. Su, H. Masuhara, S. De Gendt, S. De Feyter, J. Hofkens, H. Uji-i, *Nanoscale* **2020**, *12*, 11063.
- [182] Y. Peng, J. Cao, J. Yang, W. Yang, C. Zhang, X. Li, R. A. W. Dryfe, L. Li, I. A. Kinloch, Z. Liu, *Adv. Funct. Mater.* **2020**, *30*, 2001756.
- [183] A. Scroccarello, R. Álvarez Diduk, F. Della Pelle, C. de Carvalho Castro e. Silva, A. Idili, C. Parolo, D. Compagnone, A. Merkoçi, *ACS Sens.* **2023**, *8*, 598.
- [184] H. Masuhara, K.-i. Yuyama, *Annu. Rev. Phys. Chem.* **2021**, *72*, 565.
- [185] T. Sugiyama, T. Adachi, H. Masuhara, *Chem. Lett.* **2007**, *36*, 1480.
- [186] T. Rodgers, S. Shoji, Z. Sekkat, S. Kawata, *Phys. Rev. Lett.* **2008**, *101*, 127402.
- [187] V. N. Bagratashvili, A. O. Rybaltovskii, S. S. Ilyukhin, O. L. Zakharkina, V. Y. Panchenko, P. S. Timashev, M. A. Timofeev, S. I. Tsykina, V. I. Yusupov, A. B. Evlyukhin, B. N. Chichkov, *Laser Phys.* **2014**, *24*, 126001.
- [188] V. I. Yusupov, V. M. Chudnovskii, I. V. Kortunov, V. N. Bagratashvili, *Laser Phys. Lett.* **2011**, *8*, 214.
- [189] Z. Yan, J. Zhang, *Appl. Surf. Sci.* **2024**, *653*, 159349.
- [190] A. Dostovalov, K. Bronnikov, V. Korolkov, S. Babin, E. Mitsai, A. Mironenko, M. Tutov, D. Zhang, K. Sugioka, J. Maksimovic, T. Katkus, S. Juodkakis, A. Zhizhchenko, A. Kuchmizhak, *Nanoscale* **2020**, *12*, 13431.
- [191] G. D. Martino, F. Michaelis, A. Salmon, S. Hofmann, J. Baumberg, *Nano Lett.* **2015**, *15*, 7452.
- [192] D. Ehrlich, *Appl. Surf. Sci.* **1993**, *69*, 115.
- [193] Z. Huang, J. E. Carey, M. Liu, X. Guo, E. Mazur, J. C. Campbell, *Appl. Phys. Lett.* **2006**, *89*, 033506.
- [194] J. Dai, J. Zhu, C. Chen, F. Weng, *J. Alloys Compd.* **2016**, *685*, 784.
- [195] M. Qiao, J. Yan, L. Jiang, *Adv. Opt. Mater.* **2022**, *10*, 2101673.
- [196] A. V. Dostovalov, T. J.-Y. Derrien, S. A. Lizunov, F. Přeučil, K. A. Okotrub, T. Mocek, V. P. Korolkov, S. A. Babin, N. M. Bulgakova, *Appl. Surf. Sci.* **2019**, *491*, 650.
- [197] S. Camacho-López, R. Evans, L. Escobar-Alarcón, M. A. Camacho-López, M. A. Camacho-López, *Appl. Surf. Sci.* **2008**, *255*, 3028.
- [198] B. Öktem, I. Pavlov, S. Ilday, H. Kalaycıoğlu, A. Rybak, S. Yavaş, M. Erdoğan, F. Ö. Ilday, *Nat. Photonics* **2013**, *7*, 897.
- [199] P. Segovia-Olvera, L. Sotelo, Y. Esqueda-Barron, M. Plata, N. Ramos, S. Camacho-Lopez, *Appl. Surf. Sci.* **2022**, *606*, 154762.
- [200] A. V. Dostovalov, V. P. Korolkov, V. S. Terentyev, K. A. Okotrub, F. N. Dultsev, S. A. Babin, *Quantum Electron.* **2017**, *47*, 631.
- [201] K. Bronnikov, A. Dostovalov, V. Terentyev, S. Babin, A. Kozlov, E. Pustovalov, E. L. Gurevich, A. Zhizhchenko, A. Kuchmizhak, *Appl. Phys. Lett.* **2021**, *119*, 211106.
- [202] K. Bronnikov, S. Gladkikh, K. Okotrub, A. Simanchuk, A. Zhizhchenko, A. Kuchmizhak, A. Dostovalov, *Nanomaterials* **2022**, *12*, 306.
- [203] J. Huang, L. Jiang, X. Li, Q. Wei, Z. Wang, B. Li, L. Huang, A. Wang, Z. Wang, M. Li, L. Qu, Y. Lu, *Adv. Opt. Mater.* **2019**, *7*, 1900706.
- [204] B. Groussin, M. Martinez-Calderon, O. Beldarrain, A. Rodriguez, S. M. Olaizola, B. A. Marsh, E. Granados, *Adv. Opt. Mater.* **2023**, *12*, 2302071.
- [205] V. P. Veiko, Y. Andreeva, L. Van Cuong, D. Lutoshina, D. Polyakov, D. Sinev, V. Mikhailovskii, Y. R. Kolobov, G. Odintsova, *Optica* **2021**, *8*, 577.
- [206] J. Geng, L. Xu, W. Yan, L. Shi, M. Qiu, *Nat. Commun.* **2023**, *14*, 565.
- [207] I. Poimenidis, N. Papakosta, A. Klini, M. Farsari, S. Moustazis, P. Loukakos, *Mater. Sci. Eng., B* **2023**, *295*, 116599.
- [208] S.-g. Ryu, E. Kim, J.-h. Yoo, D. J. Hwang, B. Xiang, O. D. Dubon, A. M. Minor, C. P. Grigoropoulos, *ACS nano* **2013**, *7*, 2090.
- [209] R. Jiang, B. Li, C. Fang, J. Wang, *Adv. Mater.* **2014**, *26*, 5274.
- [210] V. G. Ageev, V. I. Konov, A. I. Krechetov, A. V. Kuzmichov, A. M. Prokhorov, in *1st Intl School on Laser Surface Microprocessing*, International Society for Optics and Photonics, (Eds.: I. W. Boyd, V. I. Konov, B. S. Luk'yanchuk), vol. 1352, SPIE, Bellingham, WA **1990**, pp. 5–17.
- [211] S. Takatani, S. Yamamoto, H. Takazawa, K. Mochiji, *J. Vac. Sci. Technol.* **1995**, *13*, 2340.
- [212] T. M. Bloomstein, D. J. Ehrlich, *Appl. Phys. Lett.* **1992**, *61*, 708.
- [213] C. I. H. Ashby, *Appl. Phys. Lett.* **1984**, *45*, 892.
- [214] C. I. H. Ashby, *Appl. Phys. Lett.* **1985**, *46*, 752.
- [215] D. J. Ehrlich, J. Osgood, R. M., T. F. Deutsch, *Appl. Phys. Lett.* **2008**, *36*, 698.
- [216] H. Niino, *Photochemical and Photophysical Etching*, Springer International Publishing, Cham, **2020**, pp. 1–13.
- [217] C. Chapados, G. Birnbaum, *J. Mol. Spectrosc.* **1988**, *132*, 323.
- [218] V. N. Bagratashvili, V. S. Doljikov, V. S. Letokhov, E. A. Ryabov, *Appl. Phys.* **1979**, *20*, 231.
- [219] W. Sesselmann, T. J. Chuang, *J. Vac. Sci. & Technology B: Microelectronics Processing and Phenomena* **1985**, *3*, 1507.
- [220] V. V. Kononenko, M. S. Komlenok, S. M. Pimenov, V. I. Konov, *Quantum Electron.* **2007**, *37*, 1043.
- [221] K. Bronnikov, S. Gladkikh, E. Mitsai, E. Modin, A. Zhizhchenko, S. Babin, A. Kuchmizhak, A. Dostovalov, *Opt. Laser Technol.* **2024**, *169*, 110049.
- [222] J. Law, P. Meigs, *J. Electrochem. Soc.* **1957**, *104*, 154.
- [223] L. Vina, M. Cardona, *Phys. Rev. B* **1984**, *29*, 6739.
- [224] P. Carey, T. Sigmon, *Appl. Surf. Sci.* **1989**, *43*, 325.
- [225] M. A. Sheehy, B. R. Tull, C. M. Friend, E. Mazur, *Mater. Sci. Eng., B* **2007**, *137*, 289.
- [226] E. Kim, C. Ko, K. Kim, Y. Chen, J. Suh, S.-G. Ryu, K. Wu, X. Meng, A. Suslu, S. Tongay, J. Wu, C. P. Grigoropoulos, *Adv. Mater.* **2016**, *28*, 341.
- [227] Y. Rho, K. Lee, L. Wang, C. Ko, Y. Chen, P. Ci, J. Pei, A. Zettl, J. Wu, C. P. Grigoropoulos, *Nat. Electron.* **2022**, *5*, 505.
- [228] C. Wu, C. Crouch, L. Zhao, J. Carey, R. Younkin, J. Levinson, E. Mazur, R. Farrell, P. Gothoskar, A. Karger, *Appl. Phys. Lett.* **2001**, *78*, 1850.
- [229] J. E. Carey, C. H. Crouch, M. Shen, E. Mazur, *Opt. Lett.* **2005**, *30*, 1773.
- [230] Y. Borodaenko, D. Pavlov, A. Cherepakhin, E. Mitsai, A. Pilnik, S. Syubaev, S. O. Gurbatov, E. Modin, A. P. Porfiev, S. N. Khonina, A. V. Shevlyagin, E. L. Gurevich, A. A. Kuchmizhak, *Adv. Mater. Technologies* **2023**, *9*, 2301567.
- [231] M.-J. Sher, M. T. Winkler, E. Mazur, *MRS bulletin* **2011**, *36*, 439.
- [232] L. D. Zarzar, B. S. Swartzentruber, B. F. Donovan, P. E. Hopkins, B. Kaehr, *ACS Appl. Mater. Interfaces* **2016**, *8*, 21134.
- [233] B. Kang, S. Han, J. Kim, S. Ko, M. Yang, *J. Phys. Chem. C* **2011**, *115*, 23664.
- [234] J. Shin, B. Jeong, J. Kim, V. B. Nam, Y. Yoon, J. Jung, S. Hong, H. Lee, H. Eom, J. Yeo, J. Choi, D. Lee, S. H. Ko, *Adv. Mater.* **2020**, *32*, 1905527.
- [235] J. Yeo, S. Hong, G. Kim, H. Lee, Y. D. Suh, I. Park, C. P. Grigoropoulos, S. H. Ko, *ACS nano* **2015**, *9*, 6059.
- [236] S. S. Chou, B. S. Swartzentruber, M. T. Janish, K. C. Meyer, L. B. Biedermann, S. Okur, D. B. Burckel, C. B. Carter, B. Kaehr, *J. Phys. Chem. Lett.* **2016**, *7*, 3736.
- [237] E. J. Broadhead, A. Monroe, K. M. Tibbetts, *Langmuir* **2021**, *37*, 3740.
- [238] Y. Borodaenko, S. Syubaev, E. Khairullina, I. Tumkin, S. Gurbatov, A. Mironenko, E. Mitsai, A. Zhizhchenko, E. Modin, E. L. Gurevich, A. A. Kuchmizhak, *Adv. Opt. Mater.* **2022**, *10*, 2201094.

- [239] S. I. Kudryashov, L. V. Nguyen, D. A. Kirilenko, P. N. Brunkov, A. A. Rudenko, N. I. Busleev, A. L. Shakhmin, A. V. Semench, R. A. Khmel'nitskiy, N. N. Melnik, I. N. Saraeva, A. A. Nastulyavichus, A. A. Ionin, E. R. Tolordava, Y. M. Romanova, *ACS Appl. Nano Mater.* **2018**, *1*, 2461.
- [240] H. Wang, A. Pyatenko, K. Kawaguchi, X. Li, Z. Swiatkowska-Warkocka, N. Koshizaki, *Angew. Chem., Int. Ed.* **2010**, *49*, 6361.
- [241] K. Niu, J. Yang, S. Kulinich, J. Sun, X. Du, *Langmuir* **2010**, *26*, 16652.
- [242] K. Niu, J. Yang, S. Kulinich, J. Sun, H. Li, X. Du, *J. Am. Chem. Soc.* **2010**, *132*, 9814.
- [243] K.-K. Kwon, H. Kim, T. Kim, C. N. Chu, *J. Mater. Process. Technol.* **2020**, *278*, 116505.
- [244] G. Kopitkovas, T. Lippert, J. Venturini, C. David, A. Wokaun, in *J. Phys.: Conf. Ser.*, vol. 59, IOP Publishing, Bristol, England **2007**, p. 526.
- [245] S. Pissadakis, R. Böhme, K. Zimmer, *Opt. Express* **2007**, *15*, 1428.
- [246] C. L. Saji, R. Sattari, B. N. Chichkov, S. Barcikowski, *J. Phys. Chem. C* **2010**, *114*, 2421.
- [247] T. Yang, J. Liu, J. Dai, Y. Han, *CrystEngComm* **2017**, *19*, 72.
- [248] J. Yeo, S. Hong, M. Wanit, H. W. Kang, D. Lee, C. P. Grigoropoulos, H. J. Sung, S. H. Ko, *Adv. Funct. Mater.* **2013**, *23*, 3316.
- [249] S. Hwang, T. Hwang, H. Kong, S. Lee, J. Yeo, *Appl. Surf. Sci.* **2021**, *552*, 149382.
- [250] H. Kong, H. Kim, S. Hwang, J. Mun, J. Yeo, *ACS Appl. Nano Mater.* **2022**, *5*, 4102.
- [251] M. P. Arciniegas, A. Castelli, S. Piazza, S. Dogan, L. Ceseracciu, R. Krahne, M. Duocastella, L. Manna, *Adv. Funct. Mater.* **2017**, *27*, 1701613.
- [252] A. Cherepakhin, A. Zhizhchenko, D. Khmelevskaia, L. Logunov, A. Kuchmizhak, S. Makarov, *Adv. Opt. Mater.* **2024**, *12*, 2302782.
- [253] M. Y. Bashouti, A. V. Povolotckaia, A. V. Povolotskiy, S. P. Tunik, S. H. Christiansen, G. Leuchs, A. A. Manshina, *RSC Adv.* **2016**, *6*, 75681.
- [254] A. C. Castonguay, N. N. Nova, L. M. Dueñas, S. McGee, M. J. K. Lodhi, Y. Yang, L. D. Zarzar, *Mater. Res. Express* **2023**, *10*, 115003.
- [255] E. Blasco, J. Müller, P. Müller, V. Trouillet, M. Schön, T. Scherer, C. Barner-Kowollik, M. Wegener, *Adv. Mater.* **2016**, *28*, 3592.
- [256] L. Yang, H. Hu, A. Scholz, F. Feist, G. Cadilha Marques, S. Kraus, N. M. Bojanowski, E. Blasco, C. Barner-Kowollik, J. Aghassi-Hagmann, M. Wegener, *Nat. Commun.* **2023**, *14*, 1103.
- [257] D. Lee, D. Paeng, H. K. Park, C. P. Grigoropoulos, *ACS Nano* **2014**, *8*, 9807.
- [258] D. Shestakov, E. Khairullina, A. Shishov, S. Khubezhov, S. Makarov, I. Tumkin, L. Logunov, *Opt. Laser Technol.* **2023**, *167*, 109777.
- [259] K. Ratautas, A. Jagminienė, I. Stankevičienė, M. Sadauskas, E. Norkus, G. Račiukaitis, *Results Phys.* **2020**, *16*, 102943.
- [260] E. M. Khairullina, K. Ratautas, M. S. Panov, V. S. Andriianov, S. Mickus, A. A. Manshina, G. Račiukaitis, I. I. Tumkin, *Microchim. Acta* **2022**, *189*, 259.
- [261] J. Zhang, T. Zhou, L. Wen, A. Zhang, *ACS Appl. Mater. Interfaces* **2016**, *8*, 33999.
- [262] E. J. Bjerneld, K. V. G. K. Murty, J. Prikulis, M. Käll, *ChemPhysChem* **2002**, *3*, 116.
- [263] J. Turkevich, P. C. Stevenson, J. Hillier, *Discuss. Faraday Soc.* **1951**, *11*, 55.
- [264] E. J. Bjerneld, F. Svedberg, M. Käll, *Nano Lett.* **2003**, *3*, 593.
- [265] K. Setoura, S. Ito, M. Yamada, H. Yamauchi, H. Miyasaka, *J. Photochem. Photobiol., A* **2017**, *344*, 168.
- [266] D. V. Mamonova, A. A. Vasileva, Y. V. Petrov, A. V. Koroleva, D. V. Danilov, I. E. Kolesnikov, G. I. Bikbaeva, J. Bachmann, A. A. Manshina, *Nanomaterials* **2022**, *12*, 146.
- [267] D. V. Mamonova, A. A. Vasileva, Y. V. Petrov, D. V. Danilov, I. E. Kolesnikov, A. A. Kalinichev, J. Bachmann, A. A. Manshina, *Materials* **2020**, *14*, 10.
- [268] O. E. Eremina, N. R. Yarenkov, G. I. Bikbaeva, O. O. Kapitanova, M. V. Samodelova, T. N. Shekhovtsova, I. E. Kolesnikov, A. V. Syuy, A. V. Arsenin, V. S. Volkov, G. I. Tselikov, S. M. Novikov, A. A. Manshina, I. A. Veselova, *Talanta* **2024**, *266*, 124970.
- [269] S. Haschke, D. Pankin, V. Mikhailovskii, M. K. S. Barr, A. Both-Engel, A. Manshina, J. Bachmann, *Beilstein J. Nanotechnol.* **2019**, *10*, 157.
- [270] M. Y. Bashouti, A. Manshina, A. Povolotckaia, A. Povolotskiy, A. Kireev, Y. Petrov, M. Mačković, E. Spiecker, I. Koshevoy, S. Tunik, S. Christiansen, *Lab Chip* **2015**, *15*, 1742.
- [271] M. A. Butt, D. Mamonova, Y. Petrov, A. Proklova, I. Kritchenkov, A. Manshina, P. Banzer, G. Leuchs, *Nanomaterials* **2020**, *10*, 1376.
- [272] S. Schlicht, A. Kireev, A. Vasileva, E. V. Grachova, S. P. Tunik, A. A. Manshina, J. Bachmann, *Nanotechnology* **2017**, *28*, 065405.
- [273] A. Vasileva, S. Haschke, V. Mikhailovskii, A. Gitlina, J. Bachmann, A. Manshina, *Nano-Struct. Nano-Obj.* **2020**, *24*, 100547.
- [274] A. A. Vasileva, D. V. Mamonova, V. Mikhailovskii, Y. V. Petrov, Y. G. Toropova, I. E. Kolesnikov, G. Leuchs, A. A. Manshina, *Nanomaterials* **2023**, *13*, 1002.
- [275] G. Shafeev, *Appl. Phys. A* **1998**, *67*, 303.
- [276] K. Kordás, J. Békési, R. Vajtai, L. Nánai, S. Leppävuori, A. Uusimäki, K. Bali, T. F. George, G. Galbács, F. Ignácz, P. Moilanen, *Appl. Surf. Sci.* **2001**, *172*, 178.
- [277] G. Shafeev, P. Hoffmann, *Appl. Surf. Sci.* **1999**, *138-139*, 455.
- [278] V. Kochemirovsky, E. Khairullina, S. Safonov, L. Logunov, I. Tumkin, L. Menchikov, *Appl. Surf. Sci.* **2013**, *280*, 494.
- [279] K. Kordás, K. Bali, S. Leppävuori, A. Uusimäki, L. Nánai, *Appl. Surf. Sci.* **2000**, *154*, 399.
- [280] C. Kindle, A. Castonguay, S. McGee, J. A. Tomko, P. E. Hopkins, L. D. Zarzar, *ACS Appl. Nano Mater.* **2019**, *2*, 2581.
- [281] I. I. Tumkin, V. A. Kochemirovsky, M. D. Bal'makov, S. V. Safonov, E. S. Zhigley, L. S. Logunov, E. V. Shishkova, *Surf. Coat. Technol.* **2015**, *264*, 187.
- [282] M. S. Panov, I. I. Tumkin, A. V. Smikhovskaia, E. M. Khairullina, D. I. Gordeychuk, V. A. Kochemirovsky, *Microelectron. Eng.* **2016**, *157*, 13.
- [283] E. M. Khairullina, I. I. Tumkin, D. D. Stupin, A. V. Smikhovskaia, A. S. Mereshchenko, A. I. Lihachev, A. V. Vasin, M. N. Ryazantsev, M. S. Panov, *ACS Omega* **2021**, *6*, 18099.
- [284] M. S. Panov, A. E. Grishankina, D. D. Stupin, A. I. Lihachev, V. N. Mironov, D. M. Strashkov, E. M. Khairullina, I. I. Tumkin, M. N. Ryazantsev, *Materials* **2020**, *13*, 5385.
- [285] A. V. Smikhovskaia, M. S. Panov, I. I. Tumkin, E. M. Khairullina, S. S. Ermakov, I. A. Balova, M. N. Ryazantsev, V. A. Kochemirovsky, *Anal. Chim. Acta* **2018**, *1044*, 138.
- [286] T. Lipateva, A. Lipatiev, S. Lotarev, G. Shakhgildyan, S. Fedotov, V. Sigaev, *Materials* **2022**, *15*, 6867.
- [287] A. C. Castonguay, N. Yi, B. Li, J. Zhao, H. Li, Y. Gao, N. N. Nova, N. Tiwari, L. D. Zarzar, H. Cheng, *ACS Appl. Mater. Interfaces* **2022**, *14*, 28163.
- [288] S. McGee, Y. Lei, J. Goff, C. J. Wilkinson, N. N. Nova, C. M. Kindle, F. Zhang, K. Fujisawa, E. Dimitrov, S. B. Sinnott, I. Dabo, M. Terrones, L. D. Zarzar, *ACS Nano* **2021**, *15*, 9796.
- [289] J. Lin, Z. Peng, Y. Liu, F. Ruiz-Zepeda, R. Ye, E. L. G. Samuel, M. J. Yacaman, B. I. Yakobson, J. M. Tour, *Nat. Commun.* **2014**, *5*, 1.
- [290] Z. Li, L. Lu, Y. Xie, W. Wang, Z. Lin, B. Tang, N. Lin, *Adv. Eng. Mater.* **2021**, *23*, 2100195.
- [291] M. Kasischke, E. Subaş, C. Bock, D.-V. Pham, E. L. Gurevich, U. Kunze, A. Ostendorf, *Appl. Surf. Sci.* **2019**, *478*, 299.
- [292] M. Kasischke, S. Maragkaki, S. Volz, A. Ostendorf, E. L. Gurevich, *Appl. Surf. Sci.* **2018**, *445*, 197.
- [293] I. A. Salimon, E. V. Zharkova, A. V. Averchenko, J. Kumar, P. Somov, O. A. Abbas, P. G. Lagoudakis, S. Mailis, *Micromachines* **2023**, *14*, 1036.

- [294] A. V. Averchenko, I. A. Salimon, E. V. Zharkova, S. Lipovskikh, P. Somov, O. A. Abbas, P. G. Lagoudakis, S. Mailis, *Mater. Today Advances* **2023**, *17*, 100351.
- [295] Z. Zhang, H. Zhu, W. Zhang, Z. Zhang, J. Lu, K. Xu, Y. Liu, V. Saetang, *Carbon* **2023**, *214*, 118356.
- [296] H. Wang, Z. Zhao, P. Liu, X. Guo, *Biosensors* **2022**, *12*, 55.
- [297] S. O'Halloran, A. Pandit, A. Heise, A. Kellett, *Adv. Sci.* **2023**, *10*, 2204072.
- [298] H. Wang, W. Zhang, D. Ladika, H. Yu, D. Gailevičius, H. Wang, C.-F. Pan, P. N. S. Nair, Y. Ke, T. Mori, J. Y. E. Chan, Q. Ruan, M. Farsari, M. Malinauskas, S. Juodkazis, M. Gu, J. K. W. Yang, *Adv. Funct. Mater.* **2023**, *33*, 2214211.
- [299] M. Göppert-Mayer, *Ann. Phys.* **2009**, *521*, 466.
- [300] S. Maruo, O. Nakamura, S. Kawata, *Opt. Lett.* **1997**, *22*, 132.
- [301] C. L. Lay, C. S. L. Koh, Y. H. Lee, G. C. Phan-Quang, H. Y. F. Sim, S. X. Leong, X. Han, I. Y. Phang, X. Y. Ling, *ACS Appl. Mater. Interfaces* **2020**, *12*, 10061.
- [302] E. Skliutas, M. Lebedevaite, E. Kabouraki, T. Baldacchini, J. Ostrauskaite, M. Vamvakaki, M. Farsari, S. Juodkazis, M. Malinauskas, *Nanophotonics* **2021**, *10*, 1211.
- [303] S. Maruo, T. Saeki, *Opt. Express* **2008**, *16*, 1174.
- [304] Y.-Y. Cao, X.-Z. Dong, N. Takeyasu, T. Tanaka, Z.-S. Zhao, X.-M. Duan, S. Kawata, *Appl. Phys. A* **2009**, *96*, 453.
- [305] Y.-Y. Cao, N. Takeyasu, T. Tanaka, X.-M. Duan, S. Kawata, *Small* **2009**, *5*, 1144.
- [306] S. Bai, D. Serien, A. Hu, K. Sugioka, *Adv. Funct. Mater.* **2018**, *28*, 1706262.
- [307] S. Bai, S. Zhang, W. Zhou, D. Ma, Y. Ma, P. Joshi, A. Hu, *Nano-Micro Lett.* **2017**, *9*, 1.
- [308] J. Jones, M. R. Snowdon, S. Rathod, P. Peng, *Flex. Print. Electron.* **2023**, *8*, 015008.
- [309] X. Zhou, W. Guo, Y. Yao, R. Peng, P. Peng, *Adv. Eng. Mater.* **2021**, *23*, 2100192.
- [310] X. Zhou, W. Guo, Q. Sun, L. Sun, P. Peng, *ACS Appl. Electron. Mater.* **2023**, *5*, 3780.
- [311] A. Shishov, A. Pochivalov, L. Nugbienyo, V. Andruch, A. Bulatov, *TrAC, Trends Anal. Chem.* **2020**, *129*, 115956.
- [312] C. M. A. Brett, *Curr. Opin. Electrochem.* **2018**, *10*, 143.
- [313] A. Shishov, D. Gordeychuk, L. Logunov, I. Tumkin, *Chem. Commun.* **2019**, *55*, 9626.
- [314] A. Shishov, D. Gordeychuk, L. Logunov, A. Levshakova, E. Andrusenko, I. Chernyshov, E. Danilova, M. Panov, E. Khairullina, I. Tumkin, *New J. Chem.* **2021**, *45*, 21896.
- [315] A. S. Levshakova, E. M. Khairullina, L. S. Logunov, M. S. Panov, A. S. Mereshchenko, V. B. Sosnovsky, D. I. Gordeychuk, A. Yu. Shishov, I. I. Tumkin, *Mater. Lett.* **2022**, *308*, 131085.
- [316] E. Khairullina, A. Shishov, D. Gordeychuk, L. Logunov, A. Levshakova, V. B. Sosnovsky, A. Koroleva, V. Mikhailovsky, E. L. Gurevich, I. Chernyshov, M. S. Panov, I. Tumkin, *J. Mater. Sci.* **2023**, *58*, 9322.
- [317] E. A. Avilova, E. M. Khairullina, A. Yu. Shishov, E. A. Eltysheva, V. Mikhailovskii, D. A. Sinev, I. I. Tumkin, *Nanomaterials* **2022**, *12*, 1127.
- [318] S. Back, B. Kang, *Opt. Lasers Eng.* **2018**, *101*, 78.
- [319] Md. K. Rahman, Z. Lu, K.-S. Kwon, *AIP Adv.* **2018**, *8*, 095008.
- [320] M. Mizoshiri, S. Arakane, J. Sakurai, S. Hata, *Appl. Phys. Express* **2016**, *9*, 036701.
- [321] M. Mizoshiri, Y. Ito, S. Arakane, J. Sakurai, S. Hata, *Jpn. J. Appl. Phys.* **2016**, *55*, 06GP05.
- [322] Y. Huang, Y. Huang, X. Xie, X. Xie, X. Xie, M. Li, M. Li, M. Xu, M. Xu, J. Long, J. Long, *Opt. Express* **2021**, *29*, 4453.
- [323] K. Bischoff, C. Esen, R. Hellmann, *Nanomaterials* **2023**, *13*, 2693.
- [324] M. Mizoshiri, K. Yoshidomi, N. Darkhanbaatar, E. M. Khairullina, I. I. Tumkin, *Nanomaterials* **2021**, *11*, 3356.
- [325] M. Mizoshiri, K. Nishitani, S. Hata, *Micromachines* **2018**, *9*, 264.
- [326] D. Paeng, D. Lee, J. Yeo, J.-H. Yoo, F. I. Allen, E. Kim, H. So, H. K. Park, A. M. Minor, C. P. Grigoropoulos, *J. Phys. Chem. C* **2015**, *119*, 6363.
- [327] S. Kefer, K. Bischoff, G.-L. Roth, J. Haubner, B. Schmauss, R. Hellmann, *Adv. Opt. Mater.* **2021**, *9*, 2002203.
- [328] G.-L. Roth, J. Haubner, S. Kefer, C. Esen, R. Hellmann, *Opt. Lasers Eng.* **2021**, *137*, 106362.
- [329] S. Arakane, M. Mizoshiri, J. Sakurai, S. Hata, *J. Micromech. Microeng.* **2017**, *27*, 055013.
- [330] M. Mizoshiri, S. Hata, *Appl. Phys. A* **2018**, *124*, 1.
- [331] K. Tamura, M. Mizoshiri, J. Sakurai, S. Hata, *Jpn. J. Appl. Phys.* **2017**, *56*, 06GN08.
- [332] I. I. Tumkin, E. M. Khairullina, M. S. Panov, K. Yoshidomi, M. Mizoshiri, *Materials* **2021**, *14*, 2493.
- [333] K. Vu Trung Nguyen, Y. Kobayashi, T. D. Tran, M. Anzai, M. Mizoshiri, *Nano-Structures & Nano-Objects* **2023**, *36*, 101062.
- [334] M. Mizoshiri, Y. Kondo, *Opt. Mater. Express* **2019**, *9*, 2828.
- [335] M. Mizoshiri, A. Tanokuchi, *Opt. Mater. Express* **2020**, *10*, 2533.
- [336] M. Mizoshiri, Y. Kondo, *Jpn. J. Appl. Phys.* **2019**, *58*, SDDF05.
- [337] M. Mizoshiri, K. Aoyama, A. Uetsuki, T. Ohishi, *Micromachines* **2019**, *10*, 401.
- [338] M. Mizoshiri, T. Hayashi, J. Narushima, T. Ohishi, *Opt. Laser Technol.* **2021**, *144*, 107418.
- [339] J. Zhang, Y. Xie, H. Xu, T. Zhou, *Ind. Eng. Chem. Res.* **2022**, *61*, 6987.
- [340] Y. Liu, M. Pharr, G. A. Salvatore, *ACS Nano* **2017**, *11*, 9614.
- [341] K. Ratautas, M. Andrulevičius, A. Jagminienė, I. Stankevičienė, E. Norkus, G. Račiukaitis, *Appl. Surf. Sci.* **2019**, *470*, 405.
- [342] M. K. Camargo, M. Uebel, M. Kurniawan, K. F. Ziegler, M. Seiler, R. Grieseler, U. Schmidt, A. Barz, J. Bliedtner, A. Bund, *Adv. Eng. Mater.* **2022**, *24*, 2100933.
- [343] P. Rytlewski, B. Jagodziński, R. Malinowski, B. Budner, K. Moraczewski, A. Wojciechowska, P. Augustyn, *Appl. Surf. Sci.* **2020**, *505*, 144429.
- [344] C. G. Akagündüz, E. Soylemez, *Adv. Eng. Mater.* **2023**, *25*, 2300907.
- [345] H. Xu, J. Feng, F. Yu, J. Huang, T. Zhou, *Ind. Eng. Chem. Res.* **2023**, *62*, 395.
- [346] J. Zhang, T. Zhou, Y. Xie, L. Wen, *Adv. Mater. Interfaces* **2017**, *4*, 1700937.
- [347] J. Zhang, J. Feng, L. Jia, H. Zhang, G. Zhang, S. Sun, T. Zhou, *ACS Appl. Mater. Interfaces* **2019**, *11*, 13714.
- [348] H. Xu, J. Zhang, J. Feng, T. Zhou, *Ind. Eng. Chem. Res.* **2021**, *60*, 8821.
- [349] H. Xu, J. Feng, C. Xiao, R. Xu, Y. Xie, T. Zhou, *ACS Appl. Mater. Interfaces* **2022**, *14*, 31411.
- [350] D. Zhang, B. Ranjan, T. Tanaka, K. Sugioka, *Int. J. Extreme Manuf.* **2020**, *2*, 015001.
- [351] S. Romashevskiy, A. Ignatov, V. Zhakhovskiy, E. Eganova, E. Pershina, N. Inogamov, S. Ashitkov, *Appl. Surf. Sci.* **2023**, *615*, 156212.
- [352] M. Senegačnik, P. Gregorčič, *Appl. Surf. Sci.* **2023**, *610*, 155486.
- [353] N. Inogamov, S. Romashevskiy, A. I. Ignatov, V. Zhakhovskiy, V. A. Khokhlov, E. M. Eganova, E. A. Pershina, S. I. Ashitkov, *JETP Lett.* **2021**, *113*, 75.
- [354] T. J.-Y. Derrien, J. Krüger, J. Bonse, *J. Opt.* **2016**, *18*, 115007.
- [355] J. Bonse, S. Gräf, *Laser Photonics Rev.* **2020**, *14*, 2000215.
- [356] C.-H. Lin, L. Jiang, Y.-H. Chai, H. Xiao, S.-J. Chen, H.-L. Tsai, *Opt. Express* **2009**, *17*, 21581.
- [357] E. J. Broadhead, K. M. Tibbetts, *Langmuir* **2020**, *36*, 10120.
- [358] N. G. Simpson, E. J. Broadhead, A. M. Casto, K. M. Tibbetts, *Langmuir* **2024**, *40*, 241.
- [359] Y. Borodaenko, E. Khairullina, A. Levshakova, A. Shmalko, I. Tumkin, S. Gurbatov, A. Mironenko, E. Mitsai, E. Modin, E. L. Gurevich, A. A. Kuchmizhak, *Nanomaterials* **2023**, *13*, 1300.

- [360] S. I. Kudryashov, A. A. Nastulyavichus, I. N. Saraeva, A. A. Rudenko, D. A. Zayarny, A. A. Ionin, *Appl. Surf. Sci.* **2020**, 519, 146204.
- [361] C. Radu, S. Simion, M. Zamfirescu, M. Ulmeanu, M. Enculescu, M. Radoiu, *J. Appl. Phys.* **2011**, 110, 034901.
- [362] D. Zhang, B. Ranjan, T. Tanaka, K. Sugioka, *ACS Appl. Nano Mater.* **2020**, 3, 1855.
- [363] D. Kochuev, K. Khorkov, D. Abramov, S. Arakelian, V. Prokoshev, *J. Surf. Invest.: X-Ray, Synchrotron Neutron Tech.* **2018**, 12, 1220.
- [364] A. Kanitz, J. Hoppius, E. Gurevich, A. Ostendorf, *Phys. Proc.* **2016**, 83, 114.
- [365] H. Wang, R. Nett, E. L. Gurevich, A. Ostendorf, *Appl. Sci.* **2021**, 11, 515.
- [366] G. Yang, *Prog. Mater. Sci.* **2007**, 52, 648.
- [367] H. Zeng, X.-W. Du, S. C. Singh, S. A. Kulinich, S. Yang, J. He, W. Cai, *Adv. Funct. Mater.* **2012**, 22, 1333.
- [368] Q. Zhang, M. Honda, S. A. Kulinich, Y. Ichikawa, *Appl. Surf. Sci.* **2021**, 541, 148438.
- [369] L. M. Frias Batista, A. Nag, V. K. Meader, K. M. Tibbetts, *Sci. China Phys., Mech. Astron.* **2022**, 65, 274202.
- [370] A. V. Shabalina, V. A. Svetlichnyi, S. A. Kulinich, *Curr. Opin. Green Sustainable Chem.* **2022**, 33, 100566.
- [371] S. Reichenberger, G. Marzun, M. Muhler, S. Barcikowski, *Chem-CatChem* **2019**, 11, 4489.
- [372] S. Ibrahimkutty, P. Wagener, T. d. S. Rolo, D. Karpov, A. Menzel, T. Baumbach, S. Barcikowski, A. Plech, *Sci. Rep.* **2015**, 5, 1.
- [373] G. Marzun, C. Streich, S. Jendrzey, S. Barcikowski, P. Wagener, *Langmuir* **2014**, 30, 11928.
- [374] A. L. Nemoikina, A. V. Shabalina, V. A. Svetlichnyi, *J. Cult. Herit.* **2019**, 39, 42.
- [375] E. D. Fakhrutdinova, A. V. Shabalina, M. A. Gerasimova, A. L. Nemoikina, O. V. Vodyankina, V. A. Svetlichnyi, *Materials* **2020**, 13, 2054.
- [376] J.-P. Sylvestre, S. Poulin, A. V. Kabashin, E. Sacher, M. Meunier, J. H. Luong, *J. Phys. Chem. B* **2004**, 108, 16864.
- [377] R. Streubel, S. Barcikowski, B. Gökce, *Opt. Lett.* **2016**, 41, 1486.
- [378] V. Amendola, M. Meneghetti, *Phys. Chem. Chem. Phys.* **2009**, 11, 3805.
- [379] K. Anikin, N. Melnik, A. Simak, G. Shafeev, V. Voronov, A. Vitukhnovsky, *Chem. Phys. Lett.* **2002**, 366, 357.
- [380] D. Amans, A.-C. Chenus, G. Ledoux, C. Dujardin, C. Reynaud, O. Sublemontier, K. Masenelli-Varlot, O. Guillois, *Diamond Relat. Mater.* **2009**, 18, 177.
- [381] T. Baati, A. Al-Kattan, M.-A. Esteve, L. Njim, Y. Ryabchikov, F. Chaspoul, M. Hammami, M. Sentis, A. V. Kabashin, D. Braguer, *Sci. Rep.* **2016**, 6, 25400.
- [382] C. L. Sajti, R. Sattari, B. N. Chichkov, S. Barcikowski, *J. Phys. Chem. C* **2010**, 114, 2421.
- [383] M. Spellauge, M. Tack, R. Streubel, M. Miertz, K. S. Exner, S. Reichenberger, S. Barcikowski, H. P. Huber, A. R. Ziefuss, *Small* **2023**, 19, 2206485.
- [384] G. S. Park, K. M. Kim, S. W. Mhin, J. W. Eun, K. B. Shim, J. H. Ryu, N. Koshizaki, *Electrochem. Solid-State Lett.* **2008**, 11, J23.
- [385] D. Amans, C. Malaterre, M. Diouf, C. Mancini, F. Chaput, G. Ledoux, G. Breton, Y. Guillin, C. Dujardin, K. Masenelli-Varlot, P. Perriat, *J. Phys. Chem. C* **2011**, 115, 5131.
- [386] Y.-S. Cho, Y.-D. Huh, C. R. Park, Y. R. Do, *Electronic Mater. Lett.* **2014**, 10, 461.
- [387] G. I. Tselikov, G. A. Ermolaev, A. A. Popov, G. V. Tikhonowski, D. A. Panova, A. S. Taradin, A. A. Vyshnevyy, A. V. Syuy, S. M. Klimentov, S. M. Novikov, A. B. Evlyukhin, A. V. Kabashin, A. V. Arsenin, K. S. Novoselov, V. S. Volkov, *Proc. Natl. Acad. Sci. USA* **2022**, 119, 2208830119.
- [388] J. Johny, Y. Li, M. Kamp, O. Prymak, S.-X. Liang, T. Krekeler, M. Ritter, L. Kienle, C. Rehbock, S. Barcikowski, S. Reichenberger, *Nano Res.* **2022**, 15, 4807.
- [389] A. S. Chernikov, G. I. Tselikov, M. Y. Gubin, A. V. Shesterikov, K. S. Khorkov, A. V. Syuy, G. A. Ermolaev, I. S. Kazantsev, R. I. Romanov, A. M. Markeev, A. A. Popov, G. V. Tikhonowski, O. O. Kapitanova, D. A. Kochuev, A. Y. Leksin, D. I. Tselikov, A. V. Arsenin, A. V. Kabashin, V. S. Volkov, A. V. Prokhorov, *J. Mater. Chem. C* **2023**, 11, 3493.
- [390] K. Sasaki, T. Nakano, W. Soliman, N. Takada, *Appl. Phys. Express* **2009**, 2, 046501.
- [391] S. Kulinich, T. Kondo, Y. Shimizu, T. Ito, *J. Appl. Phys.* **2013**, 113, 033509.
- [392] C. Rehbock, V. Merk, L. Gamrad, R. Streubel, S. Barcikowski, *Phys. Chem. Chem. Phys.* **2013**, 15, 3057.
- [393] D. T. Alexander, D. Forrer, E. Rossi, E. Lidorikis, S. Agnoli, G. D. Bernasconi, J. Butet, O. J. Martin, V. Amendola, *Nano Lett.* **2019**, 19, 5754.
- [394] V. Torresan, D. Forrer, A. Guadagnini, D. Badocco, P. Pastore, M. Casarin, A. Selloni, D. Coral, M. Ceolin, M. B. Fernandez van Raap, A. Busato, P. Marzola, A. E. Spinelli, V. Amendola, *ACS Nano* **2020**, 14, 12840.
- [395] S. Makarov, I. S. Sinev, V. A. Milichko, F. Komissarenko, D. Zuev, E. V. Ushakova, I. Mukhin, Y. F. Yu, A. I. Kuznetsov, P. Belov, I. V. Iorsh, A. N. Poddubny, A. K. Samusev, Y. S. Kivshar, *Nano Lett.* **2018**, 18, 535.
- [396] S. O. Gurbatov, V. Puzikov, D. Storozhenko, E. Modin, E. Mitsai, A. Cherepakhin, A. Shevlyagin, A. V. Gerasimenko, S. A. Kulinich, A. A. Kuchmizhak, *ACS Appl. Mater. Interfaces* **2023**, 15, 3336.
- [397] C.-Y. Shih, M. V. Shugaev, C. Wu, L. V. Zhigilei, *J. Phys. Chem. C* **2017**, 121, 16549.
- [398] Y. Ishikawa, Y. Shimizu, T. Sasaki, N. Koshizaki, *J. Colloid Interface Sci.* **2006**, 300, 612.
- [399] M. Honda, T. Goto, T. Owashi, A. G. Rozhin, S. Yamaguchi, T. Ito, S. A. Kulinich, *Phys. Chem. Chem. Phys.* **2016**, 18, 23628.
- [400] A. H. Hamad, *Chem. Phys. Lett.* **2020**, 755, 137782.
- [401] D. Zhang, Z. Li, K. Sugioka, *J. Phys.: Photonics* **2021**, 3, 042002.
- [402] A. Menéndez-Manjón, B. N. Chichkov, S. Barcikowski, *J. Phys. Chem. C* **2010**, 114, 2499.
- [403] F. Mafuné, J.-y. Kohno, Y. Takeda, T. Kondow, H. Sawabe, *J. Phys. Chem. B* **2000**, 104, 9111.
- [404] T. Tsuji, D.-H. Thang, Y. Okazaki, M. Nakanishi, Y. Tsuboi, M. Tsuji, *Appl. Surf. Sci.* **2008**, 254, 5224.
- [405] M. Koizumi, S. A. Kulinich, Y. Shimizu, T. Ito, *J. Appl. Phys.* **2013**, 114, 214301.
- [406] A. Singh, T. Salminen, M. Honkanen, J.-P. Nikkanen, T. Vuorinen, R. Kari, J. Vihinen, E. Levänen, *Nanotechnology* **2019**, 31, 085602.
- [407] K. Sasaki, N. Takada, *Pure Appl. Chem.* **2010**, 82, 1317.
- [408] T. Goto, M. Honda, S. A. Kulinich, Y. Shimizu, T. Ito, *Japanese J. Appl. Phys.* **2015**, 54, 070305.
- [409] W. Soliman, N. Takada, K. Sasaki, in *TENCON 2010-2010 IEEE Region 10 Conference*, IEEE, Piscataway, NJ **2010**, pp. 154–157.
- [410] H. Zhang, J. Liu, Y. Ye, Z. Tian, C. Liang, *Phys. Chem. Chem. Phys.* **2013**, 15, 5684.
- [411] B.-H. Lee, T. Nakayama, Y. Tokoi, T. Suzuki, K. Niihara, *J. Alloys Compd.* **2011**, 509, 1231.
- [412] A. Letzel, B. Gökce, P. Wagener, S. Ibrahimkutty, A. Menzel, A. Plech, S. Barcikowski, *J. Phys. Chem. C* **2017**, 121, 5356.
- [413] S. O. Gurbatov, V. Puzikov, A. Cherepakhin, E. Mitsai, N. Tarasenko, A. Shevlyagin, A. Sergeev, S. A. Kulinich, A. A. Kuchmizhak, *Opt. Laser Technol.* **2022**, 147, 107666.
- [414] S. Gurbatov, V. Puzikov, E. Modin, A. Shevlyagin, A. Gerasimenko, E. Mitsai, S. A. Kulinich, A. Kuchmizhak, *Materials* **2022**, 15, 8091.
- [415] S. O. Gurbatov, E. Modin, V. Puzikov, P. Tonkaev, D. Storozhenko, A. Sergeev, N. Mintcheva, S. Yamaguchi, N. N. Tarasenko, A. Chuvilin,

- S. Makarov, S. A. Kulinich, A. A. Kuchmizhak, *ACS Appl. Mater. Interfaces* **2021**, *13*, 6522.
- [416] M. Flimelová, Y. V. Ryabchikov, J. Behrends, N. M. Bulgakova, *Nanomaterials* **2023**, *13*, 764.
- [417] A. A. Popov, Z. Swiatkowska-Warkocka, M. Marszalek, G. Tselikov, I. V. Zelepukin, A. Al-Kattan, S. M. Deyev, S. M. Klimentov, T. E. Itina, A. V. Kabashin, *Nanomaterials* **2022**, *12*, 649.
- [418] N. Mintcheva, D. K. Subbiah, M. E. Turabayev, S. O. Gurbatov, J. B. B. Rayappan, A. A. Kuchmizhak, S. A. Kulinich, *Nanomaterials* **2023**, *13*, 670.
- [419] P. Shankar, M. H. Ishak, J. K. Padarti, N. Mintcheva, S. Iwamori, S. O. Gurbatov, J. H. Lee, S. A. Kulinich, *Appl. Surf. Sci.* **2020**, *531*, 147365.
- [420] V. Amendola, S. Scaramuzza, L. Litt, M. Meneghetti, G. Zuccolotto, A. Rosato, E. Nicolato, P. Marzola, G. Fracasso, C. Anselmi, M. Pinto, M. Colombatti, *Small* **2014**, *10*, 2476.
- [421] E. Fakhruddinova, O. Reutova, L. Maliy, T. Kharlamova, O. Vodyankina, V. Svetlichnyi, *Materials* **2022**, *15*, 7413.
- [422] A. V. Shabalina, E. D. Fakhruddinova, A. G. Golubovskaya, S. Kuzmin, S. Koscheev, S. A. Kulinich, V. A. Svetlichnyi, O. V. Vodyankina, *Appl. Surf. Sci.* **2022**, *575*, 151732.
- [423] E. D. Fakhruddinova, A. V. Volokitina, S. A. Kulinich, D. A. Goncharova, T. S. Kharlamova, V. A. Svetlichnyi, *Materials* **2024**, *17*, 527.
- [424] A. G. Golubovskaya, T. S. Kharlamova, E. A. Gavrilenko, E. D. Fakhruddinova, O. V. Vodyankina, S. A. Kulinich, V. A. Svetlichnyi, *J. Compos. Sci.* **2024**, *8*, 42.
- [425] A. G. Golubovskaya, D. A. Goncharova, E. D. Fakhruddinova, T. S. Kharlamova, O. V. Vodyankina, V. A. Svetlichnyi, *Mater. Chem. Phys.* **2024**, *314*, 128800.
- [426] A. V. Shabalina, T. I. Izaak, T. S. Kharlamova, D. O. Martynova, I. N. Lapin, V. A. Svetlichnyi, *Colloids Surf. A* **2018**, *553*, 80.
- [427] N. Mintcheva, P. Srinivasan, J. B. B. Rayappan, A. A. Kuchmizhak, S. Gurbatov, S. A. Kulinich, *Appl. Surf. Sci.* **2020**, *507*, 145169.
- [428] V. Amendola, M. Meneghetti, O. M. Bakr, P. Riello, S. Polizzi, D. H. Anjum, S. Fiameni, P. Arosio, T. Orlando, C. de Julian Fernandez, F. Pineider, C. Sangregorio, A. Lascialfari, *Nanoscale* **2013**, *5*, 5611.
- [429] S. Scaramuzza, S. Agnoli, V. Amendola, *Phys. Chem. Chem. Phys.* **2015**, *17*, 28076.
- [430] A. Tymoczko, M. Kamp, C. Rehbock, L. Kienle, E. Cattaruzza, S. Barcikowski, V. Amendola, *Nanoscale Horizons* **2019**, *4*, 1326.
- [431] V. Amendola, A. Guadagnini, S. Agnoli, D. Badocco, P. Pastore, G. Fracasso, M. Gerosa, F. Vurro, A. Busato, P. Marzola, *J. Colloid Interface Sci.* **2021**, *596*, 332.
- [432] A. A. Bubnov, V. S. Belov, Y. V. Kargina, G. V. Tikhonowski, A. A. Popov, A. Y. Kharin, M. V. Shestakov, A. M. Perepukhov, A. V. Syuy, V. S. Volkov, V. V. Khovaylo, S. M. Klimentov, A. V. Kabashin, V. Y. Timoshenko, *Nanomaterials* **2023**, *13*, 2256.
- [433] V. Amendola, S. Scaramuzza, S. Agnoli, G. Granozzi, M. Meneghetti, G. Campo, V. Bonanni, F. Pineider, C. Sangregorio, P. Ghigna, S. Polizzi, P. Riello, S. Fiameni, L. Nodari, *Nano Res.* **2015**, *8*, 4007.
- [434] P. Liu, H. Chen, H. Wang, J. Yan, Z. Lin, G. Yang, *J. Phys. Chem. C* **2015**, *119*, 1234.
- [435] I. N. Saraeva, N. Van Luong, S. I. Kudryashov, A. A. Rudenko, R. A. Khmelitskiy, A. L. Shakhmin, A. Y. Kharin, A. A. Ionin, D. A. Zayarny, P. Van Duong, P. H. Minh, *Journal of Photochemistry and Photobiology A: Chemistry* **2018**, *360*, 125.
- [436] A. Al-Kattan, G. Tselikov, K. Metwally, A. A. Popov, S. Mensah, A. V. Kabashin, *Nanomaterials* **2021**, *11*, 592.
- [437] E. N. Gerasimova, E. Uvarov, V. V. Yaroshenko, O. Epifanovskaya, A. Shakirova, L. S. Logunov, O. Vlasova, A. Parodi, A. A. Zamyatnin Jr, A. S. Timin, S. V. Makarov, M. V. Zyuzin, *ACS Appl. Nano Mater.* **2023**, *6*, 18848.
- [438] S. O. Gurbatov, A. Y. Zhizhchenko, V. Y. Nesterov, E. B. Modin, S. V. Zaboltnov, A. A. Kuchmizhak, *ACS Appl. Nano Mater.* **2024**, *7*, 10779.
- [439] A. Larin, A. Nominé, E. Ageev, J. Ghanbaja, L. Kolotova, S. Starikov, S. Bruyère, T. Belmonte, S. Makarov, D. Zuev, *Nanoscale* **2020**, *12*, 1013.
- [440] X. Ding, T. Sato, Y. Kawaguchi, H. Niino, *Japanese J. Appl. Phys.* **2003**, *42*, 2BL176.
- [441] K. Hatanaka, M. Kawao, Y. Tsuboi, H. Fukumura, H. Masuhara, *J. Appl. Phys.* **1997**, *82*, 5799.
- [442] X. Ding, Y. Yasui, Y. Kawaguchi, H. Niino, A. Yabe, *Appl. Phys. A: Mater. Sci. Process.* **2002**, *75*, 440.
- [443] M. Ehrhardt, P. Lorenz, B. Han, R. Zhu, K. Zimmer, *J. Laser Micro/Nanoeng.* **2018**, *13*, 47.
- [444] J. Wang, H. Niino, A. Yabe, *Appl. Phys. A* **1999**, *68*, 111.
- [445] K. Zimmer, *Int. J. Heat Mass Transfer* **2009**, *52*, 497.
- [446] Y. Kawaguchi, X. Ding, A. Narazaki, T. Sato, H. Niino, *Appl. Phys. A* **2004**, *79*, 883.
- [447] J. Long, C. Zhou, Z. Cao, X. Xie, W. Hu, *Opt. Laser Technol.* **2019**, *109*, 61.
- [448] R. Böhme, A. Braun, K. Zimmer, *Appl. Surf. Sci.* **2002**, *186*, 276.
- [449] M. Ehrhardt, G. Raciukaitis, P. Gecys, K. Zimmer, *Appl. Phys. A* **2010**, *101*, 399.
- [450] S. I. Dolgaev, A. A. Lyalin, A. V. Simakin, G. A. Shafeev, *Quantum Electron.* **1996**, *26*, 65.
- [451] S. Dolgaev, A. Lyalin, A. Simakin, V. Voronov, G. Shafeev, *Appl. Surf. Sci.* **1997**, *109*, 201.
- [452] Y. Yasui, H. Niino, Y. Kawaguchi, A. Yabe, *Appl. Surf. Sci.* **2002**, *186*, 552.
- [453] S. I. Dolgaev, M. E. Karasev, L. A. Kulevskii, A. V. Simakin, G. A. Shafeev, *Quantum Electron.* **2001**, *31*, 593.
- [454] R. Böhme, S. Pissadakis, M. Ehrhardt, D. Ruthe, K. Zimmer, *J. Phys. D: Appl. Phys.* **2006**, *39*, 1398.
- [455] A. Couairon, A. Mysyrowicz, *Phys. Rep.* **2007**, *441*, 47.
- [456] T. Sato, Y. Kawaguchi, R. Kurosaki, A. Narazaki, W. Watanabe, H. Niino, *J. Laser Micro/Nanoeng.* **2012**, *7*, 81.
- [457] R. Böhme, K. Zimmer, *Appl. Surf. Sci.* **2007**, *253*, 8091.
- [458] X. Ding, T. Sato, Y. Kawaguchi, H. Niino, *Japanese J. Appl. Phys.* **2003**, *42*, L176.
- [459] G. Kopitkovas, T. Lippert, C. David, S. Canulescu, A. Wokaun, J. Gobrecht, *Journal of Photochemistry and Photobiology A: Chemistry* **2004**, *166*, 135.
- [460] A. Rosenfeld, M. Lorenz, R. Stoian, D. Ashkenasi, *Appl. Phys. A* **1999**, *69*, S373.
- [461] K. P. Luong, R. Tanabe-Yamagishi, N. Yamada, Y. Ito, *Int. J. Electr. Mach.* **2020**, *25*, 7.
- [462] Y. Ito, S. Y. Chiah, K. P. Luong, D. Kataoka, R. Tanabe-Yamagishi, *J. Laser Micro Nanoeng.* **2020**, *15*, 111.
- [463] S. Lai, P. Lorenz, M. Ehrhardt, B. Han, D. Hirsch, I. Zagoranskiy, J. Lu, K. Zimmer, *Optics Lasers Eng.* **2019**, *122*, 245.
- [464] M. H. Hong, K. Y. Ng, Q. Xie, L. P. Shi, T. C. Chong, *Appl. Phys. A* **2008**, *93*, 153.
- [465] S. Nakashima, K. Sugioka, K. Midorikawa, *Appl. Surf. Sci.* **2009**, *255*, 249770.
- [466] Y. Okamoto, T. T. Takada, Y. M. Y. Mochizuki, *Japanese J. Appl. Phys.* **1996**, *35*, 12BL1641.
- [467] S. M. R. Nowak, G. Sepold, *Mater. Manuf. Processes* **1994**, *9*, 429.
- [468] F. Rubbi, X. Zhang, F. Delzendehrooy, B. Mao, Q. Nian, C. C. Doumanidis, Y. Liao, *J. Manuf. Processes* **2023**, *108*, 384.
- [469] K. H. Oh, S. Lee, S. Jeong, *Journal of Laser Micro Nanoengineering* **2016**, *11*, 25.
- [470] N. Jan, N. Majeed, M. Ahmad, W. A. Lone, R. John, *Chemosphere* **2022**, *302*, 134746.
- [471] P. T. Anastas, J. C. Warner, *Green chemistry: theory and practice*, Oxford University Press, Oxford **2000**.

- [472] I. Y. Khairani, G. Mínguez-Vega, C. Do nate-Buendía, B. Gökce, *Phys. Chem. Chem. Phys.* **2023**, *25*, 19380.
- [473] M. Murayama, Y. Nakayama, K. Yamazaki, Y. Hoshina, H. Watanabe, N. Fuutagawa, H. Kawanishi, T. Uemura, H. Narui, *Physica status solidi (a)* **2018**, *215*, 1700513.
- [474] S. Jendrzej, B. Gökce, M. Epple, S. Barcikowski, *ChemPhysChem* **2017**, *18*, 1012.
- [475] S. Kohsakowski, Ph.D. thesis, Dissertation, Duisburg, Essen, Universität Duisburg-Essen, 2018, **2018**.
- [476] K. Mishchik, G. Bonamis, J. Qiao, J. Lopez, E. Audouard, E. Mottay, C. Hönninger, I. Manek-Hönninger, *Opt. Lett.* **2019**, *44*, 2193.
- [477] P. L. Kramer, M. K. Windeler, K. Mecseki, E. G. Champenois, M. C. Hoffmann, F. Tavella, *Opt. Express* **2020**, *28*, 16951.
- [478] C. Kerse, H. Kalaycıoğlu, P. Elahi, B. Çetin, D. K. Kesim, Ö. Akçaalan, S. Yavaş, M. D. Aşık, B. Öktem, H. Hoogland, R. Holzwarth, F. Ö. Ilday, *Nature* **2016**, *537*, 84.
- [479] D. J. Ehrlich, P. F. Moulton, R. M. Osgood, *Opt. Lett.* **1979**, *4*, 184.
- [480] A. J. Silversmith, W. Lenth, R. M. Macfarlane, *Appl. Phys. Lett.* **1987**, *51*, 1977.
- [481] G. Qin, W. Qin, C. Wu, S. Huang, D. Zhao, J. Zhang, S. Lu, *Solid State Commun.* **2003**, *125*, 377.
- [482] H. Scheife, G. Huber, E. Heumann, S. Bär, E. Osiac, *Opt. Mater.* **2004**, *26*, 365.
- [483] P. Pues, M. Laube, S. Fischer, F. Schröder, S. Schwung, D. Rytz, T. Fiehler, U. Wittrock, T. Jüstel, *J. Lumin.* **2021**, *234*, 117987.
- [484] T.-S. D. Le, H.-P. Phan, S. Kwon, S. Park, Y. Jung, J. Min, B. J. Chun, H. Yoon, S. H. Ko, S.-W. Kim, Y.-J. Kim, *Adv. Funct. Mater.* **2022**, *32*, 2205158.
- [485] J. Scheuer, *ACS Photonics* **2020**, *7*, 1323.
- [486] P. Tonkaev, I. S. Sinev, M. V. Rybin, S. V. Makarov, Y. Kivshar, *Chem. Rev.* **2022**, *122*, 15414.
- [487] R. Paniagua-Dominguez, Y. F. Yu, E. Khaidarov, S. Choi, V. Leong, R. M. Bakker, X. Liang, Y. H. Fu, V. Valuckas, L. A. Krivitsky, A. I. Kuznetsov, *Nano Lett.* **2018**, *18*, 2124.
- [488] J. B. Mueller, N. A. Rubin, R. C. Devlin, B. Groever, F. Capasso, *Phys. Rev. Lett.* **2017**, *118*, 113901.
- [489] L. Huang, S. Zhang, T. Zentgraf, *Nanophotonics* **2018**, *7*, 1169.
- [490] A. Kristensen, J. K. Yang, S. I. Bozhevolnyi, S. Link, P. Nordlander, N. J. Halas, N. A. Mortensen, *Nat. Rev. Mater.* **2017**, *2*, 16088.
- [491] A. O. Larin, L. N. Dvoretckaia, A. M. Mozharov, I. S. Mukhin, A. B. Cherepakhin, I. I. Shishkin, E. I. Ageev, D. A. Zuev, *Adv. Mater.* **2021**, *33*, 2005886.
- [492] E. Ponkratova, E. Ageev, P. Trifonov, P. Kustov, M. Sandomirskii, M. Zhukov, A. Larin, I. Mukhin, T. Belmonte, A. Nominé, S. Bruyère, D. Zuev, *Adv. Funct. Mater.* **2022**, *32*, 2205859.
- [493] Q. Zhao, A. K. Yetisen, A. Sabouri, S. H. Yun, H. Butt, *ACS nano* **2015**, *9*, 9062.
- [494] J.-W. Tan, G. Wang, Y. Li, Y. Yu, Q.-D. Chen, *Laser Photonics Rev.* **2023**, *17*, 2200692.
- [495] J. Wu, K. Yin, S. Xiao, Z. Wu, Z. Zhu, J.-A. Duan, J. He, *Adv. Mater. Interfaces* **2021**, *8*, 2001610.
- [496] J. Langer, D. Jimenez de Aberasturi, J. Aizpurua, R. A. Alvarez-Puebla, B. Auguie, J. J. Baumberg, G. C. Bazan, S. E. Bell, A. Boisen, A. G. Brolo, J. Choo, D. Cialla-May, V. Deckert, L. Fabris, K. Faulds, F. J. G. de Abajo, R. Goodacre, D. Graham, A. J. Haes, C. L. Haynes, C. Huck, T. Itoh, M. Käll, J. Kneipp, N. A. Kotov, H. Kuang, E. C. Le Ru, H. K. Lee, J.-F. Li, X. Y. Ling, et al., *ACS nano* **2019**, *14*, 28.
- [497] H.-H. Hsiao, Y.-C. Hsu, A.-Y. Liu, J.-C. Hsieh, Y.-H. Lin, *Adv. Opt. Mater.* **2022**, *10*, 2200812.
- [498] A. Tittel, A. Leitis, M. Liu, F. Yesilkoy, D.-Y. Choi, D. N. Neshev, Y. S. Kivshar, H. Altug, *Science* **2018**, *360*, 1105.
- [499] J.-E. Park, J. Kim, J.-M. Nam, *Chem. sci.* **2017**, *8*, 4696.
- [500] D. I. Markina, S. S. Anoshkin, M. A. Masharin, S. A. Khubezhov, I. Tzibizov, D. Dolgintsev, I. N. Terterov, S. V. Makarov, A. P. Pushkarev, *ACS nano* **2023**, *17*, 1570.
- [501] Y. Borodaenko, S. Syubaev, S. Gurbatov, A. Zhizhchenko, A. Porfirev, S. Khonina, E. Mitsai, A. V. Gerasimenko, A. Shevlyagin, E. Modin, S. Juodkazis, E. L. Gurevich, A. A. Kuchmizhak, *ACS Appl. Mater. Interfaces* **2021**, *13*, 54551.
- [502] S. N. Erkizan, F. İdikut, Ö. Demirtaş, A. Goodarzi, A. K. Demir, M. Borra, I. Pavlov, A. Bek, *Adv. Opt. Mater.* **2022**, *10*, 2200233.
- [503] J. Zhang, M. Chaker, D. Ma, *J. Colloid Interface Sci.* **2017**, *489*, 138.
- [504] D. Goncharova, M. Salae, A. Volokitina, O. Magaev, V. Svetlichnyi, O. Vodyankina, *Mater. Today Chemistry* **2023**, *33*, 101709.
- [505] C. Zhu, X. Dong, X. Mei, M. Gao, K. Wang, D. Zhao, *Appl. Surf. Sci.* **2021**, *568*, 150978.
- [506] H. Liu, K.-s. Moon, J. Li, Y. Xie, J. Liu, Z. Sun, L. Lu, Y. Tang, C.-P. Wong, *Nano Energy* **2020**, *77*, 105058.
- [507] L. Fornasini, S. Scaravonati, G. Magnani, A. Morengi, M. Sidoli, D. Bersani, G. Bertoni, L. Aversa, R. Verucchi, M. Riccò, P. P. Lottici, D. Pontiroli, *Carbon* **2021**, *176*, 296.
- [508] C. Ma, J. Yan, Y. Huang, C. Wang, G. Yang, *Sci. Adv.* **2018**, *4*, eaas9894.
- [509] F. Seifkar, S. Azizian, M. Eslamipannah, B. Jaleh, *Sol. Energy Mater. Sol. Cells* **2022**, *238*, 111581.
- [510] M. Sandzhieva, D. Khmelevskaia, D. Tatarinov, L. Logunov, K. Samusev, A. Kuchmizhak, S. V. Makarov, *Nanomaterials* **2022**, *12*, 3916.
- [511] A. Furasova, P. Voroshilov, D. Saporì, K. Ladutenko, D. Baretin, A. Zakhidov, A. Di Carlo, C. Simovski, S. Makarov, *Adv. Photonics Res.* **2022**, *3*, 2100326.
- [512] A. Y. Kharin, V. V. Lysenko, A. Rogov, Y. V. Ryabchikov, A. Geloën, I. Tishchenko, O. Marty, P. G. Sennikov, R. A. Kornev, I. N. Zavestovskaya, A. V. Kabashin, V. Y. Timoshenko, *Adv. Opt. Mater.* **2019**, *7*, 1801728.
- [513] F. Ye, A. Ayub, R. Karimi, S. Wettig, J. Sanderson, K. P. Musselman, *Adv. Mater.* **2023**, *35*, 2301129.
- [514] S. Scaramuzza, C. M. De Faria, V. Coviello, D. Forrer, L. Artiglia, D. Badocco, P. Pastore, P. Ghigna, I. Postuma, L. Cansolino, C. Ferrari, S. Bortolussi, R. Vago, A. E. Spinelli, M. Bekić, M. Čolić, V. Amendola, *Adv. Funct. Mater.* **2023**, *33*, 2303366.



**Alina A. Manshina** is a professor at the institute of chemistry, St.Petersburg state university. She graduated in Physics at St.Petersburg state university where she obtained her Ph.D. in the field of laser physics. She got her habilitation in the field of solid-state chemistry. Thus, prof Manshinas work is focused on the interdisciplinary phenomena of physics and chemistry connected with laser-matter interactions, laser-induced chemical transformations, laser synthesis of functional nanomaterials, and photo-switchable nanohybrid materials for photopharmacology.



**Ilya I. Tumkin** received his Ph.D. in chemistry in St.-Petersburg University in 2016. Now he is a Postdoctoral Researcher at the Chair of Applied Laser Technologies at Ruhr University Bochum. His primary research interests include the development of innovative precursors for direct laser writing, and exploring novel approaches for fabrication of advanced flexible electronic components and sensors. With colleagues, Ilya Tumkin investigates the exciting possibilities of direct laser fabrication of metallic and composite micropatterns utilizing precursors based on Deep Eutectic Solvents and others.



**Mizue Mizoshiri** received her BS, MS, and Ph.D. degrees in materials and manufacturing science from Osaka University in 2005, 2007, and 2010, respectively. She was appointed a Research Scientist in National Institute of Advanced Industrial Science and Technology in 2010, an Assistant Professor at Nagoya University, and a Specially Appointed Associate Professor for Academia-Industry Fusion at Nagaoka University of Technology in 2018. At present, she is an Associate Professor of Micro-Nano Processing Laboratory at Nagaoka University of Technology. Her research interests include ultrafast laser processing, 3D microfabrication, and their application to fabricating microdevices.



**Evgeny L. Gurevich** received his MSc from St.-Petersburg State Technical University in Russia in 2000. In 2004 he received his Ph.D. in physics from the University of Münster in Germany. After two post-doc stays at Max-Planck Institute for Dynamics and Self-Organization in Göttingen and at ISAS - Institute for Analytical Sciences in Dortmund he was appointed as an Assistant Professor at the Ruhr-University Bochum in 2012. Since 2019 he is an Associate Professor at the University of Applied Science FH Münster, his research is focused on pattern formation and laser physics.